Aus der Klinik für Kardiologie und Pneumologie
(Prof. Dr. med. G. Hasenfuß)
der Medizinischen Fakultät der Universität Göttingen

Genetic modification in CPVT-patient-specific induced pluripotent stem cells with CRISPR/Cas9

INAUGURAL-DISSERTATION

zur Erlangung des Doktorgrades
der Medizinischen Fakultät der
Georg-August-Universität zu Göttingen

vorgelegt von

Maximilian Zimmermann

aus
Bonn

Göttingen 20.05.2019

Dekan:	Prof. Dr. rer. nat. H.K. Kroemer
Referent/in	Prof. Dr. rer. nat. K. Guan-Schmidt
Ko-Referent/in:	Prof. Dr. med. S. Hülsmann
Drittreferent/in:	Prof. Dr. med. R. Dressel
Datum der mündlichen Prüfung:	02.12.2019

Hiermit erkläre ich, die Dissertation mit dem Titel " Genetic modification in CPVT-patient-specific induced pluripotent stem cells with CRISPR/Cas9" eigenständig angefertigt und keine anderen als die von mir angegebenen Quellen und Hilfsmittel verwendet zu haben.

Göttingen, den 18.05.2019 ……

(Unterschrift)

Table of Contents

Figures

Tables

Abbreviations

°C	Degree Celsius
a.a.	Amino acid
AFP	Alpha-1-fetoprotein
ALP	Alkaline phosphatase
AP	Action potential
ATP	Adenosine triphosphate
bFGF	Basic fibroblast growth factor
BMP	Bone morphogenetic protein
bp	Base pair
bpm	Beats per minute
BSA	Bovine serum albumin
C-MYC	Cellular-Myc
Ca^{2+}	Calcium
CaM	Calmodulin
CaMK II	Ca^{2+}/calmodulin-dependent kinase II
Cas9	CRISPR-associated protein 9
CASQ2	Calsequestrin isoform 2
cDNA	Complementary DNA
CHIR	CHIR99021
CICR	Calcium-induced calcium release
CM	Cardiomyocyte
CPVT	Catecholaminergic polymorphic ventricular tachycardia
CRISPR	Clustered regulatory interspaced short palindromic repeat
crRNA	CRISPR repeat RNA
cTNT	Cardiac troponin T
Cx43	Connexin 43
d	Day
DAD	Delayed after depolarization
DAPI	4',6'-diamidine-2-phenylindol

DMEM	Dulbecco's modified Eagle's medium
DMSO	Dimethyl sulfoxide
DNA	Deoxyribonucleic acid
dNTP	Deoxyribose nucleoside triphosphate
DPBS	Dulbecco's phosphate buffered saline
DSB	Double-strand break
E. coli	Escheria coli
E8	Essential 8™ medium
EB	Embryoid bodies
ECG	Electrocardiogram
EDTA	Ethylenediaminetetraacetic acid
ESC	Embryonic stem cell
FACS	Fluorescence-activated cell sorting
FBS	Fetal bovine serum
FGF	Fibroblast growth factor
FKBP 12.6	FK506 binding protein 12.6 kDa
FOXD3	Forkhead box D3
g	Gram
g	Gravitational force
GAPDH	Glyceraldehyde-3-phosphate dehydrogenase
GDF3	Growth differentiation factor 3
GFP	Green fluorescent protein
GSK3	Glycogen synthase kinase 3
hALB	Human albumin
HDR	Homolog directed repair
HEPES	4-(2-hydroxyethyl)-1-piperazineethanesulfonic acid
I_{Ca}	Calcium influx
ICD	Implantable cardioverter defibrillator
IMDM	Iscove's modified Dulbecco's medium
IP3	Inositol 1,4,5-trisphosphate receptor
iPSC	Induced pluripotent stem cell
KLF4	Kruppel-like factor 4

l	Liter
LB	Lysogeny broth
LCSD	Left cardiac sympathetic denervation
MEF	Mouse embryonic fibroblasts
MLC2A	Myosin light chain 2a
MLC2V	Myosin light chain 2v
mRNA	Messenger ribonucleic acid
MTG	Monothioglycerol
NaCl	Sodium chloride
NCX	Na^+/Ca^{2+} exchange
NEAA	Non-essential amino acid
NHEJ	Non-homologous end joining
OCT4	Octamer-binding transcription factor 4
P/S	Penicillin/Streptomycin
PAM	Protospacer adjacent motif
PBS	Phosphate buffered saline
PCR	Polymerase chain reaction
PDE4D3	Phosphodiesterase 4D3
PFA	Paraformaldehyde
PKA	Protein kinase A
PP1	Protein phosphatase 1
PP2A	Protein phosphatase 2A
PVC	Premature ventricular contraction
PVDF	Polyvinylidene difluoride
RNA	Ribonucleic acid
rpm	Rounds per minute
RPMI	Roswell Park Memorial Institute medium
RT	Room temperature
RT-PCR	Reverse transcription-polymerase chain reaction
RyR	Ryanodine receptor
RyR1	Skeletal ryanodine receptor
RyR2	Cardiac ryanodine receptor

RyR3	Ryanodine receptor 3
SERCA	Sarcoplasmic reticulum calcium adenosine triphosphatase
SeV	Sendai virus
sgRNA	Single guide RNA
SOICR	Store overload-induced calcium release
SOX2	Sex determining region Y-box 2
SR	Sarcoplasmic reticulum
SSEA4	Stage-specific embryonic antigen-4
ssODN	Single stranded oligo desoxynucleotide
SYN	Synaptophysin
TALEN	Transcription activator-like effector nuclease
TBE	Tris/Borate/EDTA
TH	Tyrosine hydroxylase
TRA-1-60	Tumour-related antigen-1-60
tracrRNA	Transactivating crRNA
TZV	Thiazovivin
VT	Ventricular tachycardia
ZFN	Zink-finger-nuclease
α-ACT	Alpha-actinin
α-MHC	Myosin heavy chain (alpha)
αSMA	α-smooth muscle actin
β-ME	Beta-Mercaptoethanol

1 Introduction

1.1 Catecholaminergic polymorphic ventricular tachycardia

Catecholaminergic polymorphic ventricular tachycardia (CPVT) is an arrhythmic genetic cardiac disorder first described by Reid et al. (Reid et al. 1975). CPVT results from abnormal calcium (Ca^{2+}) handling in cardiomyocytes (CMs), which leads to syncope, ventricular tachycardia and sudden cardiac death at young age without structural alterations of the heart. The majority of patients carry mutations in the gene of cardiac ryanodine receptor *(RyR2)* forming the calcium release channel in the sarcoplasmic reticulum (SR). The defect causes spontaneous Ca^{2+} leak during diastole. However, the pathomechanism of the disease is not fully understood.

1.1.1 Epidemiology

CPVT is one of the most severe and lethal hereditary channelopathies with an estimated prevalence of 1:10 000 in Europe (Napolitano and Priori 2007; Hayashi et al. 2009). The mean age of onset of symptoms is 7-9 years. In exceptional cases the first syncope may occur during adulthood (Cerrone et al. 2009). Following Priori's data, 30% of the patients develop symptoms before the age of 10 and 60% of patients have approximately at least one syncopal episode before the age of 40. According to the PACES study which included 226 children with CPVT, 78% were symptomatic before the diagnoses were made (van der Werf and Wilde 2015). Because of the lack of systematic assessment in the population, realistic epidemiological data is not available.

1.1.2 Clinical presentation

The initial manifestation of CPVT is syncope triggered by physical or emotional stress during the first or second decade of life. In 30% of the cases a family history of fainting with seizure-like activity, exercise-related syncope or sudden cardiac death is known, which can lead to the diagnosis of CPVT (Sumitomo et al. 2003). Because of seizures epilepsy is often diagnosed leading to a delay in diagnosis of approximately 2 years and a mistreatment with antiepileptic drugs.

CPVT is an autosomal dominant disease (depending on the localization of the mutation). A family screening is necessary because asymptomatic carriers of a *RyR2* mutation are often detected due to family screening of an index patient (Leenhardt et al. 2012).

1.1.3 Diagnosis

An early accurate diagnosis of CPVT leads to the best possible clinical results in patients. The standard diagnosis procedures to prove CPVT are the exercise test, implantable loop recorder, holter monitoring as well as isoproterenol infusion to mimic an adrenergic flush. This can induce CPVT by ventricular arrhythmias, which appear progressively after a heart rate threshold around 120-130 beats per minute (bpm) (Leenhardt et al. 2012).

The QT interval in resting electrocardiogram (ECG) is usually normal for CPVT patients. The majority of the patients have bradycardia (≤ 60 bpm) compared with the normal heart rate of children, which is around 80-100 bpm.

CPVT can be reported by holter monitoring, which shows the acceleration of the sinus rhythm. The arrhythmias appear beyond a sinoatrial rate threshold of 120 to 130 bpm. First, isolated and monomorphic ventricular premature beats appear, which increase correlating to the heart rate in a quadrigeminy, trigeminy and bigeminy pattern. In the end phase they become polymorphic and finally they form bursts with monomorphic and bidirectional salvoes (Sumitomo et al. 2003). In the severe stage a bidirectional ventricular tachycardia (with a right bundle-branch block pattern, alternating right and left QRS axis deviation) is reported. Bursts of rapid irregular and polymorphic ventricular tachycardia (350-400 bpm) can be recorded. The final stage leads to syncope. The arrhythmic activity can be stopped in an early stage by itself and disappear in reverse order without clinical symptoms. The tachycardia can be reproduced by exercise-tests or isoproterenol infusions (Leenhardt et al. 1995). Cardiac imaging such as ECG or cardiac magnetic resonance imaging does not show structural abnormalities of the heart.

Guidelines to diagnose CPVT were developed by several experts and declared in the expert consensus statement on inherited primary arrhythmia syndromes. CPVT is diagnosed according to the expert consensus following the four definitions:

First, CPVT is diagnosed in the presence of a structurally normal heart, normal ECG and unexplained exercise or catecholamine-induced bidirectional ventricular tachycardia (VT) or polymorphic ventricular premature beats or VT in an individual ≤ 40 years of age. Second, it is diagnosed in patients (index case or family member) who have a pathogenic

mutation. Third, it is diagnosed in family members of a CPVT index case with a normal heart, who manifest exercise-induced premature ventricular contractions (PVCs) or bidirectional polymorphic VT. Fourth, it is diagnosed in the presence of a structurally normal heart and coronary arteries, normal ECG and unexplained exercise or catecholamine-induced bidirectional VT or polymorphic ventricular premature beats or VT in an individual >40 years of age (Priori et al. 2013).

1.1.4 Treatment of CPVT

The standard therapy for CPVT patients is the administration of β-blockers to prevent cardiac events like ventricular ectopy or arrhythmias. To improve the medical therapy further anti-arrhythmic drugs such as flecainide, a class Ic antiarrhythmic agent or Ca^{2+}-antagonist Verapamil can be added to the standard therapy. If the patient does not respond to medical treatment, an implantable cardioverter defibrillator (ICD) or left cardiac sympathetic denervation (LCSD) should be considered to complement the medical treatment (Priori et al. 2013; De Ferrari et al. 2015).

LCSD is a surgical treatment for CPVT patients, which treats refractory cardiac events and decreases the annual refractory cardiac events in 87% of the patients (Olde Nordkamp et al. 2014). New data show a benefit of the LCSD treatment. This causes the discussion if an ICD implantation should still be preferred towards LCSD treatment as first-line therapy for high-risk CPVT patients (De Ferrari et al. 2015). However, high-risk patients need a combination of medical therapy and interventional surgery to achieve long periods without CPVT symptoms.

Although the therapy is standardized, no specific treatment for CPVT is known because of the lack of understanding of pathomechanism. Disease modeling with induced pluripotent stem cells (iPSCs) offers the opportunity for a better understanding of genetic diseases like CPVT and may offer a new therapy approach based on genetic correction with Clustered Regularly Interspaced Short Palindromic Repeats (CRISPR) / CRISPR associated protein 9 (Cas9) (Kaminski et al. 2016).

1.1.5 Genetic background

CPVT is classified as CPVT1 and CPVT2 corresponding to the genetic background. The majority of the CPVT patients are carriers of a mutation in the *RyR2* gene with variable penetrance, which is classified as CPVT1 (Priori et al. 2002). The minority are CPVT2

patients with a recessive mutation in the cardiac *calsequestrin isoform 2* gene (*CASQ2*) (Lahat et al. 2001).

1.1.6 Ryanodine receptor

Mammalian RyR2 is a homotetramer which consists of four monomers. Each monomer has 6-10 transmembrane segments, a cytoplasmic domain functioning as scaffold for regulatory subunits and a channel domain at the carboxyl terminus (Liu et al. 2002). Four monomers are arranged as large transmembrane segments creating the channel pore (Leenhardt et al. 2012). The tetramer builds a macromolecular complex with numerous regulatory subunits such as calmodulin (CaM), FK506 binding protein known as FKBP12.6 or calstabin2, protein kinase A (PKA), Ca^{2+}/calmodulin–dependent kinase II (CaMKII), protein phosphatase 1 and 2A (PP1/PP2A), phosphodiesterase 4D3 (PDE4D3), junctin, triadin and calsequestrin (Wehrens and Marks 2004).

Three isoforms of the ryanodine receptor are known, which show a tissue-specific expression (Rossi and Sorrentino 2002). RyR1 is mainly expressed in skeletal muscles while RyR2 is mostly expressed in cardiac muscles (Marks et al. 1989; Nakai et al. 1990; Zorzato et al. 1990; Takeshima et al. 1995). RyR3 is expressed in the nervous system and at low levels in mammalian striated muscles (Hakamata et al. 1992; Ledbetter et al. 1994; Giannini et al. 1995).

RyR2 is one of the main important channels to regulate the Ca^{2+} homeostasis in heart muscle cells. The channel is localized in the sarcoplasmic reticulum (SR) and responsible for the regulation of intracellular Ca^{2+} concentration. The SR is an intracellular network functioning as Ca^{2+} storage. L-type Ca^{2+} channels located in the cell membrane regulate contraction of CMs. The L-type Ca^{2+} channel opens through depolarization of the cell membrane during an action potential (AP). The Ca^{2+} influx triggers opening of RyR2. The release of Ca^{2+} from the SR leads to increasing levels of Ca^{2+} in the cytoplasm. This mechanism is called calcium-induced calcium release (CICR) (Fabiato 1983).

Myocardial contraction is induced by high intracellular Ca^{2+} concentrations. Most of the Ca^{2+} surplus is assimilated by the SR Ca^{2+} adenosine triphosphatase (SERCA) into the SR. The remaining Ca^{2+} is ejected from the cell by the Na^{+}/ Ca^{2+} exchanger (NCX) to balance the Ca^{2+} entered with the Ca^{2+} influx (I_{Ca}). The Ca^{2+} handling is crucial for the contraction of cardiac myocytes and its dysfunctions can lead to severe cardiac diseases such as CPVT.

1.1.7 Pathophysiology of CPVT

At least 50% of CPVT patients carry mutations in the *RyR2* gene. The majority of the mutations are single base pair (bp) polymorphisms. The mutations are classified in clusters in four different hot spot regions of the coding sequence: Domain I (a.a. 77-466), II (a.a. 2246-2534), III (a.a. 3778-4201) and IV (a.a. 4497-4959) (Priori and Chen 2011, Marks et al. 2002). 10% of reported cases carry a causative RyR2 mutation, which is not located in these four domains. The channel function is depending on the domain-domain interaction. Defects in a certain domain can interrupt the intermolecular interaction of binding partners leading to different phenotypes of the disease.

The following three hypotheses describe the current stand of research for the pathophysiology of CPVT1.

Hypothesis I: The RyR2 mutation leads to an increased sensitivity to intraluminal Ca^{2+} and a reduced threshold for store overload-induced calcium release (SOICR) resulting in an earlier Ca^{2+} release from the SR during stimulation by catecholamine or stress. The large SR Ca^{2+} spillover can cause delayed after depolarization (DAD) and triggered arrhythmia. The increased SOICR is caused by increased sensitivity of RyR2 to luminal Ca^{2+} (Jiang et al. 2004) (Figure1).

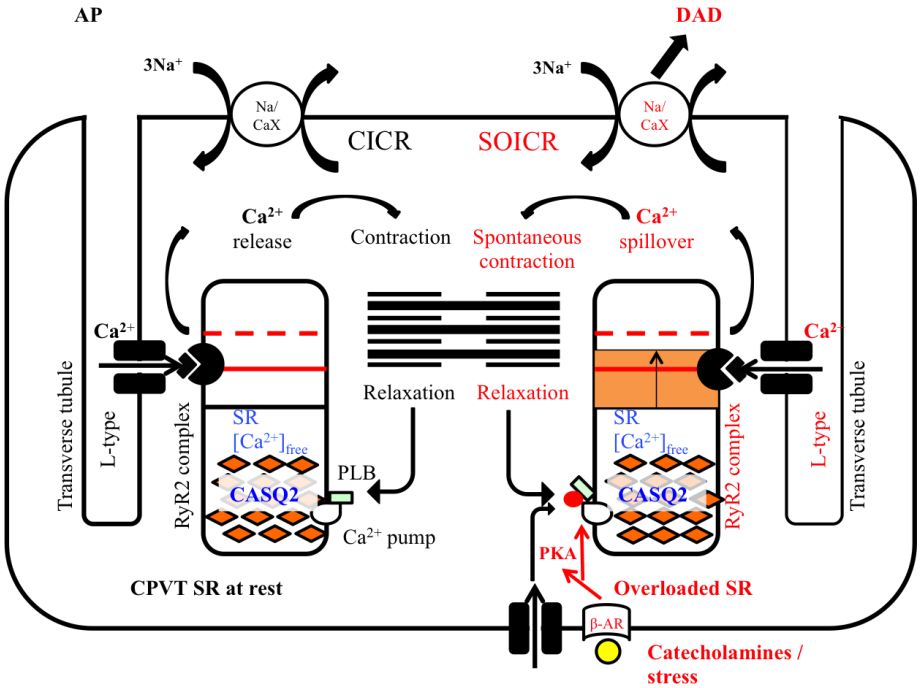

Figure 1: **The mechanisms of CICR and SOICR are schematically shown (modified according to Jiang et al. 2004).** CICR is induced by Ca^{2+} influx through the L-type channel opening when an AP occurs, which depolarizes the cell membrane at rest. The Ca^{2+} binds to RyR2. The binding causes an activation of RyR2, which leads to Ca^{2+} release

from the SR into the cytosol. The significant increase in cytosolic Ca^{2+} causes the activation of muscle contraction. During stress or the stimulation of the sarcolema by catecholamines, PKA gets activated and binds to phospholamban (PLB), a key negative regulator for SERCA2a activity. PLB phosphorylation by PKA releases its inhibition to SERCA2a activity, resulting in elevated SR Ca^{2+} uptake. The concentration of SR free Ca^{2+} gets increased and causes Ca^{2+} spillover from the SR through RyR2 into the cytosol. The threshold for the SOICR is decreased in CPVT patients by the RyR2 mutation. This leads to earlier Ca^{2+} spillover in CPVT patients causing DADs and triggering arrhythmia.

Hypothesis II: RyR2 mutation causes disruption of FKBP12.6 binding to RyR2. FKBP12.6 binding stabilizes the closed state of RyR2 during diastole. The binding affinity of FKBP12.6 for RyR2 is reduced by the mutation of the RyR2 protein. This leads to abnormal Ca^{2+} leak from the SR, especially during diastole under basal and exhibited conditions by PKA phosphorylation of RyR2 (Figure 2).

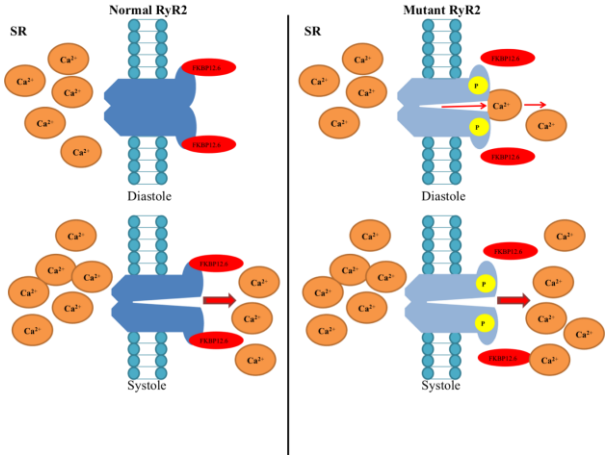

Figure 2: **Schema of reduced binding affinity of FKBP12.6 for mutant RyR2 (modified according to Liu et al. 2009).** The binding affinity of FKBP12.6 for RyR2 is reduced by RyR2 mutation causing the destabilization of the closed state of RyR2 in CPVT patients compared to normal RyR2 and phosphorylation of RyR2 by PKA induced through stress or catecholamines results in the dissociation of FKBP12.6 from RyR2. These lead to abnormal Ca^{2+} leak from the SR during diastole. .

Hypothesis III: RyR2 mutation causes disruption of domain-domain interactions. The interaction between the N-terminal and the central domain is disrupted through the mutated RyR2 protein (Oda et al. 2005; Dobrev et al. 2012). It causes a destabilized closed state of RyR2 especially under conditions of stress or the impact of catecholamines because the function of an on/off switch of the interaction between the domains is disrupted. This leads to an increase in the RyR2 sensitivity to cytoplasmic Ca^{2+} thereby causing diastolic Ca^{2+} leak which induces DADs and arrhythmias (Laver et al. 2007) (Figure 3).

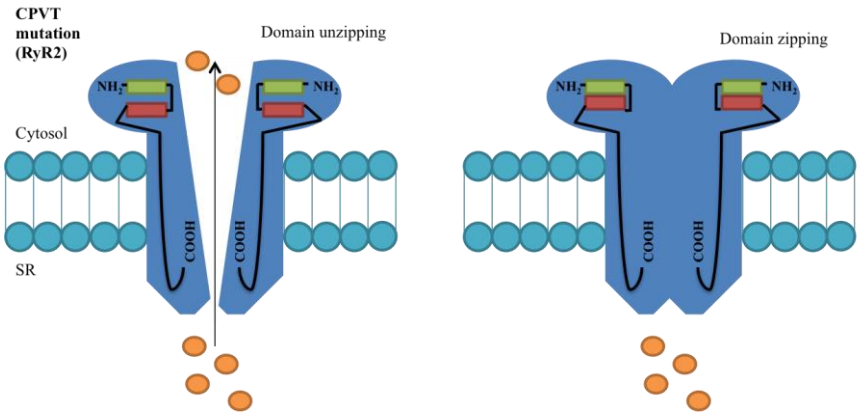

Figure 3: **Scheme of disrupted domain-domain interaction of mutant RyR2 (modified according to Dobrev et al. 2012).** Besides the FKBP12.6 binding affinity, a proper interaction between the amino terminal domain (green) and a central domain (red) of RyR2 is necessary for a normal function of RyR2. The domain interaction functions as an on/off switch between open and closed states of the channel. CPVT causes a domain unzipping, destabilizing the closed state of RyR2. A diastolic Ca^{2+} leak from the SR leads to DADs.

For a better understanding of the pathophysiology, iPSC models enable the possibility to examine CPVT patient-derived CMs *in vitro* to prove and develop theoretical concepts. Proof of concept offers the opportunity to find new therapy targets by the understanding of the different pathophysiology hypothesis and molecular pathways.

1.2 Induced pluripotent stem cells

In 2006, Takahashi and Yamanaka published their astonishing paper about reprogramming mouse embryonic or adult fibroblasts to iPSCs by introducing four transcription factors, octamer-binding transcription factor (Oct)3/4, sex determining region Y-box 2 (Sox2), cellular-Myc (c-Myc) and Kruppel-like factor 4 (Klf4). These cells showed the morphology and growth potential of embryonic stem cells (ESCs) and expressed ESC-specific marker genes (Takahashi and Yamanaka 2006). The same group created the first human iPSC (hiPSC) line with the same transcription factors (Takahashi et al. 2007).
Yu and her group from James A. Thomson's lab used a different gene combination: *OCT4*, *SOX2*, *NANOG* and *LIN28* (Yu et al. 2007).

To avoid destroying functional genes or activating oncogenes, the Sendai virus (SeV), a ribonucleic acid (RNA) virus, was used instead of the former method using lentivirus insertion containing the four transcription factors. The SeV has a completely RNA-based reproductive cycle (Fusaki et al. 2009).

Synthetically modified messenger RNA (mRNA) can also be used to generate RNA-induced pluripotent stem cells as well (Warren et al. 2010).
The biggest advantage of DNA-free methods is the prevention of uncontrollable insertions of transcription factors in the cell and viral integration inside the chromosomes leading to unwanted mutagenesis.

1.2.1 Differentiation to CMs

Patient-specific CMs are the foundation for CPVT disease models. The discovery of Takahashi and Yamaka to reprogram somatic cells to iPSCs was the main step for the establishment of patient-specific disease models. The knowledge about cardiogenesis enables the opportunity to differentiate iPSCs to CMs. By this way, the CMs have the same genetic information and characteristics like the patients *in vivo* tissue.
The differentiation is based on modulating the embryonic developmental signals controlling mesoderm induction like activin/NODAL, bone morphogenetic protein (BMP) signaling, Wnt and fibroblast growth factor (FGF) and inhibition of Wnt, BMP and TFGβ pathways for cardiac specification (Laflamme et al. 2007; Burridge et al. 2011; Kattman et al. 2011; Willems et al. 2012; Burridge et al. 2014).
The modulation of the Wnt pathway during cardiogenesis is crucial for the CM differentiation. By temporary modulation of the canonical Wnt/β-Catenin-pathway with the use of small molecules *in vitro* differentiation of iPSCs to CMs could be shown (Lian et al. 2012) and adapt to cardiac disease modeling. The Wnt pathway is biphasic activated and inactivated during cardiogenesis (Naito et al. 2006). Adapted from the physiological cardiogenesis Wnt pathway activation is induced by inhibiting glycogen synthase kinase 3 (GSK3) with CHIR99021 (CHIR) for the first two days of *in vitro* differentiation. BMP signaling is important in the late phase of iPSC differentiation to CMs (Monzen et al. 1999). BMP signaling regulates positively the cardiogenesis (Schultheiss et al. 1997). Especially BMP2/4 are expressed in the late phase of iPSC differentiation into CMs. Wnt/β-catenin signaling suppresses the expression of BMP2/4. To mimic the physiological settings during *in vitro* iPSC differentiation to CMs, the application of small molecules like IWP2 inhibits Wnt/β-catenin signaling to induce a high expression of BMP2/4.
The use of small molecules and growth factors raises the high amount and purity of *in vitro* generated CMs.

1.3 Disease modeling

The iPSC technology offers the possibility to generate patient-specific *in vitro* disease models, which help to understand molecular mechanisms of diseases. It also offers the possibility for drug screening and discovery as well as toxicity tests to develop new drugs. Patient-specific iPSCs enable the research on human disease models, which could not be recapitulated in small animal models. The genome of the iPSC derived disease models is the same to the patient, which is a big advantage in comparison to animal disease models (Kim et al. 2013).

Additionally, gene editing in iPSCs provides the opportunity to achieve specific corrections of mutations or to create gene knockout cell lines to prove the relation of genetic mutations and the correlating phenotype for a better understanding of the genetic and disease background (Colman and Dreesen 2009).

Another big field is the iPSC-based cell therapy like the transfer of *in vitro* specialized cells back to the patient, which is similar to autologous tissue transplantation to avoid immune suppression therapy. A Japanese group transplanted graft sheets with retinal pigment epithelial cells derived from patient-specific iPSCs to patients with macular degeneration. The outcome of the surgery one year after transplantation was significant and the sight of the patients was improved (Mandai et al. 2017). Adaptive scenarios are in the experimental phase like cardiac muscle patches and neuronal cell transplantation in patients with spinal cord lesions (Sugiura et al. 2016; Assinck et al. 2017).

To improve the medical treatment, disease modeling is a useful tool. A future perspective is an *in vitro* test with specific drugs for each patient, which could offer a tailor-made medication to develop a personalized medicine (Mathur et al. 2015). The *in vitro* tests enable the check for patient-specific drug metabolism and for compatibility of drugs. This can be done theoretically for each type of tissue derived from patient-specific iPSCs (Figure 4).

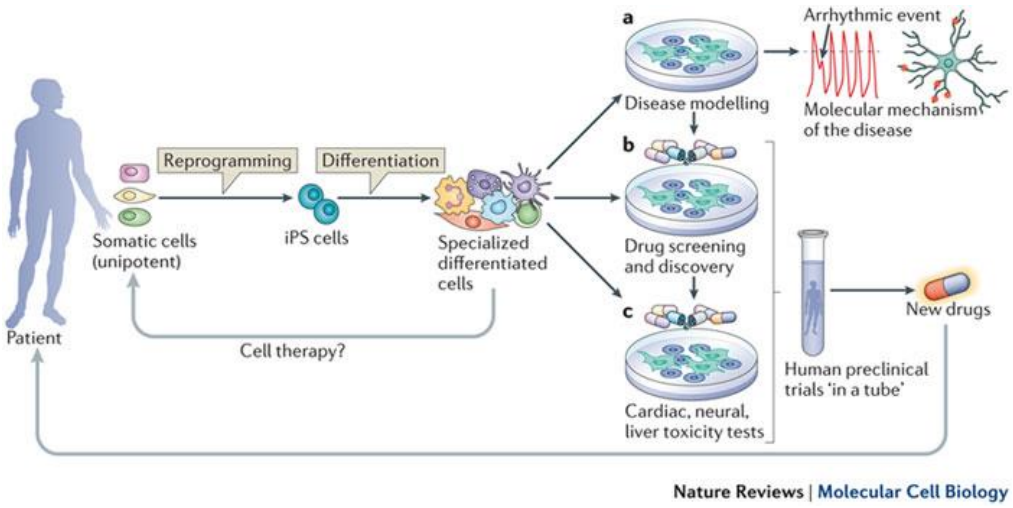

Figure 4: **Scheme of the possibilities of disease modeling using patient-specific iPSCs (Bellin et al. 2012).** Somatic cells can be reprogrammed to iPSCs and differentiated to specialized cells *in vitro*. There are different kinds of application for the *in vitro* differentiated cells. The cells can be used for cell therapy. (A) IPSCs can be used for disease modeling for a better understanding of molecular pathomechanisms. (B) Drug screening can be performed with patient-specific cells for a better determination of the effects to optimize the therapy and to develop new drugs. (C) Toxicity tests can be done. Cardiac, neural and liver toxicity tests can be performed *in vitro* to estimate the patient-specific cellular toxic reasons. Drug screening and toxicity tests represent almost a human preclinical trial in a tube. This can lead to a simplification of the drug discovery process. Reprinted by permission from Macmillan Publishers Ltd: Nature Reviews Molecular Cell Biology (Bellin et al. 2012), copyright (2012). License number 4179481218125

1.3.1 Disease modeling applied to CPVT

Modeling CPVT via iPSCs helps to understand the molecular mechanisms of the disease. Recent studies based on generated iPSC-CMs from different CPVT patients with different mutations in corresponding genes showed the typical arrhythmogenic potential of CPVT iPSC-CMs compared to control iPSC-CMs. For example, Itzhaki's group generated iPSC-CMs containing a heterozygous mutation in RyR2 (p.M4109R), Fatima's group a heterozygous mutation in RyR2 (p.F2483I) and Novak's group an autosomal recessive mutation in CASQ2 (p.D307H) (Fatima et al. 2011; Novak et al. 2012). The groups demonstrated almost similar results. There were no differences in baseline AP properties, but huge differences of the arrhythmogenic potential between control iPSC-CMs and CPVT iPSC-CMs (Itzhaki et al. 2012).

Chemicals like forskolin, an adenylate cyclase activator, or isoproterenol, a catecholamine, were used to stimulate CMs. The stimulation caused a significant higher development of DADs in CPVT iPSC-CMs compared to control iPSC-CMs. In the next step, thapsigargin was used to block SERCA and an elimination of DADs in CPVT iPSC-CMs was shown

(Itzhaki et al. 2012). Based on this, the hypothesis was confirmed that the depletion of intracellular Ca^{2+} decreases the incidence of DADs in CPVT iPSC-CMs (Fatima et al. 2011; Itzhaki et al. 2012; Novak et al. 2012). In addition, Novak's group showed differences between intracellular Ca^{2+} abnormalities of CPVT1 and CPVT2 CMs and showed that both CPVT1 and CPVT2 iPSC-CMs are less mature compared to the control group (Novak et al. 2015).

One of the future targets would be the creation of an analogous stem cell model of CPVT like the Long QT models published by Bellin *et al* in 2013. A specific correction of the N996I *KCNH2* mutation in long-QT syndrome (LQTS) to elucidate the effect of the specific mutant allele and to act as a proof-of-principle for gene therapy was done (Bellin et al. 2013). The group showed that the c.A2987T *KCNH2* mutation is the primary cause of the LQTS phenotype. The same principle of investigation needs to be done with a CPVT model to understand the pathogenic mechanism underlying specific disease phenotypes.

1.3.2 CRISPR/Cas9 systems

CRISPR/Cas9 systems are genome engineering tools for precise targeting of deoxyribonucleic acid (DNA) regions (Jinek et al. 2012).

CRISPR systems were first discovered as an adaptive immune system in bacteria to fight against viral DNA, plasmids or foreign RNA (Garneau et al. 2010). It is able to destroy RNA and DNA if they get re-infected. Three types of CRISPR loci are known, which acquire spacers from foreign DNA or RNA elements (Barrangou and Marraffini 2014). During the process of CRISPR adaptation spacers get integrated into the bacterial genome usually in the CRISPR locus, which contains partially palindromic DNA repeats. The loci rotate with repeated elements called CRISPR elements. CRISPR repeat RNA (crRNA) is the result of transcription and processing of the loci information. The crRNA guides nucleases for sequence-specific cleavage of complementary sequences. The combination of adaption of foreign genetic material, biogenesis of crRNA and targeting foreign DNA leads to a CRISPR-based adaptive immune system (Grissa et al. 2007; Karginov and Hannon 2010).

The accurate targeting by type I and II CRISPR systems is supported by protospacers assisted by system-specific CRISPR motifs called protospacer adjacent motifs (PAM) (Deveau et al. 2008). These are sequences in exogenous nucleic acid elements corresponding to CRISPR spacers. PAMs are necessary to separate the foreign DNA from

the host genome (Yusa et al. 2011). Invading sequences carrying a PAM get targeted for destruction. The PAMs are usually 2 to 5 highly conserved nucleotides. The location of the PAM depends on the CRISPR system. In Type I systems it is located on the 5' end and in Type II systems mostly on the 3' end.

Type IIA CRISPR systems are usually adapted to genomic engineering tools. The advantage of type II systems is the smaller number of Cas proteins. A single Cas9 protein is responsible in type IIA systems adapted from Streptococcus pyogenes to form the CRISPR-ribonucleoprotein (RPN) complex and for DNA cleavage with the support of a recognition lobe and a nuclease lobe. Cas9 interacts with the RNA-DNA duplex, which is responsible for the specificity of the target sequence. To simplify the genomic engineering tool one single-chain hybrid RNA contains the features of the crRNA duplex and the transactivating RNA (tracrRNA) (Jinek et al. 2012). The PAM-proximal region is responsible for the high sequence specificity. Mismatches between the first 12 nucleotides of the guide RNA (gRNA) and the DNA target are not tolerated. The most common PAM-motif is 5' NGG 3' resulting from systems based on S. pyogenes.

CRISPR/Cas9 is a RNA-guided DNA endonuclease system. Cas9 is a CRISPR associated endonuclease which forms a complex with two RNA species. The two RNAs function as guide sequences, which lead the complex to form base pairs with the DNA target. The RNA complex contains a tracrRNA and a crRNA and is engineered as a single guide RNA (sgRNA) (Figure 5).

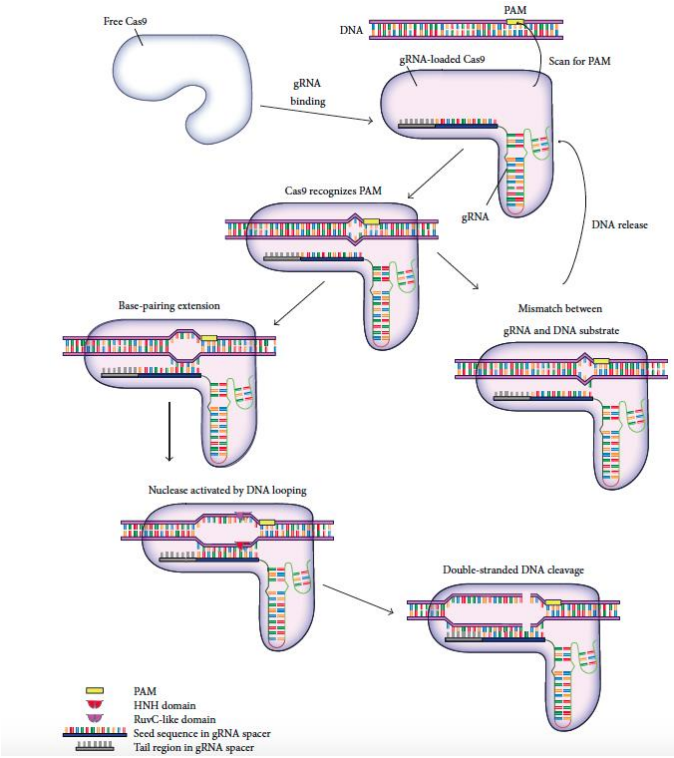

Figure 5: **Scheme of Cas9 endonuclease to trigger DNA cleavage (Shui et al. 2016).** The binding of Cas9 protein and the gRNA leads to a conformational change, which enables the gRNA to look for DNA substrate. The Recognition lobe (REC) of Cas9 scans for PAM in the genome. The PAM recognition induces a local unwinding of the dsDNA 5' to the PAM region. The unwound DNA is stabilized by protein ssDNA interaction. The base pairing between the ssDNA portion and the gRNA extends the ssDNA loop. If a critical loop size is reached Cas9 gets activated to make a double-strand cut. Cas9 remains bound to the DNA substrate. If base pairing between gRNA and ssDNA is blocked by mismatches the ssDNA loop collapses and leads to a release of the Cas9 protein. Reprinted by permission from Hindawi Publishers Ltd: Stem Cells International (Shui et al. 2016), copyright (2016). Creative Commons Attribution 4.0 International Public License

The attachment of the complex encourages Cas9 to introduce a site-specific DNA double-strand break (DSB) by two endonuclease domains. The HNH domain cleaves the complementary DNA strand thereby forming a duplex with the sgRNA. The RuvC-like domain cleaves the non-complementary DNA strand.

The design of the sgRNA is the most important part for a successful genomic manipulation. To target the wanted DNA sequence a PAM sequence on the DNA needs to be present and a 20 base pair (bp) sequence next to the wanted DSB is necessary for a successful binding of the CRISPR/Cas9 complex with the DNA. After introduction of the targeted DSB the DNA repair mechanisms are used for genetic manipulation. Gene knockouts can be forced by the introduction of small deletion or insertion mutations via non-homologous end joining (NHEJ). A targeted genetic correction or manipulation is

done by insertion of extra sequences via homology-directed repair (HDR) pathway (Sander and Joung 2014).

The CRISPR/Cas9 technology provides an affordable tool for genetic manipulation in comparison to zink-finger-nucleases (ZFN) or transcription activator-like effector nucleases (TALENs), which have significantly higher costs.

CRISPR/Cas9 offers the possibility for broad applications, for example as a tool for disease modeling in iPSCs and other model organisms. It is possible to correct point mutations to confirm if the mutation is responsible for the disease phenotype.

An American group established a disease model for cystic fibrosis. A genetic correction was done on iPSC level with CRISPR/Cas9. The group showed that the homozygous deletion of F508 in the cystic fibrosis transmembrane conductance regulator (CFTR) caused the disease phenotype. The corrected iPSCs were differentiated into mature airway epithelial cells and had a normal CFTR expression and function (Firth et al. 2015).

Another interesting field is the development of *in vitro* knockout models in hiPSCs for a better understanding of disease and cell adaption mechanisms (Chen et al. 2015).

1.4 Aims of this thesis

The thesis is part of a SFB 1002 project. The project aims to establish *in vitro* cell culture systems using patient-specific iPSCs as the foundation of disease models. IPSCs were generated from six CPVT patients with heterozygous missense mutations (R420W, A2254V, E4076K and H4742Y) in four different domains of the *RyR2* gene. The patient-specific iPSCs were generated from somatic cells. The generated hiPSCs were tested for pluripotency. Subsequently hiPSCs were differentiated to CMs and characterized. Cell biological, electrophysiological and phenotypic comparison of CMs was performed. The CMs were treated with different anti-arrhythmic drugs and new drugs were tested *in vitro*. This data was obtained in the Prof. Guan-Schmidt's lab and this thesis should amend the following aspects:

(1) In the first step of the thesis, iPSC lines generated from a CPVT patient carrying the RyR2 mutation **E4076K** are characterized for their pluripotency on mRNA and protein level using reverse transcription-polymerase chain reaction (RT-PCR), immunofluorescence staining and alkaline phosphatase staining.
(2) Patient-specific CPVT iPSCs carrying the mutation **A2254V** are used for genetic manipulations by CRISPR/Cas9.
The presumption is that the disease phenotype of CMs derived from CPVT-iPSCs is mutation-specific and not based on the genetic difference between CPVT patients and control individuals.
To prove this concept the CRISPR/Cas9 technology is used to insert a wild type gene sequence in the genome to correct the point mutation in RyR2 in the CPVT-iPSCs. In addition, the technology is used to create a RyR2 knockout model.
(3) The CRISPR/Cas9 targeted iPSCs are characterized for their pluripotency on gene expression level. The cells are differentiated to CMs and further investigation like electrophysiological analysis, Ca^{2+}-confocal analysis and molecular genetic investigations will be done. The data will be compared with the original data of the original CPVT-iPSC-CMs.

2 Materials and Methods

2.1 Materials

2.1.1 Devices

Table 1: **List of devices**

Device	Name	Supplier
Cell culture		
Centrifuge	Multifuge X3R Refrigerated Centrifuge	Thermo Fisher Scientific, Heraeus
Counting chamber	Neubauer improved	Marienfeld
Electroporator	Nucleofector™ 2b Device	Lonza
Fluorescence-activated cell sorting (FACS) cell sorter	BD FACSAria™ II sorter	BD Biosciences
Incubator	BBD6620	Heraeus Instruments
Laminar airflow cabinet	MSC-Advantage series	Thermo Fisher Scientific
Light-optical microscope	Axiovert 4CFL	Carl Zeiss
Pipette	Reference, Research plus	Eppendorf
Pipettor	Accu-jet pro	Brand
Molecular biology		
Electrophoresis	Horizontal electrophoresis system	Bio-Rad
Gel documentation	MultiImage Light Cabinet	Alpha Innotech Corporation
Photometer	Biophotometer Plus	Eppendorf
Power supply	Power Pac 3000	Bio-Rad
Tabletop centrifuge	Microcentrifuge	Eppendorf
Thermocycler	Thermocycler 48	SensoQuest

2.1.2 Consumables

Table 2: **List of consumables**

Item	Supplier	Item number
Cell culture		
0.5ml Eppendorf container	Eppendorf	# 4005233
0.5ml Eppendorf container (brown)	Eppendorf	# 0030120.155
1.5ml Eppendorf container	Eppendorf	# 4004646
2ml Eppendorf container	Eppendorf	# 4003961
15ml reaction tube	Eppendorf	# 62.554.002
50ml reaction tube	Eppendorf	# 62.547.004
24-Well cell culture plate	Eppendorf	# 0030722116
48-Well cell culture plate	Eppendorf	# 0030723112
96-Well cell culture plate	Eppendorf	# 0030730119
Cover glass, 25mm, round	Langenbrinck	# 01-0025/2
Object plate, SuperFrost Ultra Plus	Menzel	# J3800AMNZ
Steriflip 50ml	Merck Millipore	# SCGP00525
Sterifilter Millex-GS	Merck Millipore	# GLGS0250S
Object plate	Nunc	# 177380
Cover glass, 22mm, round	Omnilab	# 5161066
5ml Serological pipette	Sarstedt	# 86.1253.025
10ml Serological pipette	Sarstedt	# 86.1254.025
25ml Serological pipette	Sarstedt	# 86.1685.001
Cell scraper	Sarstedt	# 83.1830
0.1-10µl Pipette tip	Starlab	# S1111-3700 –c S1111-3700-c
10-100µl Pipette tip	Starlab	# S1112-1720 S1112-1720-c
100-1000µl Pipette tip	Starlab	# S1111-1706 S1111-1706-c

6cm Cell culture dish	Starlab	# CC7682-3359
6-Well cell culture plate	Thermo Fisher Scientific	# 140675
12-Well cell culture plate	Thermo Fisher Scientific	# 150628
Molecular biology		
Filtertips 0.1-10µl	Starlab	# S1120-3810 S1120-3810-c
Filtertips 10-100µl	Starlab	# S1122-1830 S1122-1830-c
Filtertips 100-1000µl	Starlab	# S1120-1840 S1120-1840-c
PVDF membrane Amersham Hybond P – Western blotting membranes	Sigma-Aldrich	#GE10600023
UVette®	Eppendorf	# 0030106318
Whatman gel blotting paper Grade GB003	Sigma-Aldrich	#WHA10426890

2.1.4 Chemicals, solutions and kits

Table 3: **List of chemicals, solutions and kits**

Components	Supplier	Item number
Cell culture		
0.05% Trypsin- EDTA	Life Technologies™	# 25300-054
0.25% Trypsin-EDTA	Life Technologies™	# 25200056
Albumin, human recombinant	Sigma-Aldrich	# A0237 / A9731
B27 Supplement with Insulin	Life Technologies™	# 17504044
CHIR99021	Millipore	# 361559
Collagenase B	Worthington Biochemical	# CLS-AFB
Collagenase IV	Worthington Biochemical	# CLS-4
Dimethylsulfoxide (DMSO)	Sigma-Aldrich	# D2650
DMEM/F-12	Life Technologies™	# 31331028
Dulbeccó's phosphate buffered saline (DPBS)	Life Technologies™	# 14190169
Dulbecco's modified Eagle medium (DMEM)	Life Technologies™	# 11960044
Essential 8 (E8) Basal Medium	Life Technologies™	# A1516901
Essential 8 Supplement	Life Technologies™	# A1517001
Ethanol absolute	Th. Geyer	# 1025490
Ethylenediaminetetraacetic acid (EDTA)	Carl Roth®	# 8040
Fetal Bovine Serum (FBS)	Sigma-Aldrich	# F7524
Gelatin	Sigma-Aldrich	# 48720
Geltrex (Growth Factor Reduced)	Life Technologies™	# A1413302
HEPES Buffer (pH 7.0-7.6)	Sigma-Aldrich	# H0887
Hydrochloric acid 37%	Merck	# 1025571
Iscove's modified Dulbecco's medium (IMDM)	Life Technologies™	# 12440053

IWP2	Millipore	# 681671
Knockout serum (K.O. Serum)	Life Technologies™	# 10828-028
L-Ascorbic-Acid 2-Phosphate	Sigma-Aldrich	# A8960
Methanol	J.T. Baker	# 8402
Monothioglycerol (MTG)	Sigma-Aldrich	# M6145-25ML
Non-essential Amino Acid (NEAA)	Gibco	# 11140035
Penicillin/Streptomycin (P/S)	Life Technologies™	# 15140122
Pro Survival Factor DDD00033325	Millipore	# 529659
RPMI 1640 with HEPES with GlutaMax	Life Technologies™	# 72400021
RPMI 1640 without HEPES without Glucose	Life Technologies™	# 11879020
Thiazovivin (TZV)	Millipore	# 420220
Versene Solution (0.48mM EDTA)	Life Technologies™	# 15040066
Molecular biology		
5x Green GoTaq® Reaction Buffer	Promega	# M791A
6X DNA Loading Dye	Thermo Fisher Scientific	# R0611
Agarose, peq Gold universal agarose	Peqlab	# 35-1020
Amaxa™ Human Stem Cell Nucleofector™ Kit 2 (25 RCT)	Lonza	# VPH-5022
Ammonium persulfate (APS)	Roth	#9178
Beta-Mercaptoethanol (β-ME)	Sigma-Aldrich	# M3148
cOmplete	Roche	#04693132001
Dithiothreitol (DTT)	Roth	#6908
dNTP Mix	Bioline	# BIO-39053
EndoFree Plasmid Maxi Kit (10)	Quiagen	# 12362
GeneRuler 100 bp Plus DNA Ladder	Thermo Fisher Scientific	# SM0241
Genomic Cleavage Detection Kit	GeneArt®	# A24372
GoTaq® DNA Polymerase	Promega	# M300B
GoTaq® G2 DNA Polymerase	Promega	# M7841

IGEPAL CA-630	Sigma-Aldrich	#I3021
Isopropanol	Merck Millipore	#109634
Loading buffer	Applichem	# A3481
Magnesium chloride, 25mM	Applichem	# A1036
Maxwell® 16 Cell DNA Purification Kit	Promega	# AS1020
Midori Green Advance (1 ml)	Nippon Genetics Europe GmbH	# MG04
MuLV Reverse transcriptase (50 U/µl)	Life Technologies™	# N8080018
Non-fat dry milk	Roth	#T145
Nuclease free water	Life Technologies™	# 1408217
Oligo $d(T)_{16}$ Primer	Life Technologies™	# N8080128
PCR Buffer II 10x	Life Technologies™	# N8080006
PhosStop	Roche	#04906837001
QIAquick Gel Extraction Kit (50)	Quiagen	# 28704
QuickExtract™ DNA Extraction Solution 1.0	BuccalAmp™	# QE09050
RNase Inhibitor	Life Technologies™	# N8080018
Rotiphorese gel 30	Roth	#3029
Sodium chloride	Roth	#9265.1
Sodium dodecyl sulfate (SDS)	Roth	#2326
SpeI-HF® restriction enzyme	New England BioLabs®	# R3133S
SV Total RNA isolations kit	Promega	# Z3100
SYBR® Green PCR master mix	Life Technologies™	# 4309155
Taq DNA Polymerase with ThermoPol® Buffer	New England Biolabs® Inc.	# M0267S
Tetramethylethylenediamine (TEMED)	Roth	#2367
ThermoPol® Reaction Buffer	New England Biolabs® Inc.	# B9004S
TransIT®-293 Transfection Reagent	Mirus	# MIR 2700
Tris	Roth	#5429
Tris buffer pure	Roth	# 1022840

UltraPure™ DEPC-Treated Water	Life Technologies™	# 750024
Immunostaining and alkaline phosphatase (ALP) staining		
4',6-Diamidin-2-phylindol (DAPI)	Sigma-Aldrich	# D9542
Alkaline phosphatase, Human Kit 86R	Sigma-Aldrich	# 1025719
Bovine serum albumin (BSA), 7.5%, pH 7.0	Sigma-Aldrich	# A2153
DAPI Fluoromount-G®	Southern Biotech	0100-20
Giemsa solution	Sigma-Aldrich	# GS500
Paraformaldehyde (PFA)	Sigma-Aldrich	# 158127
Triton X-100	Sigma-Aldrich	# 9002-93-1
Vectashield Mounting medium	Vector Laborites	# H-1000

2.1.5

2.1.6 Supplements, buffers and solutions

0.25% / 0.05% Trypsin-EDTA

Defreeze the new bottle and aliquot 6ml and freeze again; store at -20°C

β-Mercaptoethanol [100x]

Dilute 7µl β-ME in 10ml DPBS; store at 4°C, and prepare fresh weekly

Basic fibroblast growth factor (bFGF)

Stock solution: 100ng/µl

100µg bFGF diluted in 1ml Tris (5mM); stored at -20°C

Working solution: 5ng/µl

Stock solution diluted 1:20 in 0.1% BSA; stored at 4°C

BSA [1%]
Dilute 1ml BSA (7.5%) in 6.5ml DPBS; store at 4°C

Cell lysis buffer
20mM Tris-HCl pH 7.4, 200mM NaCl, 20mM NaF, 1% IGEPAL Ca-630, 1mM Na_3VO_4, 1mM DTT, 1 tablet of PhosStop for 10ml or 1 tablet cOmplete (EDTA-free) for 20ml; freshly prepared

CHIR99021 [12mM]
Dissolve 5mg in 0.894ml DMSO; store at -80°C

Collagenase B (400 units/ml), IV (400 units/ml)
Dissolve 400 units in 1ml RPMI 1640; store at 4°C

FBS
Heat inactivated for 30min at 56°C
Enhanced luminescence (ECL) solution
Mix 4ml of Solution SA with 400µl of Solution SB and add 1.2µl 35% H_2O_2

Gelatin [0.1%]
Dissolve 5g gelatin in 5l distilled water; autoclave

Geltrex™
Aliquot 2mg and store at -80°C; dilute directly before use in 12ml cold DMEM/F12

IWP2 [5mM]
Dissolve 10mg in 4.28ml DMSO and incubate for 10 min by 37°C; store at -20°C

MTG [150mM]
Dilute 13µl in 1ml IMDM and filtrate sterile, prepare fresh daily

Non-fat dry milk (5% w/v)
Dissolve 5g non-fat dry milk in 100ml 1 x TBS-T buffer

PFA [4%]
Dissolve 1g paraformaldehyde in 25ml DPBS; store at -80°C

SDS-loading buffer (10% w/v)
Dissolve 10g SDS in 100ml H_20

5x TBE buffer
54g Tris, 27.5g boric acid, 20ml 0.5M EDTA (pH8.0) and 1l distilled water
Triton-X 100 [0.1%]
Dilute 10µl Triton-X 100 in 990µl DPBS, dilute 1:10 in DPBS; store at 4°C

Tyrode's solution
NaCl 140 mM, KCl 5.4 mM, CaCl2 1.8 mM, MgCl2 1 mM, HEPES 10 mM, Glucose 10 mM, pH 7.4

TZV [2mM]
Dissolve 10mg in 6.8ml DMSO; store at -20°C

2.1.7 Cell culture medium

After FACS – E8 Medium

40ml	Conditioned Essential 8 Medium
40ml	Essential 8 Medium
800µl	P/S
200µl	bFGF 10ng/µl
80µl	TZV 2mM

B27 medium

500 ml RPMI 1640 with HEPES
1x B27 supplement with insulin

Cardio Culture Medium (storage up to 1 month at 4°C)

500ml	RPMI 1640 with HEPES with GlutaMax
10ml	B27 Supplement with Insulin (thaw at 4°C)

Cardio Differentiation Medium (storage for up to 1 month at 4 °C)

500ml	RPMI 1640 with HEPES with GlutaMax
250mg	Albumin, human recombinant
100mg	L-Ascorbic Acid 2-Phosphate, filter to sterilize

Cardio Digestion Medium (storage for up to 2 weeks at 4°C)

80ml	Cardio Culture Medium
20ml	Fetal Bovine Serum
100µl	TZV (2µM final)

Cardio Selection Medium

500ml	RPMI 1640-HEPES-GlutaMax
2ml	Lactate/HEPES [1M]
250mg	Albumin, human recombinant
100mg	L-Ascorbic Acid 2-Phosphate

Cryopreservation Medium feeder free 2x (storage for up to 1 week at 4 °C)

2ml	DMSO
8ml	Essential 8 Medium
20µl	2mM TZV

DMEM/F-12 modified

Sodium pyruvate, GlutaMax, Glucose 4.5g/l supplemented with:

10%	FBS
1%	P/S

Essential 8 Medium: storage up to 2 weeks at 4 °C

500ml	Essential 8 Basal Medium
10ml	Essential 8 Supplement (thaw at 4 °C)

hES Medium

78ml	DMEM/F-12
20ml	Knockout serum replacement
1ml	NEAA
1ml	β-Mercaptoethanol (100x)
10ng/ml	bFGF (freshly added each day)

Iscove-Differentiation Medium

500ml	IMDM
127ml	FBS, inactivated
6.4ml	NEAA
450µl	MTG 150mM

Lysogeny broth (LB)-Medium

5g	Yeast extract
10g	NaCl
10g	Trypton
1000ml	ddH_2O pH 7.0, autoclaved

for agar plates: 1.5% agar was added

Pre-FACS Medium:

25ml	Phenol free E8 + supplement
25µl	Thiazovivin (2mM)
250µl	P/S
1.5%	Fetal Bovine Serum
50µl	bFGF (working concentration: 10ng/ml)

2.1.8 Antibodies for immunofluorescence analysis

Table 4: **List of primary antibodies for immunofluorescence analysis**

Primary Antibody		**Dilution**		**Supplier**
Pluripotency marker				
SOX2	(mouse)	1:50	(+ 0.1% Triton-X)	R&D
OCT4	(goat)	1:40	(+ 0.1% Triton-X)	R&D
LIN28	(goat)	1:300	(+ 0.1% Triton-X)	R&D
NANOG	(goat)	1:200	(+ 0.1% Triton-X)	R&D
Tumour-related antigen-1-60 (TRA-1-60)	(mouse)	1:200		Abcam
Stage-specific embryonic antigen-4 (SSEA4)	(mouse)	1:200		Abcam
Germ layer marker				
Alpha-1-Fetoprotein (AFP)	(rabbit)	1:100		DAKO
β3-Tubulin	(mouse)	1:2000		Covance
Alpha-smooth muscle actin (α-SMA)	(mouse)	1:3000		Sigma-Aldrich
Cardiac marker				
α-Actinin	(mouse)	1:1000		Sigma-Aldrich
MLC2A	(rabbit)	1:200	(+ 0.1% Triton-X)	Protein tech

MLC2V	(mouse)	1:200	(+ 0.1% Triton-X)	Synaptic Systems
CX43 (connexin 43)	(rabbit)	1:1000		Abcam
RyR2	(mouse)	1:200		Pierce antibodies

Table 5: **List of secondary antibodies for immunofluorescence analysis**

Secondary Antibody		**Dilution**	**Supplier**
Alexa488	(donkey α-mouse)	1:1000	Life Technologies
FITC	(donkey α-rabbit)	1:200	Jackson ImmunoResearch
FITC	(goat α-mouse)	1:100	Jackson ImmunoResearch
Alexa555	(donkey α-goat)	1:1000	Life Technologies™
Cy3	(goat α-mouse)	1:300	Jackson ImmunoResearch
Cy3	(donkey α-goat)	1:500	Jackson ImmunoResearch
Alexa647	(donkey α-mouse)	1:300	Life Technologies™
Cy5	(donkey α-mouse)	1:300	Jackson ImmunoResearch

2.1.9 Primer sequences for RT-PCR

Table 6: **List of primer sequences for RT-PCR**

Gene	Primer	Sequence (5'-3')	Fragment [bp]
Pluripotency marker			
FOXD3	hu_FOXD3_for	GTGAAGCCGCCTTACTCGTAC	353
	hu_FOXD3_rev	CCGAAGCTCTGCATCATGAG	
GAPDH	hu_GAPDH_for	AGAGGCAGGGATGATGTTCT	258
	hu_GAPDH_rev	TCTGCTGATGCCCCCATGTT	
GDF3	hu_GDF3_for	TTCGCTTTCTCCCAGACCAAGGTTTC	311
	hu_GDF3_rev	TACATCCAGCAGGTTGAAGTGAACAGCACC	
LIN28	hu_LIN28_for	AGTAAGCTGCACATGGAAGG	410
	hu_LIN28_rev	ATTGTGGCTCAATTCTGTGC	
NANOG	hu_NANOG_for	AGTCCCAAAGGCAAACAACCCACTTC	164
	hu_NANOG_rev	ATCTGCTGGAGGCTGAGGTATTTCTGTCTC	
OCT4	hu_OCT4_for	AGTTTGTGCCAGGGTTTTTG	113
	hu_OCT4_rev	ACTTCACCTTCCCTCCAACC	
SOX2	hu_SOX2_for	ATGCACCGCTACGACGTGA	437
	hu_SOX2_rev	CTTTTGCACCCCTCCCATTT	
Germ layer marker			
hAFP	hu_AFP_for	ACTCCAGTAAACCCTGGTGTTG	255
	hu_AFP_rev	GAAATCTGCAATGACAGCCTCA	

hALB (human albumin)	hu_ALB_for	CCTTTGGCACAATGAAGTGGGTAACC	355
	hu_ALB_rev	CAGCAGTCAGCCATTTCACCATAG	
hα-MHC	hu_α-MHC_for	GTCATTGCTGAAACCGAGAATG	413
	hu_α-MHC_rev	GCAAAGTACTGGATGACACGCT	
hcTNT	hu_cTNT_for	GACAGAGCGGAAAAGTGGGA	305
	hu_cTNT_rev	TGAAGGAGGCCAGGCTCTAT	
hSYP	hu_SYP_for	TGCAGAACAAGTACCGAGAG	297
	hu_SYP_rev	CTGTCTCCTTAAACACGAACC	
Human Tyrosine hydroxylase (TH)	hu_TH_for	GCGGTTCATTGGGCGCAGG	215
	hu_TH_rev	CAAACACCTTCACAGCTCG	
RyR2_MUT_B marker			
CRISPR_RyR2_MUT_B	hu_CRISPR_RyR2_MUT_B_for	ACACTATGGATGGTGTTTAGAA	560
	hu_CRISPR_RyR2_MUT_B_rev	AGAACGTTGGTTCTCCTTCC	

2.1.10 Program parameters for RT-PCR

Table 7: **List of program parameters for RT-PCR**

Gene	Annealing [°C]	Cycles	Gene	Annealing [°C]	Cycles
Pluripotency marker					
FOXD3	61	38	NANOG	64	36
GAPDH	60	30	OCT4	54	34
GDF3	54	34	SOX2	60	30
LIN28	52	38			
Germ layer marker					
hAFP	58	32	hα-MHC	60	40
hALB	62	35	hSYP	60	37
hcTNT	56	35	hTH	60	35
hGAPDH	55	34			

2.1.11 Program parameters for DNA-PCR

Table 8: **List of program parameters for DNA-PCR**

Gene	**Annealing [°C]**	**Cycles**
RYR_2_MUT_B	59	35

2.1.12 Cell lines

Table 9: **List of cell lines used in the study**

Name	**Cells of Origin**	**Mutation**
Human induced pluripotent stem cell lines (generated in Prof. Dr .rer. nat. Guan-Schmidt's laboratory)		
isCPVTb1.6	Skin fibroblasts	A2254V
isCPVTc2.2	Skin fibroblasts	E4076K
isCPVTc2.3	Skin fibroblasts	E4076K
HEK-cell line		
Human embryonic kidney 293T cells (HEK293T): (University Medical Center Göttingen)		

2.1.13 Bacterial material

Table 10: **List of bacterial material**

E.coli		
Top10	F– *mcr*A Δ(*mrr-hsd*RMS-*mcr*BC) Φ80*lac*ZΔM15 Δ*lac*X74 *rec*A1 *ara*D139 Δ(*ara leu*) 7697 *gal*U *gal*K *rps*L (StrR) *end*A1 *nup*G	Kindly provided by the Department of Immunology, University Medical Center Göttingen, Thermo Fisher Scientific

2.2 Methods

All cells were cultivated under humidified air conditions with 5% carbon dioxide (CO_2) and 20% oxygen (O_2) at 37°C. All working steps were performed under sterile conditions.
Human iPSCs provided for this project were reprogrammed with the overexpression of the four Yamanaka factors (OCT4, SOX2, KLF4, c-MYC) by use of the CytoTune-iPS 2.0 Sendai reprogramming kit (Henze 2016).

2.2.1 Cell culture

2.2.1.1 Cultivation of iPSCs on feeder layer

IPSCs were cultivated on mitomycin C-inactivated mouse embryonic fibroblasts (MEFs) as feeder layers to keep them in pluripotent state. The medium was changed daily with hES+bFGF.
The cultures were examined before passaging. Differentiated areas were removed. The removal was done by suction, picking or manual passaging.
Collagenase IV was used for passaging. Collagenase IV was diluted to 200 units/ml working concentration with DMEM/F-12 and warmed to room temperature (RT). The cells were washed once with 3ml DMEM/F-12 and the supernatant was aspirated. The cells were incubated in a 6cm dish with 2.5ml Collagenase IV for 5-7 minutes at 37°C. The Collagenase IV was aspirated and the cells were rinsed once with 3ml DMEM/F-12. 3ml hES+bFGF medium was added to the cells. With the help of a cell scraper grid-like cuts across the cell layer were done. The cells were gently scraped and split onto MEFs. The ratio was depending on the confluence of the cell layer before, e.g. 80% confluence was split in a 1:4 ratio. Each 6cm dish was filled up to a total of 3ml hES+bFGF medium. The plates were labeled. The medium got changed daily.

2.2.1.2 Cultivation of iPSCs in feeder-free culture

To standardize several steps a lab intern protocol was used according to the publications of the working groups of Beers and Chen (Chen et al. 2011; Beers et al. 2012).
The human iPSCs were cultivated on 6-well culture dishes coated with Geltrex™ in Essential 8™ medium as monolayer culture. The medium was changed daily.
At 90% confluence the cells were passaged onto new culture dishes. The cells were covered with Versene Solution (EDTA solution). The supernatant was directly aspirated. The wash step was repeated. The cells were covered with Versene solution and incubated around 2-5

min depending on the cell colony size. The Versene solution promotes the detachment of the cells. EDTA is a complex binder, which binds bivalent magnesium and calcium ions. These ions stabilize the cell binding membrane proteins. The supernatant was aspirated. The cells were washed to detach with 1ml Essential 8™ Medium. The cells were transferred in Essential 8™ Medium with 2µM TZV in cell culture plate coated with Geltrex™. TZV is a selective inhibitor of the Serine/Threonine-Kinase and benefits the survival of the stem cells after passaging. The cells were passaged each 5-7 days depending on the density.

2.2.1.3 Cryopreservation on Geltrex™

Essential 8™ Medium, Cryopreservation Medium and Versene Solution were warmed to RT. The medium of hiPSCs at confluence around 70-90% was aspirated. The cells were covered with Versene solution. The Versene solution was directly aspirated. After repeating the wash step, cells were covered with Versene solution and incubated for 2-5min at RT. The supernatant was carefully removed and 1ml per 6-well of Essential 8™ Medium was rapidly added to wash the cells. 1ml of Cryopreservation Medium was given dropwise to each well. The cell suspension was carefully mixed and 0.5-1ml of the cell suspension was transferred to a labeled cryo tube. The cells were frozen at -80°C in an isopropanol freezing container for at least 2 hours and transferred to liquid nitrogen for long-term storage.

2.2.1.4 Thawing of hiPSCs on Geltrex™

The culture dishes coated with Geltrex™ and Essential 8™ Medium were warmed to RT. The solution was aspirated and Essential 8™ Medium per 6-well was added. The cryo tube was taken directly in a 37°C water bath and observed until only a small ice particle was floating.

The cells were transferred dropwise into a 15ml Falcon tube with 10ml Essential™ Medium. The cells were mixed carefully and centrifuged at 200 x g for 5 min. The supernatant was aspirated. The pellet was resuspended in Essential 8™ Medium and plated on plates coated with Geltrex™. 1µl of 2mM TZV per ml medium was added on the first day.

The medium was not changed on the second day. 1ml of fresh Essential 8™ Medium was added to the well and 1µl of 2mM TZV per ml medium was added.

2.2.1.5 Nucleofection of hiPSCs cultured on Geltrex™

The Human Stem Cell Nucleofector Kit 2 was used to transfer the CRISPR – plasmid into hiPSCs. The method is based on electroporation. Human stem cells are sensitive to the nucleofection treatment. This requires precise and fast working procedures.

The cells were cultivated to a confluence around 90%. For each nucleofection, cells in two 6-wells were needed with a total amount of 4 million.

The cells were pretreated with 1µl/ml 2mM TZV. Geltrex™ coated plates, E8 medium and Versene solution were warmed to RT. 82µl human stem cell nucleofector solution (Kit 2) and 18µl supplement 1 were mixed in a 1.5ml tube and warmed to 37°C. The Geltrex™ solution was aspirated and E8 medium (3ml per 6-well; 2ml per 12-well) was added onto the new plates. 1µl/ml 2mM TZV and 1x P/S were added on the first day.

The medium of the hiPSCs was aspirated and the cells were covered with Versene solution, which was directly aspirated without incubation. The wash step was repeated to remove Mg^{2+} and Ca^{2+}. The cells were covered with Versene solution for 4-6min with minimal movement. A longer incubation than at normal passaging was needed to obtain very small cell colonies or single cells. The solution was carefully aspirated and E8-medium was added rapidly. A 1000µl pipette was used to avoid excessive pipetting to keep the cells intact. The cell suspension was carefully mixed. The cells of both wells were collected in one 15ml Falcon tube filled with 3ml E8 medium. The cells were counted with a Thoma cell counting chamber under a light-microscope. 1.5-3 million cells were transferred in a 15ml Falcon tube and centrifuged for 3min at 200 x g. During centrifugation 4-5µg DNA (CRISPR-plasmid) and 0.6-1µl of the CRISPR-oligo were added to the prepared nucleofector mix.

The supernatant was aspirated and the cells were resuspended in the nucleofector mix. The cells were transferred to a nucleofector cuvette and the cuvette was closed with a cap. The sample had to cover the bottom of the cuvette without air bubbles. The cuvette was inserted into the nucleofector holder and program A-23 was used. The cells were diluted in 500µl E8 medium and were gently plated onto three 6-wells. Around 0.5-1 million cells per 6-well were added to the prepared plates. The plates were shacked back and forth and side to side and were incubated under standard conditions.

The medium was changed on the second day and 1µl/ml 2mM TZV was added. The cells had to regenerate for 1-2 days before selection.

2.2.1.6 FACS of hiPSCs

Pre-FACS and After-FACS medium was prepared (the mixtures are listed in 2.1.5) and warmed to 37°C. 96-well plates coated with Geltrex™ were warmed to 37°C. The old medium of nucleofected cells was aspirated and Versene solution was added and directly aspirated. The wash step was repeated. Afterwards Versene solution was added and incubated for 3-4 min. The Versene solution was aspirated and 300µl of Pre-FACS medium was added to each well (max. 4 wells). The cells were carefully resuspended and transferred to a common 15ml Falcon tube. A technician of the hematology and oncology department of the University of Goettingen did the FACS sorting. Cells with a GFP signal were sorted in a 15ml Falcon tube filled with 3ml After-FACS medium. The cell solution was carefully transferred to 96-well plates (10.000 cells per 96-well plate). The wells were filled up to ¾ with After-FACS medium. The cells were incubated under standard conditions. After 2 days half of the old medium was aspirated and After-FACS medium was added. The medium was changed every second day. The cells were passaged after two weeks to a 48-well plate, after 3 weeks to a 24-well plate, after 4 weeks to a 12-well plate and finally to a 6-well plate. The medium was changed after two weeks to E8 medium supplemented with 1µl/ml 2mM TZV. DNA was taken from the 12-well plates to do the first genetic analysis.

2.2.1.7 Mass culture for spontaneous differentiation of hiPSCs cultured on feeder layer

To confirm the potential for differentiation of hiPSCs in the three different germ layers the spontaneous differentiation was done. The iPSCs were cultured to a confluency of 90-100%. The medium was aspirated and the cells were washed once with 3ml DMEM basal medium. The cells were treated with 2.5ml 200 U/ml collagenase IV for 5 min at 37°C. The collagenase was removed and the cells were rinsed once with 3ml DMEM. 2.5ml hES+bFGF medium were added to each dish. The cells were scraped with a cell scraper in big clusters. The cells were resuspended and the clusters were transferred from two dishes to an uncoated 6cm petri dish. The embryonic bodies (EBs) were forming in suspension. After 24 hours the medium was changed to Iscove-Diff medium and was changed every 2 days until day 8. The medium change was done following a specific procedure: The EBs were collected in suspension and placed in a 15ml falcon for 5 min until the EBs were settled at the bottom of the tube. The supernatant was aspirated and fresh Iscove-Diff medium was added. The suspension was transferred to a new petri dish.

A 6cm dish for pellet collection, two 6cm dishes with 4 coverslips each for immunostaining at d8+5, d8+25 and one 24-well tissue culture plate for differentiation efficiency were coated with 0.1% gelatin and stored at 4°C overnight. The EBs were prepared for pellet collection at day 8. The medium containing the EBs was collected in a 15ml Falcon tube and centrifuged at 200 x g for 3 min. The supernatant was aspirated. The pellet was resuspended in 1ml PBS. The suspension was transferred to a 1.5ml Epi and centrifuged at 13.000 rounds per minute (rpm) for 1min. The supernatant was aspirated and the pellet was snap-frozen in liquid nitrogen. The samples were stored at -80°C for extended periods. Two samples were taken. The rest of the EBs were used for plating. The gelatin was removed. 30 EBs in 4ml Iscove-Diff medium were plated on a 6cm dish. One EB was plated in each well with 500µl Iscove-Diff medium of the 24-well plate. The EBs were cultured in Iscove-Diff medium for another 25 days. The medium was changed every 2-3 days. On day d8+25 two pellets were taken. The medium was aspirated from the dish and washed once with 3ml PBS. The PBS was aspirated and 1ml PBS was added to the dish. The cells were carefully scraped in the PBS suspension and transferred to a 1.5ml Epi. The suspension was centrifuged at 13.000 rpm for 1 min. The supernatant was aspirated and snap-frozen in liquid nitrogen. The samples were stored at -80°C for extended periods.
The efficiency counting for the spontaneous differentiation was done at d8+5, d8+10, d8+17 and d8+25. The beating areas in the 24-well plate were counted under the microscope. Three experiments should be done for each cell line.

2.2.1.8 Cardiac differentiation of iPSCs

The cardiac differentiation of hiPSCs was done according to the protocols of Lian and Burridge to obtain hiPSC-CMs (Lian et al. 2012; Lian et al. 2013; Burridge et al. 2014). Modulation of the canonical Wnt-signaling pathway effects the development of hiPSCs to mesodermal cells and cardiac progenitor cells (Lian et al. 2013; Burridge et al. 2014).
At a confluence of 80-100% hiPSCs were plated on 12-well culture dishes coated with Geltrex™ (See hiPSC-passaging). At a confluence around 85-95% the E8 Medium was replaced with 2ml Cardio Differentiation Medium per 12-well. 0.42µl of 12mM CHIR99021 (CHIR) per ml medium was added to the Cardio Differentiation Medium before. CHIR is a GSK3 inhibitor working as a Wnt-signal pathway agonist directing the development of hiPSCs to mesodermal cells. 24 hours later the medium is replaced by 2ml per 12-well of Cardio Differentiation Medium containing CHIR. 48 hours after the initiation of differentiation the medium is replaced by 2ml Cardio Differentiation Medium

with inhibitor of Wnt production 2 (IWP2, 5mM). IWP2 is a Wnt antagonist blocking the Wnt secretion. This leads to the differentiation of the cells to cardiac progenitor cells. At day four the medium was changed to Cardio Differentiation Medium without IWP2. Beginning from day eight the medium was changed to Cardio Culture Medium. On day eight the first contractile functions of the cardiomyocytes were microscopically observed. The medium was changed every 2-3 days to specify the development to cardiac muscle cells.

2.2.1.9 Cardiomyocyte digestion

Cardio Digestion medium, culture dishes coated with Geltrex™, Versene Solution, Collagenase B (400 units per ml RPMI) and 0.25% Trypsin-EDTA were warmed to 37 °C. The medium of the selected wells was aspirated and washed once with Versene Solution. The cells were covered with 37°C warmed Collagenase B (1ml per 6-well and 0.5ml per 12-well) and incubated for 1-2h at 37°C. The cell clusters were transferred in suspension in a 15ml Falcon tube. The cells were centrifuged for 5 min at 200 *g*. The supernatant was carefully aspirated and 1-2ml of 0.25% Trypsin-EDTA was added. The cell suspension was incubated for 6-10min at 37°C. Double volume of Cardio Digestion medium was added. The cells were centrifuged for 5 min at 200 *g*. The supernatant was aspirated. The cells were resuspended in 1-2ml Cardio Digestion Medium. The cell suspension was mixed carefully and a desired amount was plated on Geltrex™ coated plates or glass cover slips. The cells were incubated for 20-40min to attach. 2ml Cardio Digestion Medium was added. The Cardio Culture Medium was changed every 2-3 days.

A metabolic selection was done on day 20 by changing the medium to a glucose-free medium called Cardio Selection medium for 4-6 days. Glucose was replaced by lactate to get a higher amount of cardiomyocytes. The cells were cultivated up to day 90. The medium was changed every three to four days.

2.2.1.10 Passaging and culturing of cardiomyocytes for further analyses ($Ca^{2+}$and voltage imaging and immunostaining)

The cardiomyocytes were cultivated till day 80 – day 85 and passaged afterwards. The passaging was done according to the protocol mentioned in chapter 2.2.1.2. The amount of cells was determined to 200000 cardiomyocytes per dish. The cardiomyocytes were transferred to coverslips coated with 0.1% gelatin or Geltrex™ in 6-well culture dishes. The cardiomyocytes were cultivated for 7-10 days in Cardio Culture Medium. Cardiomyocytes

were microscopically observed and morphologically compared to control cardiomyocytes before further analysis and staining were conducted.

2.2.2 Alkaline phosphatase staining

The verification of the alkaline phosphatase (ALP) activity is a stem cell specific characteristic. The ALP staining was performed with the ALP, Human Kit 86R according to the manufactures details. The same protocol was used for iPSCs on feeder layer and iPSCs in feeder-free culture. The cells were cultivated up to a confluence of 60-70%. The cells were washed two times with 3ml PBS. After washing 2ml of fixing solution was added and incubated for 30s at RT. The fixing solution was aspirated and the cells were washed two times with 1ml-distilled water. 2ml-staining solution was added in each dish/well. The cells had to be incubated at 37°C for 15-20min. Afterwards, the cells were washed again two times with 1ml distilled water. The cells were air-dried overnight. ALP positive cells were colored red and were photographed through a light-microscope with 10x magnification.

2.2.3 Molecular biology

2.2.3.1 Pellet collection for iPSCs

The pellet collection was performed in the same procedure for iPSCs on feeder layer and iPSCs in feeder-free culture.

The medium was aspirated from the dish/well. The cells were washed once with 3ml PBS. 1.5ml PBS was added. The cells were carefully scraped in the PBS suspension by the use of a cell scraper and transferred to a 1.5ml Eppendorf tube. The cells were centrifuged at 13.000 rpm for 1 min. The supernatant was aspirated. The pellet was snap-frozen in liquid nitrogen.

The pellets were stored at -80°C for extended periods.

2.2.3.2 DNA isolation

Cell pellets were used for DNA isolation. The DNA isolation was done according to the manufactures protocol. Maxwell ® 16 DNA Purification Kit was used to isolate the DNA. The first step was modified. Instead of using 0.5ml QuickExtract Solution 150µl were used. The remaining steps were performed according to the protocol. The DNA was stored at -20°C.

2.2.3.3 RNA isolation

Cell pellets were used for RNA isolation. The isolation of the total RNA was done with the SV Total RNA Isolation Kit (Promega) according to the manufactures guidelines. The RNA concentration was measured with a spectrophotometer. 50 µl of isolated RNA were pipetted into a nuclease-free cuvette. The light had to pass through the cuvette longitudinally. The ratios of 260/280 and 260/230 were noted. Pure RNA should be around ~2.0. If the concentration was too high to be measured by the spectrophotometer, the probe was diluted 1:10 with nuclease-free water and measured again. The RNA concentration was recorded in ng/µl and adjusted to 50 ng/µl nuclease-free water. The RNA probes were stored at -80°C.

2.2.3.4 Reverse transcription reaction

To perform further gene expression analysis, messenger RNA (mRNA) was transcribed into single-stranded complementary DNA (cDNA). Polymerase chain reaction (PCR) amplifies the specific cDNA (Mullis et al. 1992).
100ng of the RNA probes were used for the reverse transcription reaction. To adapt the right amount of RNA probe, the RNA probe was diluted in nuclease free water (H_2O) and should not exceed the volume of 10.2µl. 9.8µl of reverse transcription mix were added to the reaction mixture.

Table 11: **List of mixture for the reverse transcription reaction**

Mixture for the reverse transcription reaction		
Reagents	**Volume [µl]**	
10 x PCR Buffer II	2	reverse transcription -mix
$MgCl_2$ (25mM)	4	
100mM dNTPs	0.8	
RNase Inhibitor (20U/µl)	1	
Oligo $d(T)_{16}$ (50µM)	1	
MuL V Reverse Transcriptase (50U/µl)	1	
RNA (100ng) in nuclease-free H_2O	10.2	
Total:	20	

The following program parameters were used for the reverse transcription reaction.

Table 12: **Parameters of reverse transcription reaction program**

Time [min]	**Temperature [°C]**
10	22
50	42
10	95
∞	4

The amplified cDNA was stored at -20°C.

2.2.3.5 Gene expression analysis – PCR

The cDNA was amplified with specific primers for gene expression analysis. The gene specific primer sequences are listed in 2.1.7. The PCR reaction mixture contained 24µl PCR-mix and 1µl cDNA. The negative control was a reaction mixture with water instead of cDNA.

Table 13: **List of mixture for PCR reaction**

Mixture for PCR reaction		
Reagents	**Volume [µl]**	
5x Green Buffer	5	PCR-mix
10mM dNTPs	1	
Primer forward (10µM)	1	
Primer reward (10µM)	1	
GoTaq Polymerase	0.125	
Nuclease-free H_2O	15.875	
cDNA	1	
Total:	25	

The amplification of specific cDNA fragments was done according to the following program parameters:

Table 14: **Parameters of PCR program**

	Temperature [°C]	**Time**	
Initial denaturation	95	2 min	
Repeat parameter			Amount of repeats: X
- Denaturation	95	30 sec	
- Annealing	X	30 sec	
- Elongation	72	45 sec	
Final elongation	72	10 min	
Break	4	∞	

The amount of repeats (X) and the annealing temperature are primer-specific and listed in the tables in chapter 2.1.8 and 2.1.9.

2.2.3.6 Agarose gel electrophoresis

The agarose gel electrophoresis is a molecular biological method to separate DNA fragments inside of an electrical field. The fragments were colored with a nucleic acid intercalating dye Midori Green. The colored fragments were detected under ultraviolet (UV)-light. The examined gene fragments were visualized and the primer specificity of each primer pair was proved.

An 1.5% agarose gel was made by solving 1.8g agarose in 120ml 1xTBE buffer. The solution was heated for three minutes by using a microwave. The solution had to cool down to 60°C and 4µl of Midori Green were added. The hardened gel was put in a gel electrophoresis chamber filled with 1xTBE buffer. Each pocket was loaded with 12µl of the probe. A 100 bp Ladder was used as reference. The gel electrophoresis ran for 30 min by 120 V voltage. The bands were detected under UV light.

2.2.3.7 Immunostaining

This method offers the possibility to characterize the cells on protein level. The confirmation of pluripotency and of the potential for differentiation to the three germ layers of stem cells was based on immunofluorescence staining. CMs were characterized on protein level with specific cardiac markers.

CMs, stem cells or EBs were passaged on cover slips and fixed inside the well. The medium was aspirated. The cells were washed three times with 1 x PBS. Afterwards the cells were fixed with 4% PFA for 20min at RT. The cells were washed three times with 1 x PBS and incubated in 2ml 1% BSA solution overnight at 4°C. The fixed cells could be stored at 4°C for a longer time.

Immunofluorescence staining is based on the formation of an antigen-antibody complex. A secondary antibody is linked with a fluorescent dye. The secondary antibody is able to bind the primary antigen-antibody complex.

The staining was done in a H_2O humidified chamber. All incubations were done under the exclusion of light. The antibodies used for primary staining of the pluripotency markers LIN28, OCT4, SOX2, NANOG and for the cardiac specific proteins MLC2A and MLC2V were diluted in 1%BSA and the supplement 0.1% Triton X-100 was added to the solution. Triton X-100 is able to lysate and permeable the cell membranes.

The primary antibody staining began with three times of washing the cells with 1xPBS. 200µl of primary antibody/1% BSA solution (+0.1% Triton-X) were added and incubated overnight at 4°C. The cells were washed again for three times with 1x PBS and the secondary antibody/1% BSA solution (+0.1% Triton-X) was added. The cells had to incubate for 1h at RT. The cells were washed once again with 1x PBS. Afterwards the nuclear staining with 0.4µg/ml DAPI was done for 10 min at RT. The colored cells were washed three times with 1x PBS and once with distilled water. The colored cells were sealed with Fluoromount-G or Vectashield Mounting medium onto object plates. The object plates were stored up to four weeks at 4°C. The pictures were made with a fluorescent-microscope.

Sarah Henze did the explicit immunofluorescence staining of RyR2-KO-CMs for α-actinin and RyR2.

2.2.3.8 Selection of CRISPR-clones

The selection of CRISPR-clones was done via PCR-screening. The PCR-screening was based on homologues recombination. The DNA-PCR was done according to the instruction listed in 2.2.3.5. After the PCR 0.5µl of SpeI-HF-restriction enzyme was added to the amplified DNA probes. The DNA probes were incubated at 37°C overnight. Gel electrophoresis was done afterwards according to the instructions listed in 2.2.3.6.

2.2.3.9 Genomic sequencing preparation

The positive CRISPR-clones after secondary selection were sequenced to confirm the genomic manipulation. DNA probes created with the QuickExtract Solution described in 2.2.3.2 were taken. 12µl DNA-solution was added in a 1.5ml Epi tube together with 3µl of the corresponding forward primer. Another 1.5ml Epi tube was filled with 12µl DNA and 3µl of the corresponding reverse primer. The probes were sent for genomic sequencing to the company SeqLab Sequences Laboratories GmbH in Goettingen.

2.2.3.10 Cultivation of Escheria coli (E. coli)

For cloning experiments, the E. coli strain Top10 F was used. The E. coli strain was used to perform the CRISPR project. The cells were cultivated in LB medium at 37°C and 200 rpm. The cells were cultivated on solid medium. 1.5% agar was added and the bacteria incubated at 37°C. Ampicillin 100µg/ml was added to the medium.

2.2.3.11 Transformation of competent E.coli bacteria with CRISPR plasmids

E. coli bacteria were thrown on ice for 5-10min. Afterwards 1µl of CRISPR plasmid solution was pipetted into the E.coli solution. The solution was mixed by snapping against the tube. The solution was incubated for 20min on ice. The bacteria were heat shocked at 42°C for 90 sec. Subsequently the bacteria were put on ice for 2 min for recovery. 500µl of LB medium were pipetted into the tube and were once pipetted up and down. The mixture was incubated for 1 hour at 37°C and 350 rpm to allow recovery of the heat shocked bacteria. After incubation 40-200µl of the bacteria were plated on LB-agar containing Kanamycin plates. The agar plates were incubated at 37°C overnight. A control transformation without CRISPR plasmid was performed to check that the Kanamycin was working. No colonies appeared in the control transformation.

2.2.3.12 Plasmid DNA isolation and purification from E.coli

E. coli bacteria transformed with CRISPR plasmids were incubated in appropriate volume of LB medium at 37°C. Kanamycin was added. A resistance was created through the transformation of the CRISPR plasmid. 800µl of the culture were used for a glycerin stock (200µl of 99% glycerin and 800µl bacteria culture). The isolation of plasmid DNA was done with the Maxwell® 16 DNA Purification Kit according to the manufactures instructions.

2.2.4 Transfection of HEK293T cells using Mirus TransIT®-293

For the cleavage assay of CRISPR/Cas9 the CRISPR-B-1/Cas9 plasmid was transfected in HEK293T cells using the Mirus TransIT®-293 transfection reagent. The transfection was done according to the manufacturer's protocol to obtain a high efficiency. The transfected cells were counted and pellets containing around $1x10^6$ cells were prepared by pooling 2-3 wells as described in 2.2.3.1 and used for cleavage essay.

2.2.5 Cleavage assay of CRISPR/Cas9

To detect the cleaving efficiency of the Cas9 nuclease at the target sequence, a cleavage assay of the CRISPR-B-1/Cas9 plasmid was performed. The cleavage assay was done according the manufacturer's instructions. The GeneArt® Genomic Cleavage Detection Kit was used. In summary, pellets of the transfected HEK293T cells were resuspended in 50µl cell lysis buffer/2µl protein degrader mix and a PCR was performed according to the manufacturer's instructions. 2µl of the PCR product were mixed with detection reaction buffer in a total volume of 10µl and the re-annealing reaction was started. In the next step the detection enzyme cleaved the PCR-product containing the mismatched DNA and the sample was loaded on an agarose gel using Ficoll loading buffer. No dye was used to avoid interference with band intensity measurements. The determination of the relative proportion of gene modification was done with the Alpha Imager Software.

2.2.6 Protein expression analysis

2.2.6.1 Western blot analysis

The cells were cultivated and probed for the Western blot analysis by myself. Sarah Henze performed SDS-polyacrylamide gel electrophoresis and took the images together with her probes for the CPVTc2 experiments.

2.2.6.1.1 Preparation of cell lysates

For cell lysis, frozen cell pellets were resuspended in 80-100µl cell lysis buffer and incubated for 30 min on ice. To remove bigger cell fractions, lysates were centrifuged (2,400 x g, 5 min, 4°C). The supernatant was transferred into a new reaction tube. 5µl of each sample were diluted in 95µl DPBS for measurements of protein concentrations. The protein concentration was quantified using the Pierce BCA protein assay kit according to the manufacturer´s instructions with a 96-well photometer at 562nm. The samples were

prepared for SDS-PAGE or alternatively stored at –80°C for further use. A total amount of 40µg protein lysate was mixed with SDS loading buffer and DPBS in 20µl and denatured for 30 min at 37°C before SDS-PAGE analysis.

2.2.6.1.2 SDS-polyacrylamide gel electrophoresis (SDS-PAGE)

By SDS-PAGE charged proteins are separated according to their molecular weight. The separation gel was mixed according to Table 15 and poured between two glass plates separated by spacers and fixed with clamps. Solutions for the separation gel were covered with a thin layer of isopropanol. The isopropanol was decanted after polymerization. A stacking gel was poured on top. A comb was inserted. After polymerization of the stacking gel, the whole gel was attached to an electrophoresis chamber, filled with 1x running buffer. The samples were loaded together with a prestained molecular weight marker. Electrophoresis was performed at constant amperage of 30mA for approximately 2 hours. To visualize the separated proteins, the gels were further processed by immunoblotting

Table 15: Components for separation and stacking gel

Separation gel 12ml	6%	12%	15%	Stacking gel 7.5ml	2 gels
Rotiphorese gel 30	2ml	4.8ml	6ml		1ml
4x Tris/SDS pH 8.8	3ml	3ml	3ml	4x Tris/SDS pH 6.8	1.88ml
ddH_20	6.6ml	4.2ml	3ml		4.62ml
10% APS	48µl	48µl	48µl		37.5µl
Temed	18µl	18µl	18µl		15µl

2.2.6.1.3 Protein transfer and detection

Proteins, which were separated by SDS gel electrophoresis, were transferred to polyvinylidene difluoride (PVDF) membranes using the Wet/Tank blotting system. Four filter papers were batched in 1x transfer buffer. The PVDF membrane was activated according to the manufacturer's instructions. Two filter papers were placed on the black site of the holder cassette. The SDS gel was placed above the PVDF membrane and two additional filter papers. The protein transfer was cooled with ice during the blotting (400 mA, 2h).

3% BSA/TBS-T or non-fat dry milk was used to block the free binding sites on the PVDF membrane (60 min, RT). Primary antibodies diluted in 1-3% BSA/TBS-T (4°C, overnight)

were used for the immunostaining together with the HRP-conjugated secondary antibodies diluted in 1% BSA/TBS-T (60 min, RT). The membrane was washed three times with TBS-T during the incubation period. By adding ECL reagents the antigens of interest were detected. The results were documented with a chemiluminescence detection system.

2.2.7 Calcium imaging

The cells were prepared for calcium imaging by myself. Lukas Cyganek performed the confocal measurements and Sarah Henze helped with the analysis.

For calcium imaging, cells were digested and plated on Geltrex-coated 25mm glass coverslips and afterwards incubated in B27 medium 5 to 7 days before the calcium recording. At day 86-118 cells were used and washed twice with Tyrode's solution. In the next step cells were incubated for 30 minutes with 5µl fluo-4/AM fluorescent calcium indicator and 0.02% [w/v] pluronic F-127 in Tyrode's solution at 20-22°C. Afterwards the cells were washed twice with Tyrode's solution. The cells were paced by using a recording chamber with platinum electrodes in Tyrode's solution at 20-22°C. The medium was changed every 10 minutes. The field stimulation was performed at 0.25Hz (18V, 3ms duration) and the calcium recording was performed. LSM 710 confocal microscopy system with a 63x 1.4 NA oil objective in line scan mode (512 pixels, 45µm, 1057.7Hz, 20,000 cycles) exciting at 488nm and collecting emission at 490-540nm was used to capture images. The analysis of the intracellular calcium concentration variation was performed using ImageJ and Microsoft Excel. The calcium concentration change was analyzed as a function of the time. During diastolic phase a defined plot per recording (500ms, 25µm) was analyzed by ImageJ Spark Master (settings: 1057.70lps; 0.088µm; Fl. U. 0; criteria 3.3; intervals 3).

2.3 Vote of the Ethics Committee

All experiments were done according to the vote of the ethics committee. The application number of the vote of ethics committee of the University Clinic Goettingen is DK_89_2015.

3 Results

3.1 Characterization of iPSC lines

Disease models using iPSCs for CPVT patients with different mutations were established in the lab. Skin biopsies were taken from CPVT patients for the generation of iPSCs. The iPSCs were generated via SeV transduction containing the Yamanaka factors *KLF4, C-MYC, OCT4* and *SOX2* (Fusaki et al. 2009). The CPVT disease models for this project were based on iPSCs from CPVT patients b1 and c2, who had a missense mutation A2254V or E4076K at different loci, respectively.

The human iPSC line isCPVTb1.6 was previously characterized in feeder culture conditions for the pluripotency after successful reprogramming in the lab and was used for the CRISPR experiments. Characterization of iPSCs includes ALP, gene expression and protein expression of pluripotency-associated markers and the proof of the differentiation potential in all three germ layers. Immunofluorescence staining enables the characterization of the cells on protein level. The RT-PCR method as a gene expression analysis allows characterization on mRNA level. The proof of ALP activity was done, because of the high activity in pluripotent stem cells.

In this study, the two iPSC lines isCPVTc2.2 and isCPVTc.2.3, which were generated from CPVT patient c2, were fully characterized.

3.1.1 Alkaline phosphatase staining of the human iPSC lines

ALP is a hydrolase enzyme which shows high activity in undifferentiated ESCs and iPSCs (Wobus et al. 1984; Pease et al. 1990; Kim and Wyckoff 1991). The high alkaline phosphatase activity was verified as red precipitate in the analyzed iPSC lines isCPVTc2.2 and isCPVTc2.3 (Figure 6).

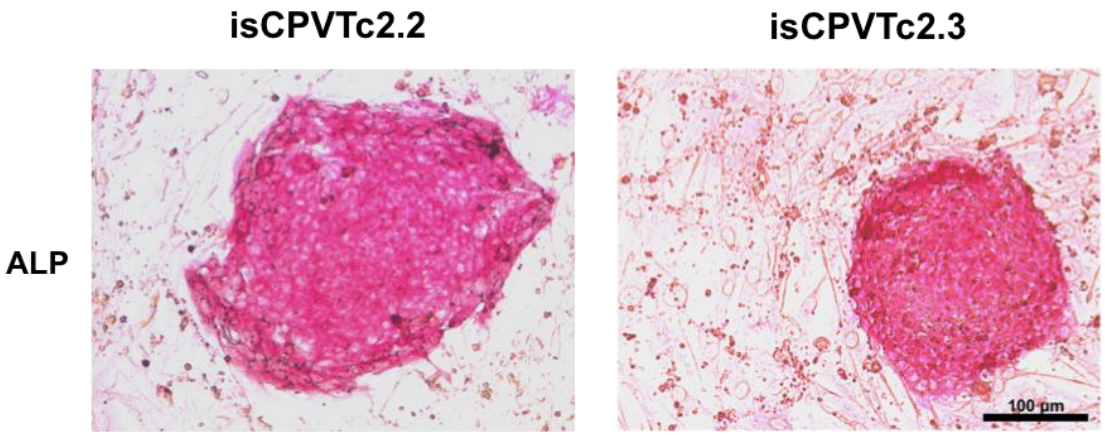

Figure 6: **Alkaline phosphatase staining of the human iPSC lines isCPVTc2.2 and isCPVTc2.3.** The figure shows ALP staining (10x) of isCPVTc2.2 and isCPVTc2.3 cultured on MEFs. The red staining in all iPSC lines proved the high enzymatic activity. The pictures were taken without phase contrast and with automatic white balance. (Scale bar: 100 µm)

3.1.2 Proof of the expression of pluripotency-associated marker genes at mRNA level

The analysis of cellular gene expression patterns of the iPSC lines was carried out by the use of RT-PCR. As proof of pluripotency the iPSC lines were examined for the expression of pluripotent stem cell-specific marker genes. *SOX2, OCT4, NANOG, LIN28, GDF3* and *FOXD3* were used as pluripotency markers (Reubinoff et al. 2000; Hanna et al. 2002; Chambers et al. 2003; Richards et al. 2004; Levine and Brivanlou 2006; Zhang and Cui 2014). Human ESCs were used as positive control. MEFs and patient-specific fibroblasts were used as negative controls (Figure 7).

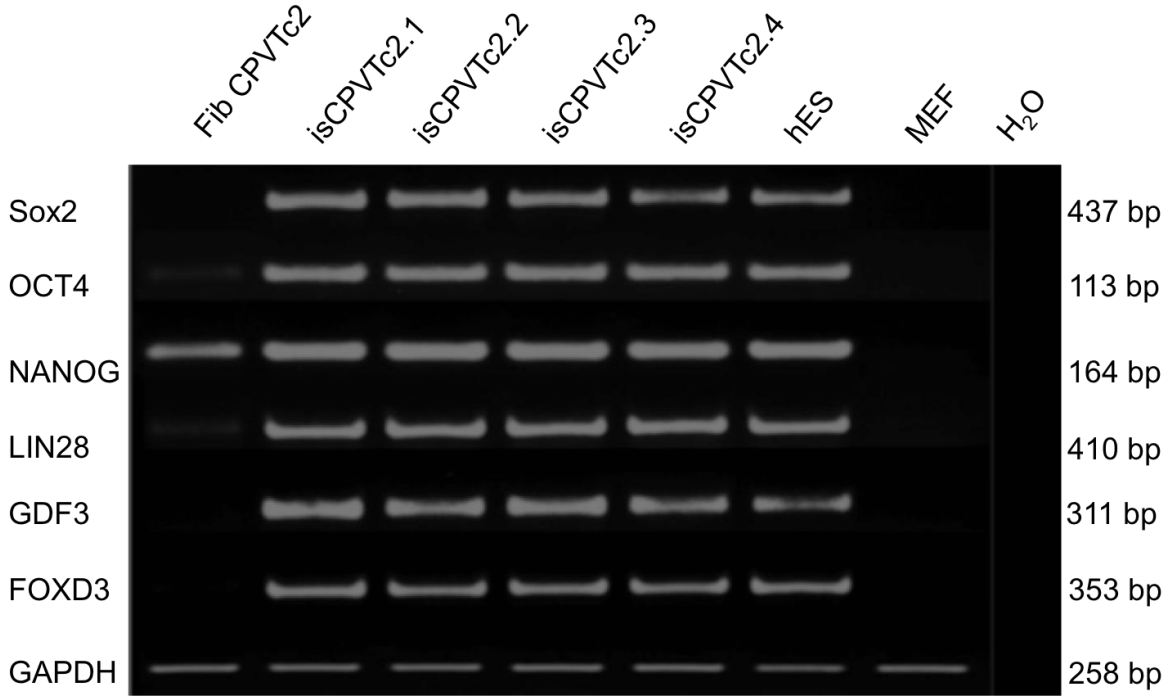

Figure 7: **Proof of pluripotent stem cell-specific marker gene expression on mRNA level.** Gel electrophoresis of RT-PCR products are shown. The following marker genes were proved on their expression at mRNA level: SOX2 (437bp), OCT4 (113bp), NANOG (164bp), LIN28 (410bp), GDF3 (311bp) and FOXD3 (353bp). GAPDH (258bp) was used as intern control. The iPSC lines isCPVTc2.1, isCPVTc2.2, isCPVTc2.3 and isCPVTc2.4 were proved. The positive control was done with human ESCs. The negative control was done with MEFs and patient-specific skin fibroblasts (Fib CPVTc2). The pluripotency-associated markers were detected in all pluripotent stem cell lines.

The pluripotency factors *SOX2*, *OCT4*, *NANOG*, *LIN28*, *GDF3* and *FOXD3* were expressed in all iPSC lines analyzed and showed a corresponding expression pattern to human ESCs used as positive control. These pluripotency genes were expressed at very low levels in their parental fibroblasts. The intern control *GAPDH* showed in all probes a similar intensity. The MEFs used for negative control showed no expression of stem cell specific marker genes.

3.1.3 Proof of the expression of pluripotency-associated markers at protein level

For demonstrating the pluripotency of iPSCs at protein level immunofluorescence staining was performed. The iPSCs were fixed with 4% PFA and stained with antibodies against pluripotency-specific proteins OCT4, SOX2, LIN28, NANOG, SSEA4 and tumour-related antigen-1-60 (TRA-1-60) and their corresponding secondary antibodies. The cells were microscopically examined. OCT4, SOX2 and NANOG are important pluripotency factors, which are expressed in the cell nucleus. The antibodies against SSEA4 and TRA-1-60

detect antigens at the cell surface of pluripotent stem cells. The LIN28 antibody binds to cytoplasmic antigens (Brimble et al. 2007; Schopperle and DeWolf 2007). The nucleus staining was done with DAPI, which is detectable with UV light with a wavelength of 461nm. Figure 8 shows blue nucleus staining with DAPI and the pluripotency markers OCT4 SOX2 and NANOG are colored in red. The cytoplasmic marker LIN28 is colored in red. The expression of surface markers SSEA4 and TRA-1-60 was proved in the two iPSC lines analyzed. The DAPI staining is overlaid with the antibody staining in the figure (Figure 8).

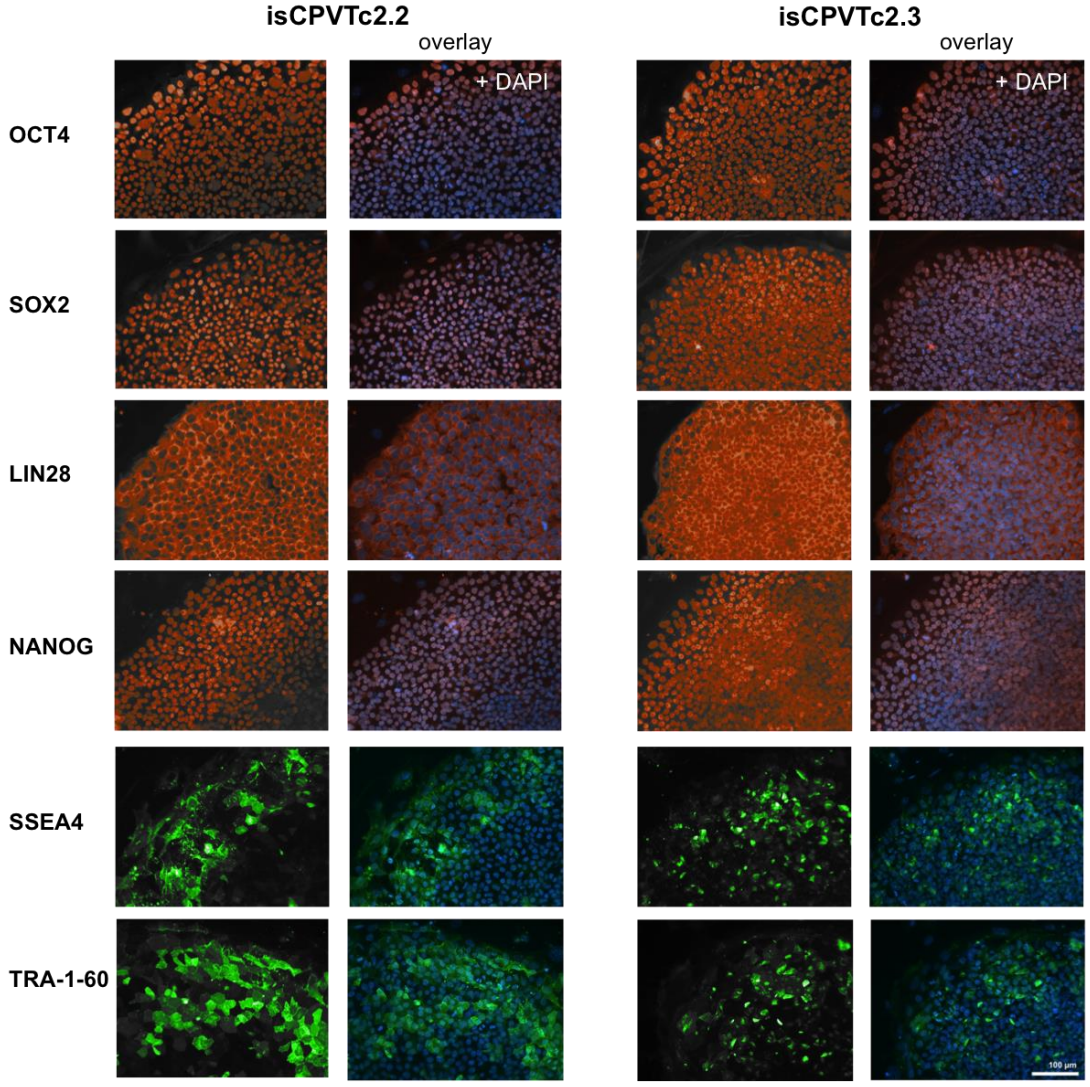

Figure 8: **Proof of the expression of pluripotency-associated markers at protein level.** The immunofluorescence staining of pluripotent stem cell-associated markers is shown and also in an overlaid picture with DAPI. The transcription factors OCT4, SOX2 and NANOG, the surface markers SSEA4 and TRA-1-60 and the cytoplasmic marker LIN28 are expressed in all examined iPSC lines. The pictures were taken with a 20x image enlargement. The protein expression of pluripotency-associated markers was proven in both iPSC lines isCPVTc2.2 and isCPVTc2.3. (Scale bar: 100µm)

3.1.4 Proof of the iPSC differentiation potential *in vitro*

The spontaneous differentiation of human iPSCs was done according to the established protocol of the stem cell laboratory at the cardiology and pulmonology department. To prove the differentiation potential of iPSCs into all three germ layers ectoderm, mesoderm and endoderm, immunofluorescence staining was done for two cell lines. The differentiated EBs were fixed with 4% PFA and stained with germ layer-specific antibodies and visualized with fluorescence marked secondary antibodies. β3-tubulin, which is a neuron-specific isoform of the tubulin, was used as ectodermal marker. The α smooth muscle actin (α-SMA) was used as mesodermal marker and the glycoprotein alpha-1-fetoprotein (AFP) was used as endodermal marker (Pekkanen-Mattila et al. 2010; Martí et al. 2013). The expression of the germ layer-specific markers was shown in both iPSC lines after differentiation (Figure 9).

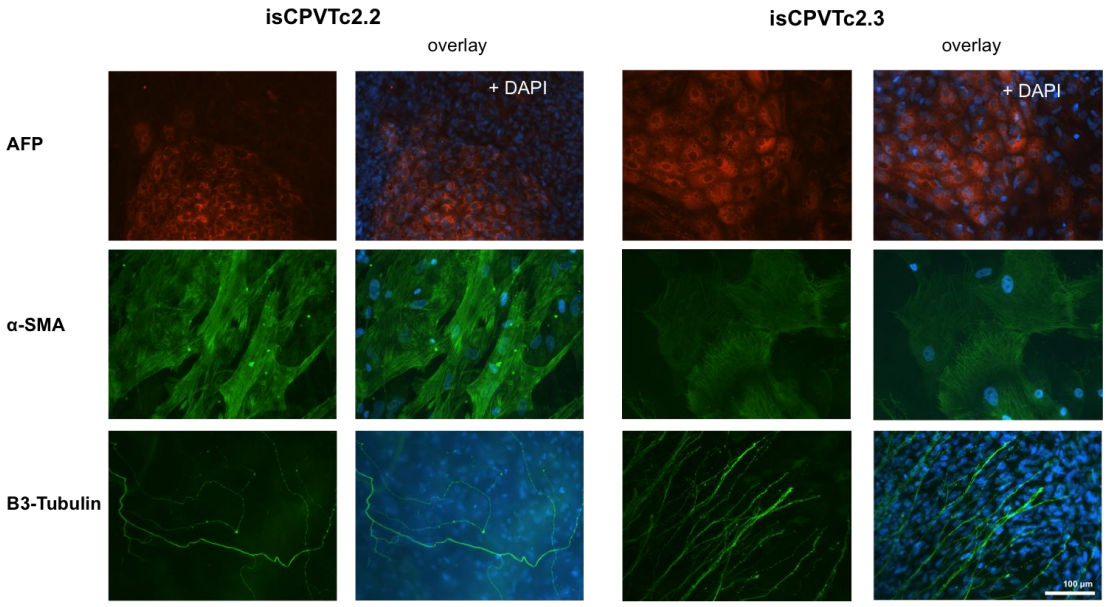

Figure 9: **Proof of the expression of germ layer-specific markers at protein level.** The figure shows the immunofluorescence staining of antibodies specific for three germ layers and also in an overlaid picture with DAPI. The following germ layer-specific markers were stained: AFP (endoderm) α-SMA (mesoderm) and β3-tubulin (ectoderm). The pictures were taken with a 20x image enlargement. At d8+25 protein markers of the three germ layers were proved in both iPSC lines. (Scale bar: 100µm)

3.2 CRISPR/Cas9-mediated gene editing of *RyR2*

One patient-specific iPSC line isCPVTb1.6, which contains the mutation A2254V in RyR2, was used for the CRISPR/Cas9 mediated genetic-targeting. The missense mutation is localized in the genomic sequence expressing the cytosolic part of RyR2. The missense mutation A2254V in isCPVTb1.6 was confirmed by sequencing previously.

3.2.1 CRISPR/Cas9 design

The combined and customized CRISPR/Cas9 plasmid (Figure 10) was designed and generated including the gRNA sequence with a 22bp RyR2-targeting region. The CRISPR/Cas9 plasmid contains the gRNA, a Cas9 enzyme and GFP for selection of positive transfected cells. Several gRNAs were designed, bioinformatic analysis of off-target prediction of the gRNAs was performed by Sigma-Aldrich and a gRNA (Crispr1) with 2 off-targets at 3 mismatches was used in this study (Figure 11), which gave the lowest amount of off-targets and about 34bp away from the mutant site (c.C6761T). The designed plasmid CRISPR-B-1/Cas9 was ordered at Sigma-Aldrich (Figure 10).

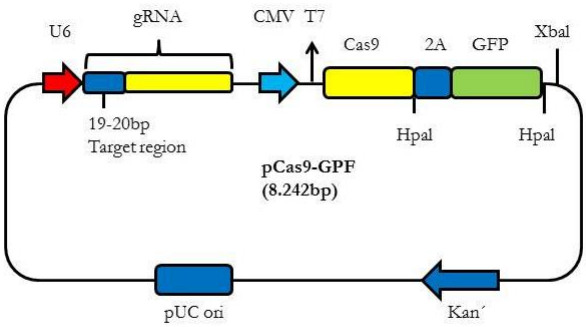

Figure 10**: The combined customized CRISPR-B-1/Cas9 recognizes a specific 22-bp binding site for the domain b of RyR2.**

The mutation C>T in exon 44 of RyR2 causes an amino acid change from alanine (GCA) to valine (GTA). Additionally, the mutation leads to the generation of a SpeI (ACTAGT) restriction site. A single strand oligodeoxynucleotide (ssODN) was designed as a template to correct the C>T mutation in RyR2 (Figure 11 and 12). The designed ssODN carried the T>C correction and a total of 107 nucleotides of homologous sequence flanking the mutation site. The SpeI restriction site should be destroyed after the genetic correction.

The mutated restriction site after genetic correction can be further used for a primary screening (Figure 11).

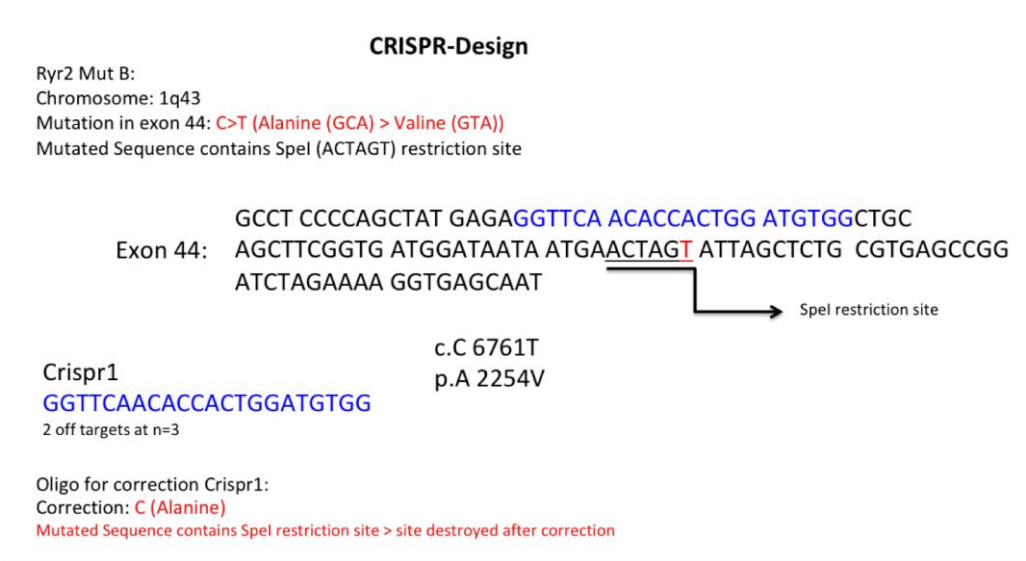

Figure 11: **CRISPR/Cas9 design for the RyR2 mutation c.C6761T. Crispr1 was designed according the binding characteristics of the sgRNA of the CRISPR/Cas9 complex.** The sgRNA binds best at a PAM sequence and about 34bp away from the mutant site (c.C6761T). The ssODN was designed as a template for the genetic correction. The genetic correction causes a destruction of the SpeI restriction enzyme binding site additionally.

Forward and reverse primers were designed for genomic sequencing flanking the respective exon. The fragment defined through the primer contains 560bps. Genomic sequencing was used to show the genetic correction or the creation of a knockout model on base level.

	Sequence
ssODN for CRISPR1	5‘- GCCTCCCCAGCTATGAGAGGTTCAACACCACTGG ATGTGGCTGCAGCTTCGGTGATGGATAATA ATGAACTAGCATTAGCTCTGCGTGAGCCGG ATCTAGAAAAGGT-3’

Figure 12: **Design of ssODN for CRISPR1**

3.2.2 Cleavage assay

The CRISPR-B-1/Cas9 cleavage efficacy was tested with a cleavage assay. HEK 293T cells were transfected using Mirus TransIT®-293 Transfection Reagent with the CRISPR-B-1/Cas9 plasmid (Figure 13). The DNA samples of the transfected cells were amplified using primers flanking the RyR2 mutation region, used for the cleavage assay to detect deletions or insertions (indel) and analyzed on agarose gel.

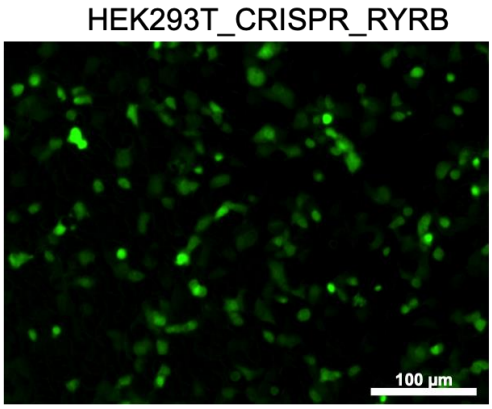

Figure 13: **Representative image of HEK293T cells expressing the CRISPR-B-1/Cas9 plasmid including a GFP signal.** The HEK293T cells were transfected with the CRISPR-B-1/Cas9 plamid using Mirus TransIT®-293 Transfection Reagent. The GFP signal was detectable after 24-48 hours. (Scale bar: 100 µm)

The intensity of the digested and undigested bands was quantified. The plasmid CRISPR-B-1/Cas9 had an estimated cleavage efficiency of 15-20%. The positive control had cleavage efficiency around 21-24%.

3.2.3 Generation of CRISPR-B-1/Cas9-targeted iPSC lines

Figure 14 shows the strategy for generating CRISPR/Cas9-targeted CPVT-iPSC lines. The CRISPR-B-1/Cas9 gene-targeting plasmid and ssODN were introduced by nucleofection into isCPVTb1.6 iPSCs to generate CRISPR-B-1/Cas9-targeted hiPSC clones. Different methods were used to improve the transfection efficiency. Nucleofection showed the best outcome. In the next step transfected cells were sorted via FACS for GFP positive cells. Flow cytometry analysis showed that the GFP positive rate of living transfected cells ranged around 1-3% (Figure 15).

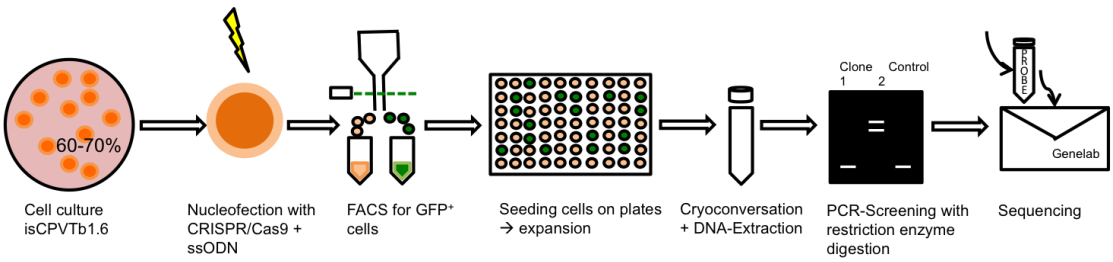

Figure 14: **Strategy for generating CRISPR/Cas9-targeted CPVT-iPSC lines.** CRISPR-B-1/Cas9 gene-targeting plasmid was introduced into isCPVTb1.6 iPSCs by nucleofection using 2 million cells mixed with 4µg plasmid and 3.3µg ssODNs as donor DNA. 24 hours after nucleofection, GFP positive iPSCs were sorted by FACS. 2-7 x 10^3 cells were seeded on each Geltrex coated 96-well plate (1-10 cells per well) in a 1:1 mix of E8 and MEF-conditioned E8 medium supplemented with additional bFGF (10 ng/ml), TZV, 1x P/S (first week), which was changed every third day. After 10-

18 days single colonies were transferred into Geltrex-coated 48-well plates. Confluent cells in 48-well plates were transferred onto two wells of 24 well plates for cryopreservation and DNA extraction, respectively. Genomic DNA was isolated and analyzed for targeted integration by PCR and SpeI restriction digestion. Negative digested cell clones were sequenced.

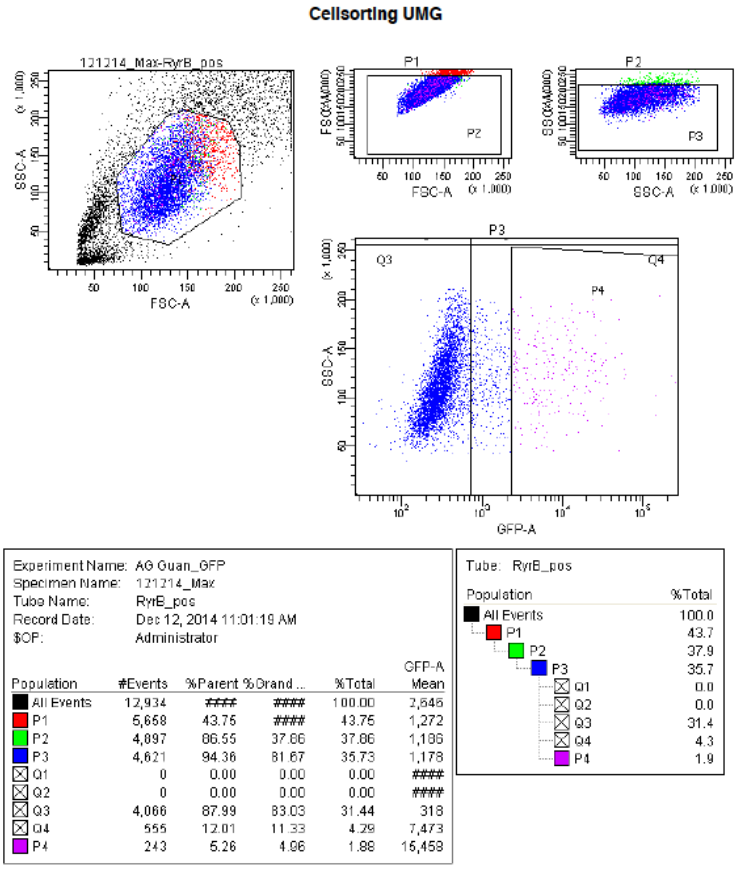

Population	#Events	%Parent	%Grand ...	%Total	GFP-A Mean
All Events	12,934	####	####	100.00	2,646
P1	5,658	43.75	####	43.75	1,272
P2	4,897	86.55	37.86	37.86	1,186
P3	4,621	94.36	81.67	35.73	1,178
Q1	0	0.00	0.00	0.00	####
Q2	0	0.00	0.00	0.00	####
Q3	4,066	87.99	83.03	31.44	318
Q4	555	12.01	11.33	4.29	7,473
P4	243	5.26	4.96	1.88	15,458

Figure 15: **Example: FACS sorting for GFP positive cells.** The CRISPR-B-1/Cas9 gene-targeting plasmid and ssODN were introduced by nucleofection into isCPVTb1.6 iPSCs. 24 hours after nucleofection the cell sorting via FACS was done according to the intensity of the GFP positive signal. Population P4 matches for GFP positive cells after nucleofection. Population P4 was sorted and cultivated for further analysis afterwards. The transfection efficiency of iPSCs ranged between 1-3%.

The primary screening of positive clones for HDR was done by restriction digestion. The binding site of the restriction enzyme was destroyed through the genetic correction (Figures 11 and 12).

An edited genome by the CRISPR-B-1/Cas9 in combination with ssODNs for HDR should be accompanied with a mutated SpeI restriction site in isCPVTb1.6 patient cell line and successfully genome edited iPSC lines should display only one DNA fragment compared to two fragments in isCPVTb1.6 iPSC line (Figure 16).

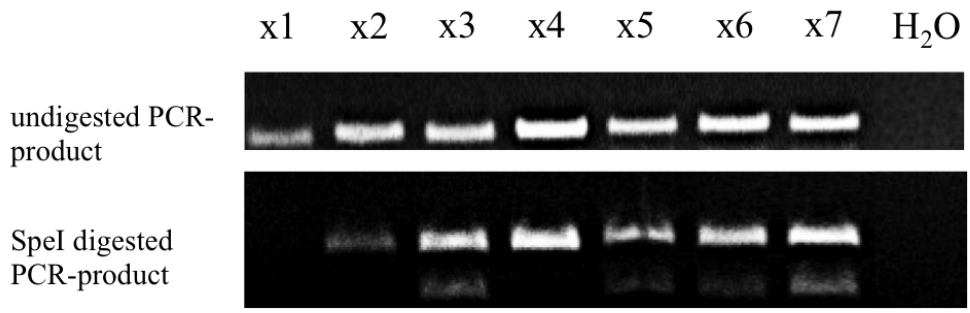

Figure 16: **Representative PCR and restriction digestion shows positive not-digested CRISPR-targeted clones (X2, X4).** The CRISPR/Cas9 complex destroyed the restriction site in genomic edited clones. No digested fragments are shown after digestion with SpeI in the CRISPR-targeted clones. The other cells show digested fragments after digestion.

In total, 68 GFP positive clones derived from isCPVTb1.6 cell line were expanded and screened for correction of mutation via PCR and subsequent restriction enzyme digestion. The primary screening showed two targeted clones (X2 and X4). Sequencing of the genome of two clones X2 and X4 showed an integration of the ssODNs close to CRISPR-B-1/Cas9 cleavage site in clone X4 as well as additional deletions in the genome of clone X2 and clone X4 (Figure 17).

Clone	Origin	ssODN	Sequence
X2	isCPVT b1.6	CRISPR-Oligo-b1	Allele 1: 5'-GCCTCCCCAGCTATGANAGGTTCAACACCMNNGGN------3' Allele 2: 5'- GCCTCCCCAGCTATGANAGGTTCAACACC------3'
X4	isCPVTb1.6	CRISPR-Oligo-b1	Allele 1: 5'-GCCTCCCCAGCTATGAGAGGTTCAACACCA----ATGTGGCTGCAGCTTCGGTGATGGATAATAATGAACTAGCATTAGCTCTGCGTGAGCCGGATCTAGAAAAGGT-3' Allele 2: 5'-GCCTCCCCAGCTATGAGAGGTTCAACACCA----ATGTGGCTGCAGCTTCGGTGATGGATAATAATGAACTAGCATTAGCTCTGCGTGAGCCGGATCTAGAAAAGGT-3'
b1.6 WT	isCPVT b1.6	-	Allele 1: Mutation in exon 44 C>T 5'-GCCTCCCCAGCTATGAGAGGTTCAACACCACTGGATGTGGCTGCAGCTTCGGTGATGGATAATAATGAACTAGTATTAGCTCTGCGTGAGCCGGATCTAGAAAAGGT-3'

			Allele 2: 5'- GCCTCCCCAGCTATGAGAGGTTCAACACCACTGGAT GTGGCTGCAGCTTCGGTGATGGATAATAATGAACT AGCATTAGCTCTGCGTGAGCCGGATCTAGAAAAGG T-3'

Figure 17: **Sequencing of CRISPR-B-1/Cas9-targeted clones.** Both clones were sequenced to test if the genetic correction or the creation of a KO-cell line worked. The clones were preselected by restriction enzyme digestion. Clone X4 had a homozygous deletion of 4 bps.

However, no isogenic corrected isCPVTb1 cell lines were created with CRISPR-B-1/Cas9. Instead, iPSC lines with a RyR2 knockout were generated with CRISPR-B-1/Cas9. The generated X4 clone of isCPVTb1 iPSCs showed the integration of the ssODNs, but had a homozygous nucleotide deletion of 4bps. The deletion caused a reading frameshift with a premature stop codon at the a.a. position 2246 in the cytosolic domain of RyR2, which causes the loss of the transmembrane domain of the RyR2 receptor. As a result the channel pore of the RyR2 is not formed anymore, and the generated isCPVTb1.6_X4 is a cell line with complete knockout of RyR2. The isCPVTb1.6_X2 clone showed an analogous pattern. The generated X2 clone had several nonsense mutations early before the targeted sequence at the a.a. position 2245. The manipulated base sequence caused a reading frame shift, which causes the loss of the transmembrane domain of the RyR2 receptor as well as in clone X4. It did not show a successful genetic correction of the defined locus.. isCPVTb1.6_X2 was not further examined because the cultivation and differentiation process to CMs was problematic. Further studies were performed with the isCPVTb1.6_X4 cell line.

To show that the CRSPR-B-1/Cas9-targeted clone (X4) has the similar pluripotent characteristics like non-transfected isCPVT1.6 iPSCs, different methods to prove pluripotency were used. The pluripotency was proved at mRNA level with RT-PCR and at protein level with immunostaining.

The first step was to show a high ALP activity with alkaline phosphatase staining, which is a marker for undifferentiated ESCs and iPSCs (Figure 18).

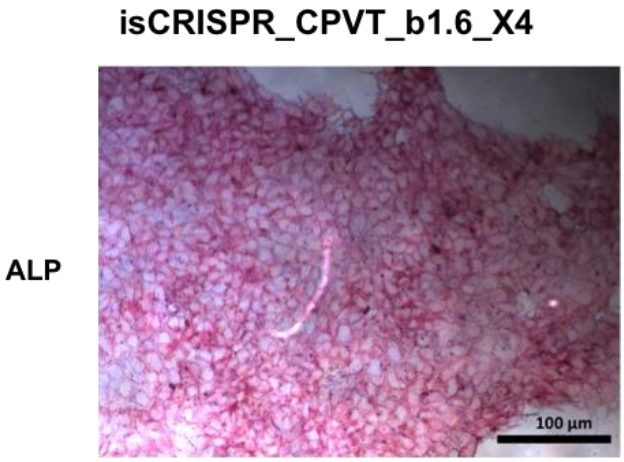

Figure 18: **Alkaline phosphatase staining of the CRISPR-B-1/Cas9-targeted clone X4.** The figure shows ALP staining (10x) of isCPVTb1.6_X4 cultured on Geltrex. The red staining proved the high enzymatic activity. The picture was taken without phase contrast and with automatic white balance. (Scale bar: 100µm)

The CRISPR-B-1/Cas9-targeted clone X4 was examined for the expression of pluripotent stem cell-specific marker genes on mRNA level. *SOX2, OCT4, NANOG, LIN28, GDF3* and *FOXD3* were used as pluripotency markers. Human ESCs were used as positive control. MEFs were used as negative control. The pluripotency factors *SOX2, OCT4, NANOG, LIN28, GDF3* and *FOXD3* were expressed in the CRISPR-B-1/Cas9-targeted clone X4 and showed a corresponding expression pattern similar to its parental cell line isCPVTb1.6 and to human ESCs. GAPDH was used as an intern control and showed in all probes a similar intensity. No expressions of pluripotent stem cell-specific marker genes were shown in MEF cells (Figure 19).

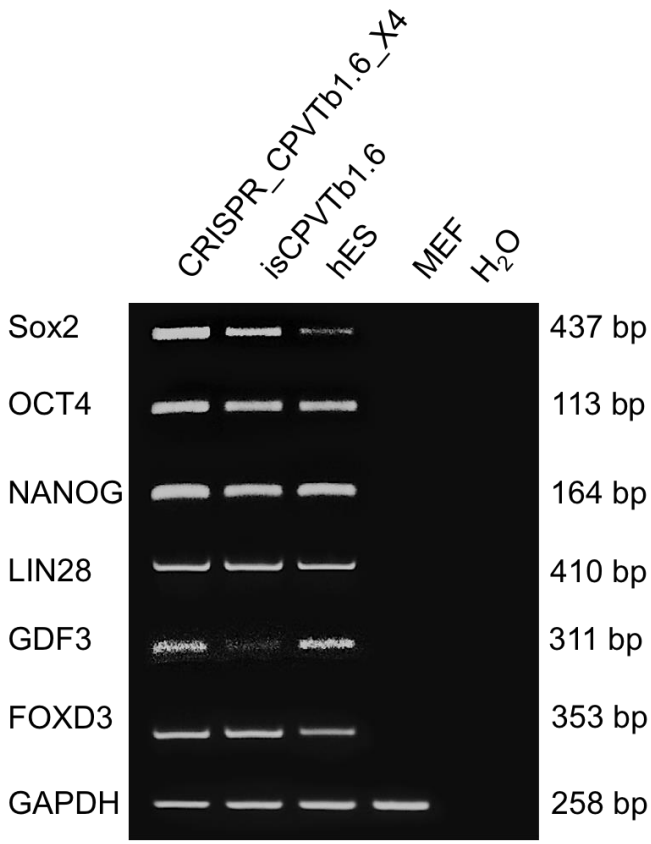

Figure 19: **Proof of pluripotent stem cell-specific marker gene expression on mRNA level.** Gel electrophoretic separations of products of RT-PCR are shown. The following marker genes were proved on their expression at mRNA level: SOX2 (437bp), OCT4 (113bp), NANOG (164bp), LIN28 (410bp), GDF3 (311bp) and FOXD3 (353bp). GAPDH (258bp) was used as internal control. The iPSC line isCPVTb1.6_X4 showed similar expression as isCPVTb1.6. The positive control was done with human ESCs. The negative control was done with MEF cells. The pluripotency-associated markers were detected in all stem cell lines.

For demonstrating the pluripotency of the CRISPR-B-1/Cas9-targeted clone X4 at protein level immunofluorescences staining was performed according to the standardized protocol. The cells were fixed with paraformaldehyde and stained with antibodies against pluripotency-specific proteins OCT4, SOX2, LIN28, NANOG, SSEA4 and TRA-1-60 and their corresponding secondary antibodies. OCT4, SOX2, LIN 28 and NANOG were expressed in the CRISPR-B-1/Cas9-targeted clone X4. The expression of surface markers SSEA4 and TRA-1-60 was also proved in the CRISPR-B-1/Cas9 targeted clone X4 (Figure 20).

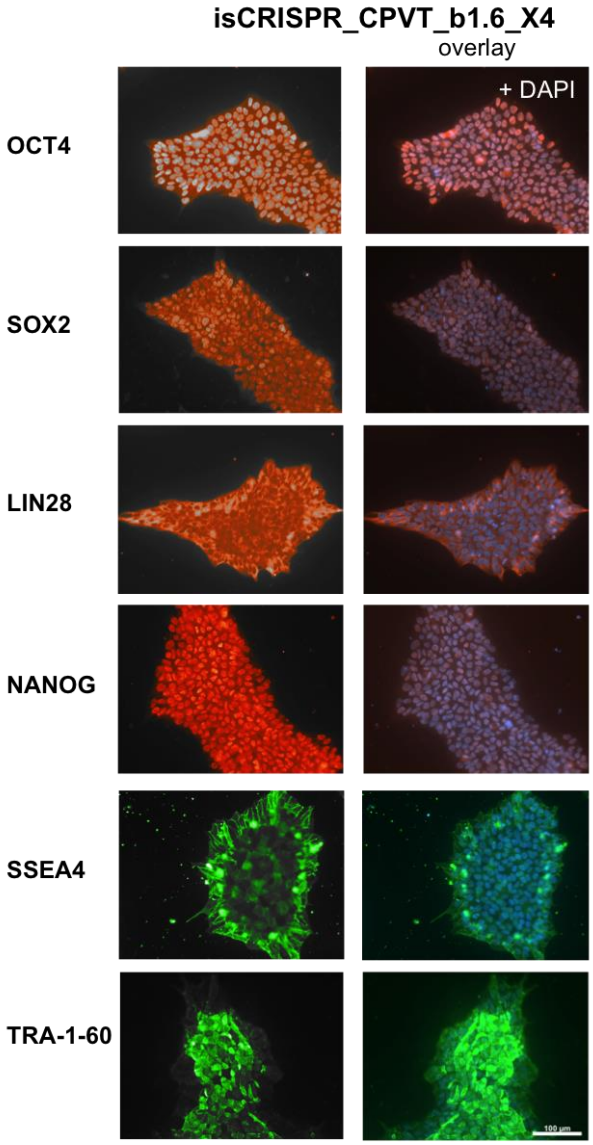

Figure 20: **Proof of the expression of pluripotency-associated marker at protein level.** The immunofluorescence staining of pluripotent stem cell-associated markers are shown and also in an overlaid picture with DAPI. The transcription factors OCT4, SOX2 and NANOG, the surface markers SSEA4 and TRA-1-60 and the cytoplasmic marker LIN28 are expressed in the examined stem cell line. The pictures were taken with a 20x image enlargement. The protein expression of pluripotency-associated markers was proven in the stem cell line. (Scale bar: 100µm)

The expression of pluripotency-associated markers was shown at mRNA and protein level. The CRISPR-B-1/Cas9-targeted clone X4 showed similar pluripotent characteristics like the non-transfected iPSCs.

After the proof of pluripotency, the CRISPR-B-1/Cas9-targeted clone X4 was differentiated into CMs for further analysis.

3.3 Cardiac differentiation

The *in vitro* differentiation of human iPSCs to cardiomyocytes was performed according to established protocols. The canonical Wnt/β-catenin signaling pathway plays a crucial role for the differentiation of iPSCs into CMs (Lian et al. 2012; Lian et al. 2013; Burridge et al. 2014). Figure 21 shows the chronological sequence of the *in vitro* differentiation protocol.

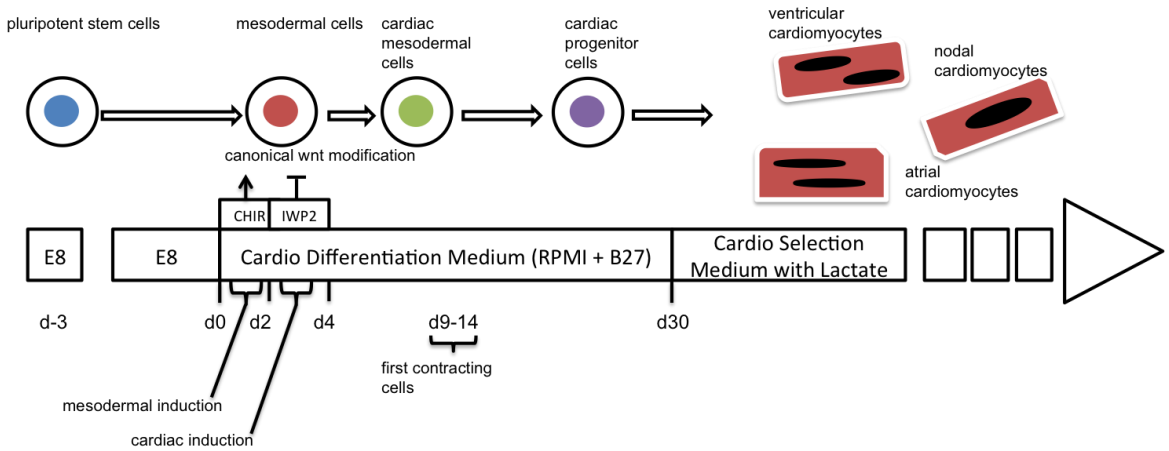

Figure 21: **Scheme of the *in vitro* differentiation protocol of human iPSCs to cardiomyocytes**. The human iPSCs were cultivated in E8 medium on Geltrex™ coated plates. After reaching a confluent cell density the mesodermal induction was started by adding CHIR [5µM] for 48h. The cardiac induction was accomplished by adding IWP2 [5µM] for another 48h. (day =d)

The isCPVTb1.6 iPSCs and the CRISPR/Cas9-targeted clone X4 were cultivated in E8 medium on Geltrex™ coated plates to a confluent cell density. The mesodermal induction got started by adding CHIR99021 [5µM] for 48h. By adding IWP2 [5µM] for another 48h the cardiac induction was accomplished. The cells were cultivated in Cardio Differentiation Medium up to day 90, while the majority of the cells show already contractile functions from day 8/9 on. A metabolic selection was performed after day 20 by using a glucose-free medium for 4-6 days with the addition of lactate to reach a high amount of CMs. The maturation of CMs to an adult-similar phenotype was carried out in a longtime culture in Cardio Culture Medium up to day 90. CMs were examined on their cell biological and functional characteristics.

First microscopically observations showed a different spontaneous beating cluster of the RyR_X4_KO_CMs compared to control isCPVTb1.6_CMs. RyR_X4_KO_CMs were beating slower and the beating pattern was not that synchronized as in control isCPVTb1.6_CMs.

3.3.1 RyR2 gene expression in RyR2-KO-CMs

The RyR2_X4_KO-CMs showed unexpectedly contractile functions, even though the RyR2 protein was destroyed by the CRISPR/Cas9 system. The CMs were screened at first for *RyR2* expression on mRNA level. The isCPVTb1.6_X4_RYR2-KO-CMs showed the similar level of gene expression for *RyR2* as the control isCPVTb1.6-CMs. GAPDH was used as a standard reference gene (Figure 22).

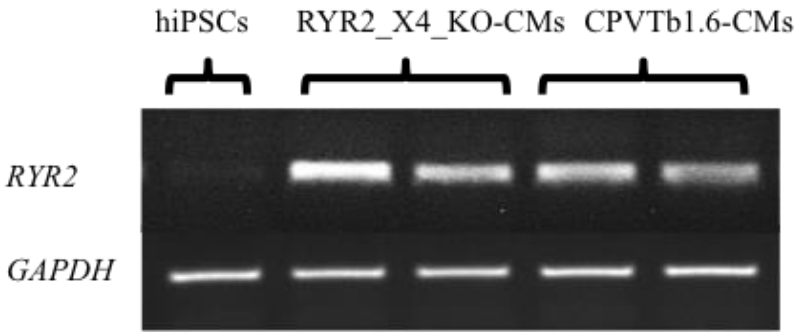

3.3.2

Figure 22: **Gene expression of *RyR2* in CRISPR-B-1/Cas9-edited isCPVTb1.6_X4-derived CMs.** The CRISPR-B-1/Cas9 manipulated iPSCs (isCPVTb1.6_X4) and control iPSCs (isCPVTb1.6) were directly differentiated into CMs and cultivated up to 90 days. The mRNA was isolated from the CMs and reverse transcribed into cDNA. The RyR2_X4_KO-CMs showed the same expression pattern for *RyR2* as isCPVTb1.6-CMs. Undifferentiated hiPSCs were used as negative control. GAPDH was used as a reference gene and was expressed by all of samples.

3.3.3 Immunofluorescence staining of RyR2-KO-CMs

To prove the ability of genetic manipulated isCPVTb1.6_X4 iPSCs to differentiate into RyR2-KO-CMs immunofluorescence staining was done. The isCPVTb1.6_X4_RYR2-KO -CMs were fixed with 4% paraformaldehyde around day 90. The isCPVTb1.6_X4_RYR2-KO-CMs were stained simultaneously against the proteins MLC2A and MLC2V, CX43 and α-actinin (Figure 23), or α-actinin and RyR2 (Figure 24).

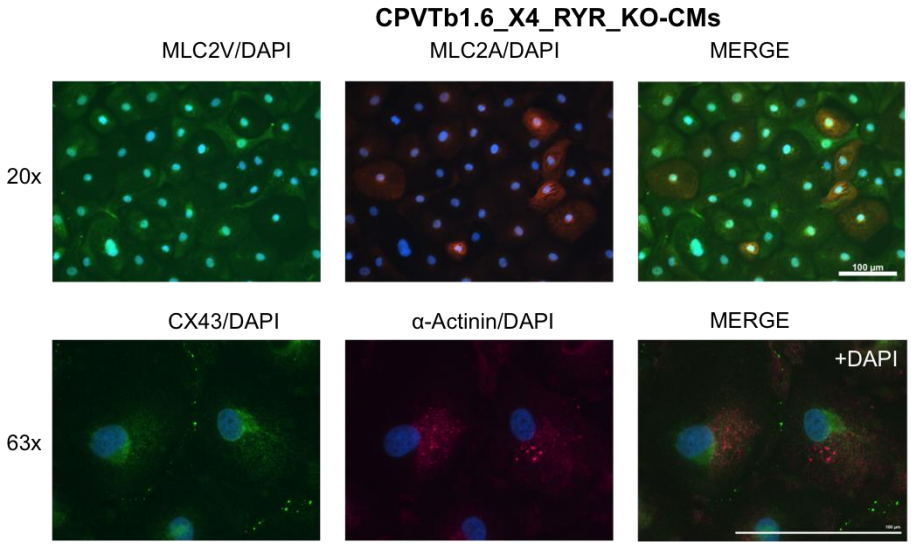

Figure 23: **Immunofluorescence staining of cardiac specific markers MLC2V, MLC2A, CX43 and α-actinin.** The simultaneous immunofluorescence staining of MLC2A and MLC2V is shown in an overlaid picture with DAPI in the first row. The pictures were taken with a 20x image enlargement. The second row shows the simultaneous immunofluorescence staining of the gap junction protein CX43 and the z-disc specific marker α-actinin in an overlaid picture with DAPI. The pictures were taken with a 63x image enlargement. (Scale bar: 100µm)

The immunofluorescence staining against CX43 and the z-disc-associated protein α-actinin showed that the majority of differentiated RyR2-KO cells were CMs. The immunofluorescence staining with the antibodies against MLC2V and MLC2A showed that most cells were positive for the ventricular marker MLC2V. Previous study showed that MLC2V is ventricular restricted and that MLC2A is highly expressed in the human atrium, but at low levels in the human ventricle (Lopes et al. 2006). The isCPVTb1.6_X4_RYR2-KO-CMs showed typical protein expression of MLC2V, MLC2A and CX43 like normal CMs.

As expected, immunofluorescence imaging showed no staining of RyR2 located in the SR in isCPVTb1.6_X4_RYR2-KO-CMs compared to isCPVTb1.6 iPSC-CMs, assuming that the RyR2 protein was not expressed in isCPVTb1.6_X4_RYR2-KO-CMs, however, typical sarcomere structures were indicated by α-actinin staining in isCPVTb1.6_X4_RYR2-KO-CMs similar to control isCPVTb1.6 iPSC-CMs. Control CMs showed a striated pattern of RyR2 as well as normal α-actinin staining (Figure 24). The RyR2 protein is responsible for the Ca^{2+} homeostasis in CMs. Nevertheless the isCPVTb1.6_X4_RYR2-KO-CMs showed unexpected contractile functions.

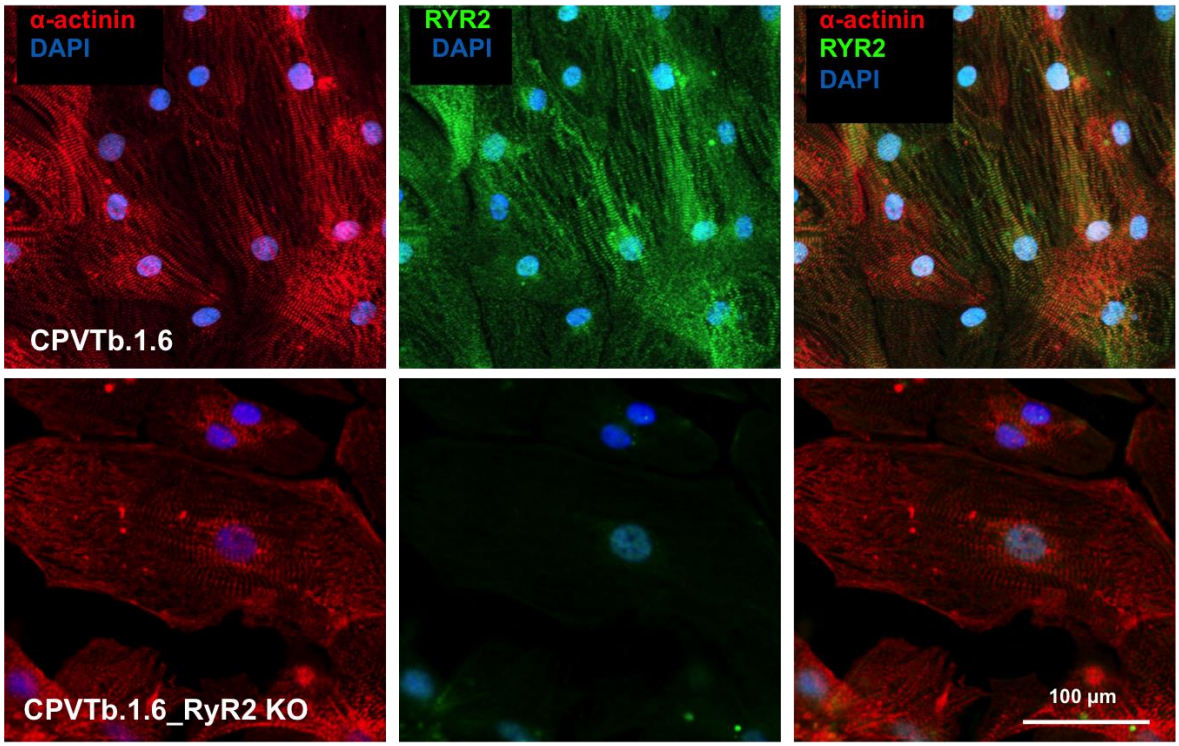

Figure 24: **Immunofluorescence staining of cardiac specific marker α-actinin and RyR2.** Immunofluorescence imaging showed no staining of RyR2 in RyR2-KO-CMs, but normal sarcomere structures indicated by alpha-actinin staining. Control CMs showed a striated pattern of the RyR2 as well as normal alpha-actinin staining. Images were taken by Sarah Henze (Scale bar: 100µm)

3.3.4 Western blot analysis of RyR2-KO-cardiomyocytes

RyR2-KO-CMs from isCPVTb1.6-X4 were analyzed for RyR2 protein expression via Western blot with the antibody recognizing the full length protein of RyR2. CMs derived from the origin iPSC line isCPVTb1.6 were used as control. Whereas the RyR2 protein was detected in CMs derived from the control cell line isCPVTb1.6, Western blot analysis showed no detectable RyR2 protein in RyR2-KO-CMs. CTNT was used to determine the CM proportion and no obvious differences could be detected in CM amount in the different samples (Figure 25). This analysis further confirmed the successful generation of a RyR2 protein knockout iPSC line.

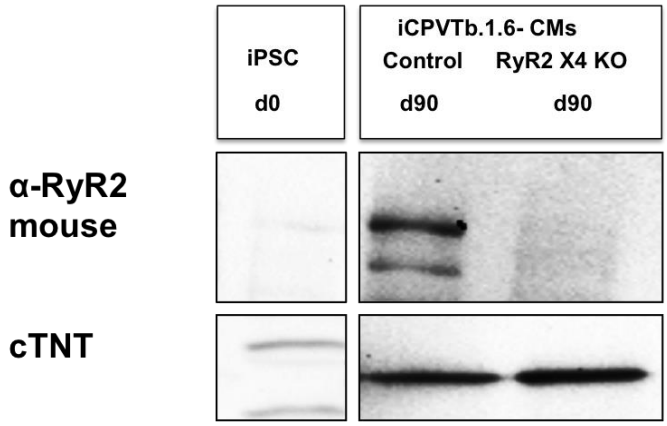

Figure 25: **Western blot analysis of the RyR2 protein in RyR2-KO-CMs.** The RyR2 protein was not detectable in RyR2-KO-CMs. The KO cell line from one iPSC patient was tested (CPVTb1.6-X4) with the antibody recognizing the full length protein of RyR2 (α-RyR2 mouse). cTNT was used to determine the CM proportion. Images were taken by Sarah Henze.

3.3.5 Calcium imaging of RyR2-KO-CMs

Confocal calcium imaging offers optical tracking of Ca^{2+}-transients in cells via fluorescence linked signal recognition. Ca^{2+} plays a crucial role for the CM contraction. An untypical Ca^{2+} homeostasis in the KO-CMs derived from isCPVTb1.6_X4 iPSC line was expected, because of the non-expression of RyR2. RyR2 plays a crucial role during the Ca^{2+} homeostasis. It releases Ca^{2+} from the SR into the cytoplasm during a contractile phase, which is essential for the contraction induced by high intracellular Ca^{2+} concentration. The KO-CMs differentiated from isCPVTb1.6_X4_RYR2-KO iPSC line were examined for their calcium cycling characteristics.

The KO-CMs from the cell line isCPVTb1.6_X4 as well as CMs from the control isCPVTb1.6 were examined around day 90. Fluo-4/AM- a calcium-sensitive dye, was used during the confocal laser scanning microscopy to test the calcium cycling characteristics of the CMs. Calcium sparks during calcium imaging are the microscopic release of Ca^{2+}, which corresponds approximately with the Ca^{2+} release from the SR especially via RyR2 into the cytoplasm during diastole.

The calcium imaging of RyR2-KO-CMs showed no calcium sparks when they were paced at 0.25 Hz in comparison to the control CMs (isCPVTb1.6-Control). This confirms the absence of a defect RyR2 like in CMs derived from CPVT patients.

Ca^{2+} transients were measured by confocal line scan imaging. RyR2-KO-CMs showed smaller amplitudes and a slower decrease to baseline in comparison to the control CMs, when they were stimulated with 0.25 Hz. (Figure 26).

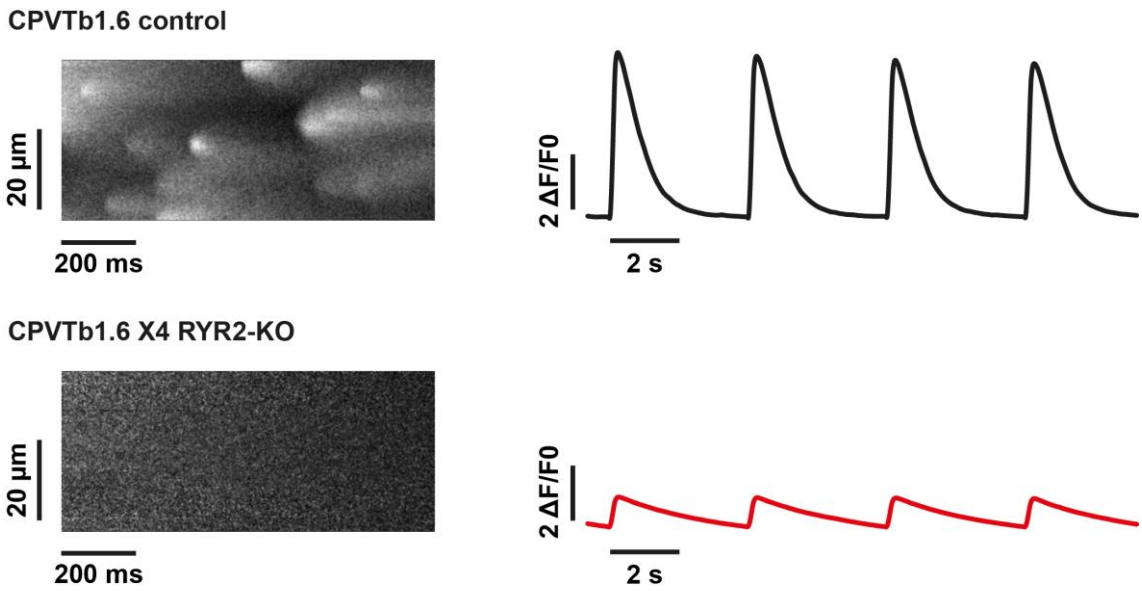

Figure 26: **Calcium imaging of RyR2-KO CMs.** All CMs were loaded with fluo-4/AM around day 90 and were stimulated with 0.25 Hz. No calcium sparks were detected in the RyR2-KO-CMs stimulated with 0.25Hz. The control CPVT-CMs showed Ca^{2+}sparks under stimulated conditions. Ca^{2+}transients were shown by the use of confocal line scan imaging. The amplitudes of the Ca^{2+} transients were smaller and the decrease of the Ca^{2+} to baseline was slower in RyR2-KO CMs (red graph) compared to the data of the control-CMs (black graph Images were taken by Sarah Henze and Lukas Cyganek

4 Discussion

CPVT is a genetic cardiac disorder leading to sudden cardiac death in young patients without structural abnormalities of the heart. Over 150 mutations in the *RyR2* gene causing CPVT1 have been identified so far (Lehnart et al. 2008). Thereof, several mutations have been studied in either transgenic mice or cell models. Abnormal Ca^{2+} handling in CMs causes severe arrhythmia during physical or emotional stress through missense mutations in the *RyR2* or *CASQ2* gene (Jiang et al. 2002; Cerrone et al. 2009).

The aim of the thesis was to establish an *in vitro* disease model using hiPSCs from CPVT1 patients. The patients carry a heterozygous missense mutation in the *RyR2* gene. Two iPSC lines (isCPVTc2.2 and isCPVTc2.3) from one CPVT patient, who was heterozygous for a point mutation in the *RyR2* gene (E4076K), were characterized for their pluripotency within this study. According to the standardized pluripotency characterization procedure, pluripotency-associated markers were shown on both mRNA and protein level. Germ layer-specific markers were shown as well on protein level.

The second aim was to correct a point mutation in the *RyR2* gene from a second patient (A2254V) and to create a knockout cell line of the RyR2 protein via CRISPR/Cas9-based genome editing. 68 cell clones were tested for genome editing after hiPSC transfection and expansion. One CRISPR/Cas9 targeted cell clone (X4) had four homozygous nucleotide deletions on both alleles of the genome causing a frame shift, which finally resulted in a premature stop codon in the *RyR2* gene. The point mutation A2254V in the *RyR2* gene was corrected as well. By this way, we have not only managed to correct the point mutation in the *RyR2* gene, but also managed to create a RyR2-KO hiPSC line. However, we have not been able to create a corrected RyR2 cell line alone. The engineered RyR2-knockout hiPSC line was examined for pluripotency-associated markers and differentiated into functional CMs for further analysis. The RyR2-KO-CMs showed no detectable RyR2 protein expression, which was shown by using Western blot analysis. In addition, an analysis of the Ca^{2+} handling in the RyR2-knockout CMs was performed and the results were compared to control CPVT-CMs. The RyR2-KO-CMs showed no Ca^{2+} sparks under stimulated conditions with 0.25 Hz in comparison to the control CPVT-CMs, which showed the CPVT-specific Ca^{2+} sparks via Ca^{2+} imaging.

4.1 Establishing hiPSCs from CPVT patients

Yamanaka's work in 2006 and 2007 was a breakthrough for the medical world. It laid the foundation for the generation of hiPSCs from somatic cells by reprogramming them with defined factors (Takahashi and Yamanaka 2006; Takahashi et al. 2007). HiPSCs are used for patient specific disease models and for therapeutic applications as well as in drug discovery and in regenerative medicine.

The CPVT iPSC lines used in this study were generated by reprogramming of fibroblasts from the CPVT-patients with the SeV through the overexpression of the four Yamanaka factors OCT4, SOX2, KLF4 and C-MYC. SeV was chosen due to its replication, which takes place exclusively in the cytoplasm of infected cells. This in turn minimizes the risk of unwanted integration into the host genome (Li et al. 2000). By this way, the generated hiPSCs were transgene-free (Fusaki et al. 2009).

The process of reprogramming somatic cells to hiPSCs is currently not fully comprehensible. It contains the suppression of somatic cell-specific genes and the activation of pluripotency specific transcription network. A change in the metabolic system from oxidative phosphorylation in somatic cells to a glycolysis-based metabolism in hiPSCs and a mesenchymal to epithelial transition are additionally induced (Samavarchi-Tehrani et al. 2010; Zhang et al. 2012). In this study, the isCPVTc2.2 and isCPVT2.3 iPSCs are proved to be positive for the transcription factors like the "core factors" OCT4, NANOG and SOX2 and additionally LIN28, FOXD3, GDF3, SSEA4 and TRA-1-60, which are necessary to maintain pluripotency in hESCs and hiPSCs. The maintenance of the pluripotency network of ESCs and hiPSCs is based on the expression and activation of the transcription factors including OCT, SOX2 and NANOG (Boyer et al. 2005). SOX2 and OCT4 bind DNA co-operatively to activate the transcription of key pluripotency factors. Both factors maintain their own expression through a feedforward auto-regulatory loop of pluripotency (Chambers and Tomlinson 2009). NANOG functions in combination with OCT4 in order to maintain pluripotency and to sustain self-renewal of ESCs (Cavaleri and Schöler 2003; Chambers et al. 2003). NANOG and KLF4 have common targets and are important for the self-renewal as well as the regulation of the transcription of pluripotency factors (Jiang et al. 2008). The reprogramming of somatic cells is not fully dependable on C-MYC but its expression plays an important role in increasing the reprogramming efficiency. C-MYC influences cell proliferation, biosynthetic pathways and metabolism (Nakagawa et al. 2010; Nakagawa et al. 2016).

Other factors as LIN28, FOXD3, GDF3, SSEA4 and TRA-1-60 are also highly expressed in hESCs and down-regulated in differentiated cells (Boyer et al. 2005; Kim et al. 2008). The generated hiPSCs in this study showed the same characteristics as hESCs. The morphology and the ALP expression as well as the mRNA expression of pluripotency-associated markers like *OCT4, SOX2, NANOG, LIN28, FOXD3* and *GDF3* were comparable to the characteristics of hESCs. Additionally, OCT4, SOX2, LIN28, NANOG, SSEA4 and TRA-1-60 were expressed on protein level. These characteristics show that the ectopic expression of *OCT4, SOX2, KLF4* and *C-MYC* during reprogramming activated the expression of endogenous pluripotency genes and proteins, which were maintained during long-term culture (Kim et al. 2008; Fusaki et al. 2009).

An important characteristic of hiPSCs is the potential to differentiate into derivatives of all three germ layers (Itskovitz-Eldor et al. 2000; Sheridan et al. 2012). The expression of specific markers for each of the three germ layers was shown after spontaneous *in vitro* differentiation of the CPVT-hiPSCs on protein level, which ultimately demonstrates that the cells are pluripotent. The expression of the associated germ layer-specific marker on mRNA level could not have been shown, due to a laboratory mistake in the spontaneous mass culture experiment. This experiment should be repeated in the future to fulfill the standardized characterization of the isCPVTc2 cell lines.

To verify the cell line identity, patient-specific isCPVTc2.2 and isCPVTc2.3 lines were sequenced in the lab before starting the thesis work. The previous sequencing confirmed the heterogeneous missense mutation in the *RyR2* gene (E4076K) (data not shown).

In summary, the analyzed two CPVT-hiPSC lines (isCPVTc2.2 and isCPVTc2.3) have similar characteristics as hESCs and meet the standards of fully reprogrammed hiPSCs.

4.2 CRISPR/Cas9

CRISPR/Cas9 systems originally function as an adaptive immune system in bacteria against viral DNA, plasmids or foreign RNA. The systems have been adapted to genome engineering tools, which are able to generate DSBs in predicted regions of the eukaryotic genome in order to generate either knock-outs or knock-ins and to correct endogenous genetic mutations. To the current state of research it is the most efficient technology for genome editing (Garneau et al. 2010; Jinek et al. 2012; Doudna and Charpentier 2014).

CRISPR/Cas9 was chosen in this project for genome editing because of the broad advantages in comparison to ZNF and TALEN. The major advantage of the

CRISPR/Cas9 technology is the simplicity of the target design. The DNA-binding moiety in CRISPR/Cas9 uses RNA, whereas ZFN and TALEN use protein, which makes the design more complex. Also, the costs for the CRISPR/Cas9 technology are much lower in comparison to ZNF and TALEN, caused by the simplicity of the CRISPR/Cas9 design and the possibility to use standard cloning procedures and oligo syntheses to multiply the system. A further advantage of the CRISPR/Cas9 technology is the possibility to introduce multiple DSBs in the same cell via expression of distinct guide RNAs, which is called multiplexing (Kabadi et al. 2014).

The ability to design custom-specific CRISPR/Cas9 complexes offers the opportunity to manipulate biological organisms on almost every arbitrary location of the genome. On the one hand, this renders the opportunity for a potential treatment of genetic disorders by correcting disease-causing mutations. On the other hand, the potential for unethical genetic manipulations, which is causing a huge discourse in the society (Musunuru 2017) could be an outcome. The CRISPR/Cas9 complex is guided by a 20-nucleotide crRNA, which is complementary to the targeted DNA sequence in a defined location where the DSB should occur. The DSB is repaired either by NHEJ or by HDR repair mechanisms. The repair of the broken DNA by NHEJ might introduce unspecific small indel. Conversely the HDR repair mechanism leads to a targeted genetic correction or manipulation in the presence of a donor DNA plasmid or ssODN flanking the DSB site (Sander and Joung 2014).

We established a protocol for the use of CRISPR/Cas9 to manipulate isCPVTb1.6 iPSCs. The isCPVTb1.6 hiPSCs were transfected with ssODNs and a CRISPR/Cas9 combined plasmid. The aims of this experiment were primarily to create a frameshift in the *RyR2* gene by unspecific deletions via NHEJ to create homozygous RyR2 knockout cell lines and secondly to correct the point mutation (A2254V) in the *RyR2* gene causing the disease phenotype by HDR. This should prove the hypothesis that the observed CPVT-phenotype in isCPVTb1.6 iPSC-CMs is caused by the point mutation in the *RyR2* gene and can be annihilated in CRISPR/Cas9 corrected CMs.

A 20 bp sequence in close proximity to the intended DSB was chosen for a successful binding of the CRISPR/Cas9 complex on the DNA guided by a gRNA. The ssODNs were designed as a template, which contains the corrected sequence for the genetic correction of the point mutation via HDR. Ideally, the mutation should be in close proximity (<20 bp) to the targeted site of the nuclease to guarantee high targeting frequencies (Hsu et al. 2013). In this study, the gRNA was designed with the help of an online tool to minimize the

mismatch and off-target activity. The mismatch activity was predicted to be low. Two off-target sites where detected. The PAM was 34 bp close to the targeted site. The gRNA was included into the CRISPR plasmid construct and ordered at Sigma Aldrich.

A mismatch-specific endonuclease assay was performed to measure the direct *RyR2* interruption induced by the designed CRISPR/Cas9 plasmid. The cleavage efficiency was around 15-20%, which resembles the value of the positive control of the kit. One of the key limitations for successful CRISPR/Cas9 experiments in human cells is that they prefer to take the NHEJ pathway to repair a DSB instead of using the precise HDR pathway (Chapman et al. 2012). The amount of successful CRISPR-mediated gene knockout experiments via NHEJ-induced indel mutations predominates the amount of successful precise corrections of point mutations or introductions of sequence fragments via HDR in hiPSCs. Only a few working groups have been able to correct missense mutations in hiPSCs by using CRISPR/Cas9 (Chang et al. 2015; Huang et al. 2015; Tang et al. 2016; Turan et al. 2016).

These groups used either plasmids containing the designed CRISPR/Cas9 complex and the gRNA and ssODNs, which were transfected into iPSCs via nucleofection, or adenoviral mediated genome editing. For our gene editing experiments, we used ssODNs together with CRISPR/Cas9 plasmids to induce HDR. The transfection efficiency after nucleofection was below 5%, which is typical for hiPSCs as a difficult-to-transfect cell type. However, the positive-transfected CPVT-hiPSCs could be sorted by an additional GFP signal within the plasmid. FACS was used to select the GFP^+ cells. Just a small amount of transfected CPVT-hiPSCs survived the cell sorting, which was limiting the experiment. In spite of the low transfection efficiency and the low survival rate, 68 iPSC clones were screened after hiPSC transfection and after cell sorting and expansion. One of the reasons for the low survival rate after the transfection of the hiPSCs could be the After-FACS medium, which may have too less nutrients. A more nutrient hiPSC medium like StemMACS iPS Brew XF medium could be used in future experiments in order to increase the survival rate of the transfected hiPSCs by inducing a faster recovery after stressful situations. Valamehr's working group had a higher survival rate while using a survival cocktail with different small inhibitors compared to our results with the single use of TZV (Valamehr et al. 2012). A combination of these two approaches could be the key for a higher survival rate after nucleofection in future experiments. A further troubleshooting event for the low survival rate could be the quantity and quality of the Cas9 and sgRNA

plasmid, which was produced with maxiprep. It is essential to ensure a high concentration of the plasmid > 2mg/ml and that endotoxin-free materials are used. If there is a difference in the survival of the transfected and control cells, the DNA quantity needs to be controlled. Furthermore the sg RNA should not target a gene which is essential for cell survival, which leads to troubleshooting events (Byrne and Church 2015).

Our results showed that <4% of the cell clones, which were analyzed by PCR and restriction digestion, displayed a genomic modification.

After PCR and restriction enzyme digestion with SpeI, one sequenced clone isCRISPR_CPVTb1.6_X4 had a ssODN based sequence in its genome. The clone had additionally integrated indels in the *RyR2* gene besides the desired correction of the point mutation. The second sequenced clone isCRISPR_CPVTb1.6_X2 had integrated indels earlier in the genome, leading to a complete destruction of the *RyR2* gene. One possibility is that CRISPR/Cas9 could cleave the DNA again after a first HDR-mediated genomic correction. Some studies showed an increase of HDR efficiency without further indels by using ssODNs with silent missense mutations to prevent inadvertent cleaves by CRISPR/Cas9 after HDR (Paquet et al. 2016). Our study failed to confirm this hypothesis after using a new designed ssODN with a silent missense mutation. We were not able to cultivate a single clone using the new designed ssODNs.

In addition, because of the failure to create a clone with an isolated genetic correction instead of additional unspecific indels, we assume that HDR works inefficient in hiPSCs. The use of small molecules to increase the efficiency of CRISPR/Cas9 mediated gene editing in hiPSCs improved the amount of HDR after DSB in diverse studies (Maruyama et al. 2015; Yu et al. 2015).

The major challenge of the CRISPR/Cas9 technology is the high off-target activity. In comparison to other gene editing technologies like TALEN, CRISPR/Cas9 shows a higher and unspecific off-target activity (Frock et al. 2015). Several working groups are investigating new approaches to reduce the off-target activity to push the technology ahead to clinical standards for disease treatment without unspecific off-target mutagenesis. An approach to reduce the off-target activity of the CRISPR/Cas9 plasmid is a better design of the sgRNA. Half of the human genome consists of repeated sequences concluding that a high specificity of the sgRNA is needed to sustain minimal off-target activity. To achieve a minimal off-target activity, the use of web-based bioinformatics tools and algorithms was established. However, the use of these tools has limitations. The off-target activity and the

cleavage activity are influenced by many factors, which delimitate the predictions of the algorithms. Pelletier's group showed that the use of sgRNA with a PAM-distal complementary and with a minimum guide length of 17 nucleotides reduces the off-target activity and engaged the Cas9 targeted cleavage. The sequences distal to PAM should trigger a conformational change of Cas9 to boost the CRISPR/Cas9 DNA target cleavage (Cencic et al. 2014). However, the possible mismatch tolerance of Cas9-sgRNA complexes fosters the off-target cuts in the genomic DNA. Although we ordered a custom designed CRISPR/Cas9 plasmid at Sigma-Aldrich with low predicted off-target effects via bioinformatics tools, a tolerance of mismatches exists. The state of science is the avoidance of off-target activity for a precise genome editing (Hsu et al. 2013; Cho et al. 2014; O'Geen et al. 2015; Zhang et al. 2015). Another strategy to reduce off-target activity is to weaken interactions between Cas9 and the non-complementary DNA strand. A positive electric cloud is formed among the minor binding channel of the nuclease (NUC) lobe and creates a pulling force of the NUC lobe. The NUC lobe is elementary to separate the non-target DNA from the gRNA-target DNA heteroduplex while unwinding the double strand protospacer DNA and during the formation of the gRNA-target DNA heteroduplex. CRISPR-Cas9 DSB specificity changes, if there are modifications in the positively charged amino acids of the NUC lobe. This changes the positive electric density along the minor binding channel of the NUC lobe. A balanced system needs to be designed. Pulling forces, which are too strong, as well as weak pulling forces result in a higher off-target DSB activity through a misbalanced interaction between the gRNA and the non-target DNA. Due to positive charged amino acids the pulling force is strong and weakens the hydrogen bonds between the two strands of the protospacer DNA. The detachment of the gRNA from the non-target DNA becomes easier and the formation of a heteroduplex with the target DNA strand is favored. The outlook is a systematical identification of amino acids responsible for each base pair position of the protospacer sequence for targeted engineering of each DNA site with almost no off-target activity (Slaymaker et al. 2016; Zhang et al. 2016). A further approach is the use of SpCas9-HF1, a high-fidelity variant harboring alterations designed to reduce non-specific DNA contacts. Joung's working group showed data with almost no off-target activity in comparison to the standard SpCas9. The high-fidelity variant can be used to target non-repetitive sequences that do not have closely matched sites elsewhere in the genome (Kleinstiver et al. 2016).

Avoiding off-target activity is necessary for future *in vitro* and especially *in vivo* studies and therapeutic use of CRISPR/Cas9 to eliminate the risk of off-target mutagenesis (Lee et al. 2016a). This can be achieved by a specific design, accessibility of sgRNA and an identification of amino acids responsible for each base pair positon of the protospacer sequence. A gRNA truncation and a gRNA elongation is discussed to reach a lower off-target activity and a higher on-target activity (Kim et al. 2015). By increasing the overall length from 20 to 40 bp a higher specificity for the Cas9 nickases can be reached (Tsai et al. 2014). Furthermore Cas9 orthologs with different PAM requirements for example with longer PAM sequences as Staphylococcus aureus Cas9, Streptococcus thermophilus Cas9 and Neisseria meningitidis Cas9. These Cas9 orthologous have been already adopted for genome editing in mammalian cells and a lower off-target activity was detected (Ran et al. 2015; Lee et al. 2016b; Müller et al. 2016).

4.3 Generation of CMs out of CRISPR/Cas9 targeted hiPSCs

In this study we have not been able to correct the missense mutation in the *RyR2* gene in hiPSCs derived from the CPVT patient b1. The designed CRISPR/Cas9 vectors introduced additionally indels after HDR. However, this resulted in a successful genetic alteration in the *RyR2* gene, which was the second aim of our protocol. The CRISPR/Cas9 targeted hiPSC clone displayed a correction of the mutation and an additional homozygous deletion in the *RyR2* gene, which was confirmed by genetic sequencing. The deletion of 4 bps caused a frameshift of the coding sequence and resulted in a premature termination codon and a truncated RyR2 protein.

The CRISPR/Cas9 targeted CPVT-hiPSCs were examined for the maintenance of pluripotency after genetic manipulation. The CRISPR/Cas9 targeted CPVT-hiPSCs showed similar characteristics like the patient-specific iPSCs or hESCs. The morphology and ALP activities and the mRNA expression of pluripotency related markers like *OCT4, SOX2, NANOG, LIN28, FOXD3* and *GDF3* were comparable to parental isCPVTb1.6 iPSC and hESC characteristics. Additionally, OCT4, SOX2, LIN28, NANOG, SSEA4 and TRA-1-60 were expressed on protein level. The expression of the pluripotency related markers on mRNA and protein level showed that there was no manipulation of the pluripotency characteristics in the CRISPR/Cas9-targeted CPVT-hiPSCs after genomic editing.

Based on our literature research, no knockout hiPSC line of the *RyR2* gene exists so far. The RyR2 function was usually analyzed in mouse knockout models instead of in hiPSC-derived CMs. Takeshima et al. showed in 1998 that mice with a homozygous deletion of *RyR2* had an embryonic lethality around day 10 through cardiac arrest (Takeshima et al. 1998). This leads to the assumption that functional RyR2 is essential for mammalian survival. Heterozygous mice had alterations in ECG recordings and membrane potential measured in urinary bladder smooth muscle cells (Hotta et al. 2007). Bround et al. showed that adult mice developed brachycardiac and intermittent tachycardiac arrhythmias after reducing the amount of RyR2 in an inducible cardiac-specific heterozygous knockout mice model (Bround et al. 2012). These studies show that RyR2 is essential for a normal cardiac function and thus demonstrate the importance of a better understanding of its function for future drug targets. The translation from mouse models to human models is limited. The animal model CMs for *in vivo* studies display major differences in cellular electrophysiology and limitations in predicting drug responses compared to human CMs. This animated us to create hiPSC-derived CMs from the generated homozygous *RyR2*-KO-hiPSCs (isCPVTb1.6_RyR2_X4_KO) for further investigation of the RyR2 function and possible adaption and compensation mechanisms in the Ca^{2+} cycling.

The *RyR2*-KO-hiPSCs were differentiated into CMs according to our standardized protocol, which imitates the embryonic developmental signals. First, activation of the WNT signaling pathway induced mesoderm formation. Inhibiting the WNT, BMP and TGFβ pathways induced the cardiac specification subsequently (Burridge et al. 2011; Kattman et al. 2011).

CMs were selected around day 20 through metabolic selection, where glucose was replaced with lactate for 4-6 days to obtain a high amount of pure CMs (Tohyama et al. 2013). Glucose deprivation gains the proportion of pure CMs from 85% $TNNT2^{+}$ to >95%, which is beneficial for further analyses (Burridge et al. 2014). Experiments without metabolic selection showed a high amount of CMs overgrown with neural or fibroblast-like cell types. The generated CMs were cultivated up to day 90 to reach a higher maturation phenotype resembling CMs at fetal stages, assuming that the characteristics of iPSC-CMs could correlate with the characteristics of heart muscle cells of CPVT patients. CPVT patients develop first symptoms during childhood and young adolescence, when the embryonic development of the heart is already completed. Our aim was to compare the *RyR2*-KO-CMs with CMs derived from CPVT patients without genetic manipulation. The

RyR2-KO-CMs showed an aberrant beating cluster compared to CPVT-CMs. The beating was slower and displayed a delayed onset of first contractions during cardiac differentiation. The data of this study showed that *RyR2*-KO-CMs had no difference in *RyR2* mRNA expression compared to the corresponding CPVT-CMs, whereas on protein level RyR2 was not detectable in CRISPR/Cas9-edited CMs in comparison to CPVT-CMs assessed by Western blot analysis. Both *RyR2*-KO-CMs and CPVT-CMs showed comparable expression of typical cardiac markers like MLC2v, MLC2A, α-ACT, and CX43 and displayed well-organized sarcomeric structures. CX43 was used as a marker for gap junctions, which are important for cell-to-cell contact and electrical signals between CMs. The expression of sarcomere and gap junction proteins, which are elementary for the cardiac function, in *RyR2*-KO-CMs was comparable to the expression in CPVT-CMs. Only RyR2 was not detectable on protein level in *RyR2*-KO-CMs, whereas α-ACT as a marker for cross-striation was detectable by immunofluorescence staining. The conclusion based on this data is that the frame shift induced a fully degraded RyR2 protein in *RyR2*-KO-CMs.

Against our expectations, *RyR2*-KO-CMs contract after cardiac differentiation. Functional analyses via calcium imaging showed that no uncontrolled Ca^{2+} sparks were detectable in *RyR2*-KO-CMs, whereas CPVT-CMs showed typical Ca^{2+} sparks, when they were stimulated with 0.25Hz during Ca^{2+}imaging. The amplitudes of Ca^{2+} transients in *RyR2*-KO-CMs were smaller compared to the amplitudes of the control CPVT-CMs (Henze 2016). The calcium transients displayed a different shape leading to the assumption that IP3 or different Ca^{2+} homeostasis proteins regulate the Ca^{2+} release. This results in a different Ca^{2+} homeostasis pattern compared to the physiological RyR2-mediated Ca^{2+} release. The small amplitudes of the Ca^{2+} transients in *RyR2*-KO-CMs could be a result of a failure in the Ca^{2+} release from the SR through RyR2. We speculate that compensatory mechanisms might regulate the Ca^{2+} homeostasis in CMs without the RyR2 protein. CMs need to adapt the expression of Ca^{2+} regulatory proteins to compensate for the loss of function of the RyR2. One hypothesis is that CMs generated from hiPSCs resemble immature CMs with an immature functioning of the SR in terms of their Ca^{2+} handling compared to adult CMs (Lee et al. 2011). During early cardiogenesis, IP3 is upregulated already at day 5.5 whereas RyR2 upregulation does not begin until day 8.5 in mouse models. IP3 is responsible for the Ca^{2+} homeostasis in early CMs (Rosemblit et al. 1999). The IP3-gated Ca^{2+} release may compensate for the function of the missing RyR2 in RyR2-

KO-CMs. This Ca^{2+} release is sufficient to induce the cardiac contraction in early stage of cardiogenesis (Janowski et al. 2010). Supporting the hypothesis that IP3 compensates for the RyR2 function, Go et al. showed that RyR2 is downregulated and IP3 is upregulated during end-stage heart failure when fetal gene programs are reactivated as a compensatory response (Go et al. 1995). Further compensatory mechanisms could be the activation of the Fas signaling pathway as observed in heart failure patients. The Fas receptor activation induces the phospholipase C, which activates 1,4,5-IP3 leading to a Ca^{2+} release from the SR (Barac et al. 2005). The role of mitochondrial Ca^{2+} release is not fully understood yet, but it could be a further mechanism to resemble the loss of function of RyR2It is postulated that Ca^{2+} and ROS release from the mitochondria can be induced through direct protein-protein interaction initiated by shear/flow forces. The mitochondrial Ca^{2+} release is a response to mechanical forces like the cell contraction (Beutner et al. 2001; Belmonte and Morad 2008). NCX1 is a Na^{+}/Ca^{2+} exchanger protein, which is able to function in forward and reverse modes. In reverse mode, NCX1 is capable of Ca^{2+} influx. In early cardiogenesis NCX1 functions in reverse mode. Through the Ca^{2+} influx, NCX1 has a major role in generating the Ca^{2+} transient at the earliest stage of cardiac contraction (Iwamoto 2004). The NCX1 may compensate for the RyR2 function in early stage of cardiogenesis, when a functional SR is not yet required and the Ca^{2+} homeostasis is regulated by NCX1 and other proteins (Tyser et al. 2016). Future investigation should be performed to figure out which compensatory mechanisms occur in RyR2-KO-CMs.

Heart failure studies with animal models and human heart tissue showed significant changes in the expression of proteins associated with the excitation-contraction coupling. The RyR2 expression is decreased by up to 25% in rabbit or up to 30% in canine models of aortic insufficiency, 48% in a canine model of chronic heart failure by pacing and 35% in human heart failure (Go et al. 1995; Ai et al. 2005; Kubalova et al. 2005; Song et al. 2005). These studies lead to the assumption that the compensatory mechanisms in these models could be comparable to our knockout model. The expression of SERCA is suppressed and the degree of the damage could correlate with the severity of symptoms seen in human failing compared to non-failing hearts (Hasenfuss et al. 1994). In addition, the NCX expression in heart failure patients is increased. The exact function of the NCX in human heart failure has not yet been definitely established. The Ca^{2+} influx via the NCX can increase the SR Ca^{2+} content in CMs. These effect was shown in CMs from infarcted hearts with a modest NCX activity (Litwin and Zhang 2006). The combination of increased

NCX and decreased SERCA expression leads to increased cellular extrusion and a decreased Ca^{2+} store in the SR (Hasenfuss et al. 1994; Reinecke et al. 1996; Litwin and Zhang 2006). This limits the cytosolic Ca^{2+} available for contractile protein maintenance (Blayney and Lai 2009).

Further investigation of possible compensatory mechanisms for the loss of function of the RyR2 in *RyR2*-KO-CMs could aid our understanding of molecular mechanisms controlling calcium handling during early cardiogenesis and in human heart failure.

4.4 Conclusions and outlook

The findings of this study underlie that patient-specific hiPSCs are a promising tool for studying human diseases and for detailed investigation of mutations in the *RyR2* gene of CPVT patients. A RyR2 knockout model for a better understanding of the RyR2 channel and the Ca^{2+} homeostasis in CMs complemented the CPVT disease model. CPVT-hiPSCs were successfully characterized and differentiated into ventricular-like CMs. The establishment of these protocols was essential for further investigations especially for the CRISPR/Cas9 assisted genome editing in hiPSCs and the following differentiation into CMs.

CRISPR/Cas9 systems were used for genome editing in hiPSCs derived from one CPVT patient. CRISPR/Cas9 edited hiPSCs were generated, yet it was not possible to create isogenic corrected controls of the hiPSCs derived from the CPVT patient.

A further approach to prove the concept of the disease phenotype of a specific point mutation would be to introduce the mutation in healthy hiPSCs to generate heterozygous hiPSCs with the mutation and study the mutation-specific phenotype. These genetic manipulated cells could be compared with CPVT-patient derived hiPSCs. The primary recruiting of CPVT-patients would not be necessary and it would be easier and faster to create more mutations in the *RyR2* gene. The big disadvantage of this study design is that the cells would not be patient specific anymore, which does not take the patient-specific genetic factors into account and not fit well with the approach of personalized medicine. Furthermore, new experiments could be designed using new approaches to reduce the re-cutting possibility and the off-target activity in CRISPR/Cas9 systems.

A homozygous CRISPR/Cas9-edited hiPSC line with a complete knockout of the RyR2 protein was generated in this study. The isCPVTb1.6_RyR2_X4_KO-CMs show no detectable expression of the RyR2 protein. CMs derived from isCPVTb1.6_RyR2_X4_KO

have altered Ca^{2+} transients with respect to amplitude and shape. The RyR2_X4_KO-CMs are a useful model for further studies to examine the Ca^{2+} homoeostasis in these CMs with a loss of the RyR2 protein. The Ca^{2+} homoeostasis can be compared with the Ca^{2+} homeostasis in CMs of patients with severe heart failure or with the Ca^{2+} homoeostasis during early CM differentiation because of the modified expression profile of calcium channel proteins during cardiogenesis. The future understanding of the compensatory mechanisms of the genome-edited CMs can lead to a better understanding of the RyR2 function.

5 Abstract

CPVT is a genetic cardiac disorder leading to sudden cardiac death in young patients without structural abnormalities of the heart. Abnormal Ca^{2+} handling in CMs causes severe arrhythmia during physical or emotional stress through missense mutations in the *RyR2* or *CASQ2* gene. Over 150 mutations in the *RyR2* gene causing CPVT1 have been identified so far. The exact underlying pathomechanism causing a typical disease pattern induced by point mutations is not yet fully explored. The objective of this research is to contribute to the establishment of *in vitro* disease models for CPVT with hiPSCs as a source for CMs.

CPVT disease models of this project were based on hiPSCs from CPVT patients b1 and c2, who respectively had a missense mutation A2254V or E4076K at different loci. In this study pluripotency was proven in hiPSCs from CPVT patient c2. The differentiation potential of hiPSCs into all three germ layers ectoderm, mesoderm and endoderm was verified as well. The hiPSCs from CPVT patient b1 were characterized in previous studies.

For further investigation of the point mutation-based phenotype in CPVT patients CRISPR/Cas9 technology was applied for genome editing in hiPSCs from the CPVT patient b1. The study failed to fulfill the aim to correct the single point mutation in hiPSCs from patient b1 to generate an isogenic corrected control cell line. Nevertheless, homogeneous CRISPR/Cas9-edited hiPSCs with a knockout of the RYR2 protein were generated, characterized for pluripotency-associated marker and differentiated into CMs. The CRISPR/Cas9-edited CMs with homozygous deletions in *RYR2* showed normal RYR2 mRNA expression, but no expression of the RYR2 protein. The CRISPR/Cas9 edited CMs showed a typical expression pattern for the remaining cardiac marker on mRNA and protein level. Surprisingly, RyR2_X4_KO-CMs were able to contract without the expression of RYR2 protein compared to the control CPVT-CMs and showed no CPVT typical Ca^{2+} leak.

In conclusion, the data of this study show that patient-specific hiPSCs are useful tools to create CPVT disease models. Even though an isogenic corrected control cell line could not be generated in this study, CRISPR/Cas9 systems are a promising tool for genetic manipulation in hiPSCs.

RyR2_X4_KO-CMs offer the possibility to analyze the compensatory adaption mechanism for a sufficient Ca^{2+}cycling without functioning RYR2 protein. As a result, future drug targets can be developed.

6 References

Ai X, Curran JW, Shannon TR, Bers DM, Pogwizd SM (2005): Ca2+/Calmodulin–Dependent Protein Kinase Modulates Cardiac Ryanodine Receptor Phosphorylation and Sarcoplasmic Reticulum Ca2+ Leak in Heart Failure. Circ Res 97, 1314–1322

Assinck P, Duncan GJ, Hilton BJ, Plemel JR, Tetzlaff W (2017): Cell transplantation therapy for spinal cord injury. Nat Neurosci 20, 637–647

Barac YD, Zeevi-Levin N, Yaniv G, Reiter I, Milman F, Shilkrut M, Coleman R, Abassi Z, Binah O (2005): The 1,4,5-inositol trisphosphate pathway is a key component in Fas-mediated hypertrophy in neonatal rat ventricular myocytes. Cardiovasc Res 68, 75–86

Barrangou R, Marraffini LA (2014): CRISPR-Cas systems: prokaryotes upgrade to adaptive immunity. Mol Cell 54, 234–244

Beers J, Gulbranson DR, George N, Siniscalchi LI, Jones J, Thomson JA, Chen G (2012): Passaging and colony expansion of human pluripotent stem cells by enzyme-free dissociation in chemically defined culture conditions. Nat Protoc 7, 2029–2040

Bellin M, Marchetto MC, Gage FH, Mummery CL (2012): Induced pluripotent stem cells: the new patient? Nat Rev Mol Cell Biol 13, 713–726

Bellin M, Casini S, Davis RP, D'Aniello C, Haas J, Ward-van Oostwaard D, Tertoolen LGJ, Jung CB, Elliott DA, Welling A, et al. (2013): Isogenic human pluripotent stem cell pairs reveal the role of a KCNH2 mutation in long-QT syndrome. EMBO J 32, 3161–3175

Belmonte S, Morad M (2008): 'Pressure–flow'-triggered intracellular Ca2+ transients in rat cardiac myocytes: possible mechanisms and role of mitochondria. J Physiol 586, 1379

Beutner G, Sharma VK, Giovannucci DR, Yule DI, Sheu S-S (2001): Identification of a Ryanodine Receptor in Rat Heart Mitochondria. J Biol Chem 276, 21482–21488

Blayney LM, Lai FA (2009): Ryanodine receptor-mediated arrhythmias and sudden cardiac death. Pharmacol Ther 123, 151–177

Boyer LA, Lee TI, Cole MF, Johnstone SE, Levine SS, Zucker JP, Guenther MG, Kumar RM, Murray HL, Jenner RG, et al. (2005): Core Transcriptional Regulatory Circuitry in Human Embryonic Stem Cells. Cell 122, 947

Brimble SN, Sherrer ES, Uhl EW, Wang E, Kelly S, Merrill AH, Robins AJ, Schulz TC (2007): The Cell Surface Glycosphingolipids SSEA-3 and SSEA-4 Are Not Essential for Human ESC Pluripotency. Stem Cells 25, 54–62

Bround MJ, Asghari P, Wambolt RB, Bohunek L, Smits C, Philit M, Kieffer TJ, Lakatta EG, Boheler KR, Moore ED, et al. (2012): Cardiac ryanodine receptors control heart rate and rhythmicity in adult mice. Cardiovasc Res 96, 372-380

Burridge PW, Thompson S, Millrod MA, Weinberg S, Yuan X, Peters A, Mahairaki V, Koliatsos VE, Tung L, Zambidis ET (2011): A Universal System for Highly Efficient Cardiac Differentiation of Human Induced Pluripotent Stem Cells That Eliminates Interline Variability. PLoS ONE 6

Burridge PW, Matsa E, Shukla P, Lin ZC, Churko JM, Ebert AD, Lan F, Diecke S, Huber B, Mordwinkin NM, et al. (2014): Chemically Defined and Small Molecule-Based Generation of Human Cardiomyocytes. Nat Methods 11, 855–860

Byrne SM, Church GM (2015): Crispr-mediated Gene Targeting of Human Induced Pluripotent Stem Cells. Curr Protoc Stem Cell Biol 2015, 5A.8.1

Cavaleri F, Schöler HR (2003): Nanog. Cell 113, 551–552

Cencic R, Miura H, Malina A, Robert F, Ethier S, Schmeing TM, Dostie J, Pelletier J (2014): Protospacer Adjacent Motif (PAM)-Distal Sequences Engage CRISPR Cas9 DNA Target Cleavage. PLoS ONE 9

Cerrone M, Napolitano C, Priori SG (2009): Catecholaminergic polymorphic ventricular tachycardia: A paradigm to understand mechanisms of arrhythmias associated to impaired Ca2+ regulation. Heart Rhythm 6, 1652–1659

Chambers I, Tomlinson SR (2009): The transcriptional foundation of pluripotency. Dev Camb Engl 136, 2311–2322

Chambers I, Colby D, Robertson M, Nichols J, Lee S, Tweedie S, Smith A (2003): Functional Expression Cloning of Nanog, a Pluripotency Sustaining Factor in Embryonic Stem Cells. Cell 113, 643–655

Chang C-W, Lai Y-S, Westin E, Khodadadi-Jamayran A, Pawlik KM, Lamb LS Jr, Goldman FD, Townes TM (2015): Modeling Human Severe Combined Immunodeficiency and Correction by CRISPR/Cas9-Enhanced Gene Targeting. Cell Rep 12, 1668–1677

Chapman JR, Taylor MRG, Boulton SJ (2012): Playing the End Game: DNA Double-Strand Break Repair Pathway Choice. Mol Cell 47, 497–510

Chen G, Gulbranson DR, Hou Z, Bolin JM, Ruotti V, Probasco MD, Smuga-Otto K, Howden SE, Diol NR, Propson NE, et al. (2011): Chemically defined conditions for human iPS cell derivation and culture. Nat Methods 8, 424–429

Chen Y, Cao J, Xiong M, Petersen AJ, Dong Y, Tao Y, Huang CT-L, Du Z, Zhang S-C (2015): Engineering Human Stem Cell Lines with Inducible Gene Knockout using CRISPR/Cas9. Cell Stem Cell 17, 233–244

Cho SW, Kim S, Kim Y, Kweon J, Kim HS, Bae S, Kim J-S (2014): Analysis of off-target effects of CRISPR/Cas-derived RNA-guided endonucleases and nickases. Genome Res 24, 132

Colman A, Dreesen O (2009): Pluripotent Stem Cells and Disease Modeling. Cell Stem Cell 5, 244–247

De Ferrari GM, Dusi V, Spazzolini C, Bos JM, Abrams DJ, Berul CI, Crotti L, Davis AM, Eldar M, Kharlap M, et al. (2015): Clinical Management of Catecholaminergic Polymorphic Ventricular Tachycardia: The Role of Left Cardiac Sympathetic Denervation. Circulation 131, 2185–2193

Deveau H, Barrangou R, Garneau JE, Labonté J, Fremaux C, Boyaval P, Romero DA, Horvath P, Moineau S (2008): Phage Response to CRISPR-Encoded Resistance in Streptococcus thermophilus. J Bacteriol 190, 1390–1400

Dobrev D, Carlsson L, Nattel S (2012): Novel molecular targets for atrial fibrillation therapy. Nat Rev Drug Discov 11, 275–291

Doudna JA, Charpentier E (2014): The new frontier of genome engineering with CRISPR-Cas9. Science 346, 1258096

Fabiato A (1983): Calcium-induced release of calcium from the cardiac sarcoplasmic reticulum. Am J Physiol - Cell Physiol 245, C1–C14

Fatima A, Xu G, Shao K, Papadopoulos S, Lehmann M, Arnáiz-Cot JJ, Rosa AO, Nguemo F, Matzkies M, Dittmann S, et al. (2011): In vitro Modeling of Ryanodine Receptor 2 Dysfunction Using Human Induced Pluripotent Stem Cells. Cell Physiol Biochem 28, 579–592

Firth AL, Menon T, Parker GS, Qualls SJ, Lewis BM, Ke E, Dargitz CT, Wright R, Khanna A, Gage FH, Verma IM (2015): Functional Gene Correction for Cystic Fibrosis in Lung Epithelial Cells Generated From Patient iPSCs. Cell Rep 12, 1385–1390

Frock RL, Hu J, Meyers RM, Ho Y-J, Kii E, Alt FW (2015): Genome-wide detection of DNA double-stranded breaks induced by engineered nucleases. Nat Biotechnol 33, 179–186

Fusaki N, Ban H, Nishiyama A, Saeki K, Hasegawa M (2009): Efficient induction of transgene-free human pluripotent stem cells using a vector based on Sendai virus, an RNA virus that does not integrate into the host genome. Proc Jpn Acad Ser B Phys Biol Sci 85, 348–362

Garneau JE, Dupuis M-È, Villion M, Romero DA, Barrangou R, Boyaval P, Fremaux C, Horvath P, Magadán AH, Moineau S (2010): The CRISPR/Cas bacterial immune system cleaves bacteriophage and plasmid DNA. Nature 468, 67–71

Giannini G, Conti A, Mammarella S, Scrobogna M, Sorrentino V (1995): The ryanodine receptor/calcium channel genes are widely and differentially expressed in murine brain and peripheral tissues. J Cell Biol 128, 893–904

Go LO, Moschella MC, Watras J, Handa KK, Fyfe BS, Marks AR (1995): Differential regulation of two types of intracellular calcium release channels during end-stage heart failure. J Clin Invest 95, 888

Grissa I, Vergnaud G, Pourcel C (2007): The CRISPRdb database and tools to display CRISPRs and to generate dictionaries of spacers and repeats. BMC Bioinformatics 8, 172

Hakamata Y, Nakai J, Takeshima H, Imoto K (1992): Primary structure and distribution of a novel ryanodine receptor/calcium release channel from rabbit brain. FEBS Lett 312, 229–235

Hanna LA, Foreman RK, Tarasenko IA, Kessler DS, Labosky PA (2002): Requirement for Foxd3 in maintaining pluripotent cells of the early mouse embryo. Genes Dev 16, 2650–2661

Hasenfuss G, Reinecke H, Studer R, Meyer M, Pieske B, Holtz J, Holubarsch C, Posival H, Just H, Drexler H (1994): Relation between myocardial function and expression of sarcoplasmic reticulum Ca(2+)-ATPase in failing and nonfailing human myocardium. Circ Res 75, 434–442

Hayashi M, Denjoy I, Extramiana F, Maltret A, Buisson NR, Lupoglazoff J-M, Klug D, Hayashi M, Takatsuki S, Villain E, et al. (2009): Incidence and Risk Factors of Arrhythmic Events in Catecholaminergic Polymorphic Ventricular Tachycardia. Circulation 119, 2426–2434

Henze S: Induced pluripotent stem cell-derived cardiomyocytes as model for studying CPVT caused by mutations in RYR2. Biol. Diss. Göttingen 2016

Hotta S, Morimura K, Ohya S, Muraki K, Takeshima H, Imaizumi Y (2007): Ryanodine receptor type 2 deficiency changes excitation–contraction coupling and membrane potential in urinary bladder smooth muscle. J Physiol 582, 489

Hsu PD, Scott DA, Weinstein JA, Ran FA, Konermann S, Agarwala V, Li Y, Fine EJ, Wu X, Shalem O, et al. (2013): DNA targeting specificity of RNA-guided Cas9 nucleases. Nat Biotechnol 31, 827

Huang X, Wang Y, Yan W, Smith C, Ye Z, Wang J, Gao Y, Mendelsohn L, Cheng L (2015): Production of gene-corrected adult beta globin protein in human erythrocytes differentiated from patient iPSCs after genome editing of the sickle point mutation. Stem Cells Dayt Ohio 33, 1470

Itskovitz-Eldor J, Schuldiner M, Karsenti D, Eden A, Yanuka O, Amit M, Soreq H, Benvenisty N (2000): Differentiation of human embryonic stem cells into embryoid bodies compromising the three embryonic germ layers. Mol Med 6, 88

Itzhaki I, Maizels L, Huber I, Gepstein A, Arbel G, Caspi O, Miller L, Belhassen B, Nof E, Glikson M, Gepstein L (2012): Modeling of Catecholaminergic Polymorphic Ventricular Tachycardia With Patient-Specific Human-Induced Pluripotent Stem Cells. J Am Coll Cardiol 60, 990–1000

Iwamoto T (2004): Forefront of Na^+/Ca^{2+} Exchanger Studies: Molecular Pharmacology of Na^+/Ca^{2+} Exchange Inhibitors. J Pharmacol Sci 96, 27–32

Janowski E, Berríos M, Cleemann L, Morad M (2010): Developmental aspects of cardiac Ca2+ signaling: interplay between RyR- and IP3R-gated Ca2+ stores. Am J Physiol - Heart Circ Physiol 298, H1939

Jiang D, Xiao B, Yang D, Wang R, Choi P, Zhang L, Cheng H, Chen SRW (2004): RyR2 mutations linked to ventricular tachycardia and sudden death reduce the threshold for store-overload-induced Ca2+ release (SOICR). Proc Natl Acad Sci U S A 101, 13062–13067

Jiang J, Chan Y-S, Loh Y-H, Cai J, Tong G-Q, Lim C-A, Robson P, Zhong S, Ng H-H (2008): A core Klf circuitry regulates self-renewal of embryonic stem cells. Nat Cell Biol 10, 353–360

Jiang Y, Lee A, Chen J, Cadene M, Chait BT, MacKinnon R (2002): The open pore conformation of potassium channels. Nature 417, 523–526

Jinek M, Chylinski K, Fonfara I, Hauer M, Doudna JA, Charpentier E (2012): A Programmable Dual-RNA–Guided DNA Endonuclease in Adaptive Bacterial Immunity. Science 337, 816–821

Kabadi AM, Ousterout DG, Hilton IB, Gersbach CA (2014): Multiplex CRISPR/Cas9-based genome engineering from a single lentiviral vector. Nucleic Acids Res 42, e147

Kaminski R, Chen Y, Fischer T, Tedaldi E, Napoli A, Zhang Y, Karn J, Hu W, Khalili K (2016): Elimination of HIV-1 Genomes from Human T-lymphoid Cells by CRISPR/Cas9 Gene Editing. Sci Rep 6

Karginov FV, Hannon GJ (2010): The CRISPR system: small RNA-guided defense in bacteria and archaea. Mol Cell 37, 7

Kattman SJ, Witty AD, Gagliardi M, Dubois NC, Niapour M, Hotta A, Ellis J, Keller G (2011): Stage-Specific Optimization of Activin/Nodal and BMP Signaling Promotes Cardiac Differentiation of Mouse and Human Pluripotent Stem Cell Lines. Cell Stem Cell 8, 228–240

Kim C, Wong J, Wen J, Wang S, Wang C, Spiering S, Kan NG, Forcales S, Puri PL, Leone TC, et al. (2013): Studying arrhythmogenic right ventricular dysplasia with patient-specific iPSCs. Nature 494, 105–110

Kim D, Bae S, Park J, Kim E, Kim S, Yu HR, Hwang J, Kim J-I, Kim J-S (2015): Digenome-seq: genome-wide profiling of CRISPR-Cas9 off-target effects in human cells. Nat Methods 12, 237–243

Kim EE, Wyckoff HW (1991): Reaction mechanism of alkaline phosphatase based on crystal structures. J Mol Biol 218, 449–464

Kim J, Chu J, Shen X, Wang J, Orkin SH (2008): An extended transcriptional network for pluripotency of embryonic stem cells. Cell 132

Kleinstiver BP, Pattanayak V, Prew MS, Tsai SQ, Nguyen N, Zheng Z, Joung JK (2016): High-fidelity CRISPR-Cas9 variants with undetectable genome-wide off-targets. Nature 529, 490–495

Kubalova Z, Terentyev D, Viatchenko-Karpinski S, Nishijima Y, Györke I, Terentyeva R, da Cuñha DNQ, Sridhar A, Feldman DS, Hamlin RL, et al. (2005): Abnormal intrastore calcium signaling in chronic heart failure. Proc Natl Acad Sci U S A 102, 14104–14109

Laflamme MA, Chen KY, Naumova AV, Muskheli V, Fugate JA, Dupras SK, Reinecke H, Xu C, Hassanipour M, Police S, et al. (2007): Cardiomyocytes derived from human embryonic stem cells in pro-survival factors enhance function of infarcted rat hearts. Nat Biotechnol 25, 1015–1024

Lahat H, Pras E, Olender T, Avidan N, Ben-Asher E, Man O, Levy-Nissenbaum E, Khoury A, Lorber A, Goldman B, et al. (2001): A Missense Mutation in a Highly Conserved Region of CASQ2 Is Associated with Autosomal Recessive Catecholamine-Induced Polymorphic Ventricular Tachycardia in Bedouin Families from Israel. Am J Hum Genet 69, 1378–1384

Laver DR, Honen BN, Lamb GD, Ikemoto N (2007): A domain peptide of the cardiac ryanodine receptor regulates channel sensitivity to luminal Ca2+ via cytoplasmic Ca2+ sites. Eur Biophys J 37, 455–467

Ledbetter MW, Preiner JK, Louis CF, Mickelson JR (1994): Tissue distribution of ryanodine receptor isoforms and alleles determined by reverse transcription polymerase chain reaction. J Biol Chem 269, 31544–31551

Lee CM, Cradick TJ, Fine EJ, Bao G (2016a): Nuclease Target Site Selection for Maximizing On-target Activity and Minimizing Off-target Effects in Genome Editing. Mol Ther 24, 475

Lee CM, Cradick TJ, Bao G (2016b): The Neisseria meningitidis CRISPR-Cas9 System Enables Specific Genome Editing in Mammalian Cells. Mol Ther 24, 645–654
Lee Y-K, Ng K-M, Lai W-H, Chan Y-C, Lau Y-M, Lian Q, Tse H-F, Siu C-W (2011): Calcium Homeostasis in Human Induced Pluripotent Stem Cell-Derived Cardiomyocytes. Stem Cell Rev 7, 976

Leenhardt A, Lucet V, Denjoy I, Grau F, Ngoc DD, Coumel P (1995): Catecholaminergic Polymorphic Ventricular Tachycardia in Children A 7-Year Follow-up of 21 Patients. Circulation 91, 1512–1519

Leenhardt A, Denjoy I, Guicheney P (2012): Catecholaminergic Polymorphic Ventricular Tachycardia. Circ Arrhythm Electrophysiol 5, 1044–1052

Lehnart SE, Mongillo M, Bellinger A, Lindegger N, Chen B-X, Hsueh W, Reiken S, Wronska A, Drew LJ, Ward CW, et al. (2008): Leaky Ca2+ release channel/ryanodine receptor 2 causes seizures and sudden cardiac death in mice. J Clin Invest 118, 2230–2245

Levine AJ, Brivanlou AH (2006): GDF3, a BMP inhibitor, regulates cell fate in stem cells and early embryos. Development 133, 209–216

Li H-O, Zhu Y-F, Asakawa M, Kuma H, Hirata T, Ueda Y, Lee Y-S, Fukumura M, Iida A, Kato A, et al. (2000): A Cytoplasmic RNA Vector Derived from Nontransmissible Sendai Virus with Efficient Gene Transfer and Expression. J Virol 74, 6564

Lian X, Hsiao C, Wilson G, Zhu K, Hazeltine LB, Azarin SM, Raval KK, Zhang J, Kamp TJ, Palecek SP (2012): Robust cardiomyocyte differentiation from human pluripotent stem cells via temporal modulation of canonical Wnt signaling. Proc Natl Acad Sci U S A 109, E1848–E1857

Lian X, Zhang J, Azarin SM, Zhu K, Hazeltine LB, Bao X, Hsiao C, Kamp TJ, Palecek SP (2013): Directed cardiomyocyte differentiation from human pluripotent stem cells by modulating Wnt/β-catenin signaling under fully defined conditions. Nat Protoc 8, 162–175

Litwin SE, Zhang D (2006): Enhanced Sodium- Calcium Exchange in the Infarcted Heart. Ann N Y Acad Sci 976, 446–453

Liu N, Rizzi N, Boveri L, Priori SG (2009): Ryanodine receptor and calsequestrin in arrhythmogenesis: What we have learnt from genetic diseases and transgenic mice. J Mol Cell Cardiol 46, 149–159

Liu Z, Zhang J, Li P, Chen SRW, Wagenknecht T (2002): Three-dimensional Reconstruction of the Recombinant Type 2 Ryanodine Receptor and Localization of Its Divergent Region 1. J Biol Chem 277, 46712–46719

Lopes SMC de S, Hassink RJ, Feijen A, Rooijen MA van, Doevendans PA, Tertoolen L, Rivière AB de la, Mummery CL (2006): Patterning the heart, a template for human cardiomyocyte development. Dev Dyn 235, 1994–2002

Mandai M, Watanabe A, Kurimoto Y, Hirami Y, Morinaga C, Daimon T, Fujihara M, Akimaru H, Sakai N, Shibata Y, et al. (2017): Autologous Induced Stem-Cell–Derived Retinal Cells for Macular Degeneration. N Engl J Med 376, 1038–1046

Marks AR, Tempst P, Hwang KS, Taubman MB, Inui M, Chadwick C, Fleischer S, Nadal-Ginard B (1989): Molecular cloning and characterization of the ryanodine receptor/junctional channel complex cDNA from skeletal muscle sarcoplasmic reticulum. Proc Natl Acad Sci 86, 8683–8687

Marks AR, Priori S, Memmi M, Kontula K, Laitinen PJ (2002): Involvement of the cardiac ryanodine receptor/calcium release channel in catecholaminergic polymorphic ventricular tachycardia. J Cell Physiol 190, 1–6

Martí M, Mulero L, Pardo C, Morera C, Carrió M, Laricchia-Robbio L, Esteban CR, Belmonte JCI (2013): Characterization of pluripotent stem cells. Nat Protoc 8, 223–253

Maruyama T, Dougan SK, Truttmann M, Bilate AM, Ingram JR, Ploegh HL (2015): Inhibition of non-homologous end joining increases the efficiency of CRISPR/Cas9-mediated precise [TM: inserted] genome editing. Nat Biotechnol 33, 538

Mathur A, Loskill P, Shao K, Huebsch N, Hong S, Marcus SG, Marks N, Mandegar M, Conklin BR, Lee LP, Healy KE (2015): Human iPSC-based Cardiac Microphysiological System For Drug Screening Applications. Sci Rep 5

Monzen K, Shiojima I, Hiroi Y, Kudoh S, Oka T, Takimoto E, Hayashi D, Hosoda T, Habara-Ohkubo A, Nakaoka T, et al. (1999): Bone Morphogenetic Proteins Induce Cardiomyocyte Differentiation through the Mitogen-Activated Protein Kinase Kinase Kinase TAK1 and Cardiac Transcription Factors Csx/Nkx-2.5 and GATA-4. Mol Cell Biol 19, 7096

Müller M, Lee CM, Gasiunas G, Davis TH, Cradick TJ, Siksnys V, Bao G, Cathomen T, Mussolino C (2016): Streptococcus thermophilus CRISPR-Cas9 Systems Enable Specific Editing of the Human Genome. Mol Ther 24, 636–644

Mullis K, Faloona F, Scharf S, Saiki R, Horn G, Erlich H (1992): Specific enzymatic amplification of DNA in vitro: the polymerase chain reaction. 1986. Biotechnol Read Mass 24, 17–27

Musunuru K (2017): The Hope and Hype of CRISPR-Cas9 Genome Editing: A Review. JAMA Cardiol 2, 914-919

Naito AT, Shiojima I, Akazawa H, Hidaka K, Morisaki T, Kikuchi A, Komuro I (2006): Developmental stage-specific biphasic roles of Wnt/β-catenin signaling in cardiomyogenesis and hematopoiesis. Proc Natl Acad Sci U S A 103, 19812

Nakagawa M, Takizawa N, Narita M, Ichisaka T, Yamanaka S (2010): Promotion of direct reprogramming by transformation-deficient Myc. Proc Natl Acad Sci U S A 107, 14152-14157

Nakagawa M, Karagiannis P, Yamanaka S (2016): When Myc's asleep, embryonic stem cells are dormant. EMBO J 35, 801-802

Nakai J, Imagawa T, Hakamata Y, Shigekawa M, Takeshima H, Numa S (1990): Primary structure and functional expression from cDN A of the cardiac ryanodine receptor/calcium release channel. FEBS Lett 271, 169–177

Napolitano C, Priori SG (2007): Diagnosis and treatment of catecholaminergic polymorphic ventricular tachycardia. Heart Rhythm 4, 675–678

Novak A, Barad L, Zeevi-Levin N, Shick R, Shtrichman R, Lorber A, Itskovitz-Eldor J, Binah O (2012): Cardiomyocytes generated from CPVTD307H patients are arrhythmogenic in response to β-adrenergic stimulation. J Cell Mol Med 16, 468–482

Novak A, Barad L, Lorber A, Gherghiceanu M, Reiter I, Eisen B, Eldor L, Itskovitz-Eldor J, Eldar M, Arad M, Binah O (2015): Functional abnormalities in iPSC-derived cardiomyocytes generated from CPVT1 and CPVT2 patients carrying ryanodine or calsequestrin mutations. J Cell Mol Med n/a-n/a

Oda T, Yano M, Yamamoto T, Tokuhisa T, Okuda S, Doi M, Ohkusa T, Ikeda Y, Kobayashi S, Ikemoto N, Matsuzaki M (2005): Defective Regulation of Interdomain Interactions Within the Ryanodine Receptor Plays a Key Role in the Pathogenesis of Heart Failure. Circulation 111, 3400–3410

O'Geen H, Henry IM, Bhakta MS, Meckler JF, Segal DJ (2015): A genome-wide analysis of Cas9 binding specificity using ChIP-seq and targeted sequence capture. Nucleic Acids Res 43, 3389

Olde Nordkamp LRA, Driessen AHG, Odero A, Blom NA, Koolbergen DR, Schwartz PJ, Wilde AAM (2014): Left cardiac sympathetic denervation in the Netherlands for the treatment of inherited arrhythmia syndromes. Neth Heart J 22, 160–166

Paquet D, Kwart D, Chen A, Sproul A, Jacob S, Teo S, Olsen KM, Gregg A, Noggle S, Tessier-Lavigne M (2016): Efficient introduction of specific homozygous and heterozygous mutations using CRISPR/Cas9. Nature 533, 125–129

Pease S, Braghetta P, Gearing D, Grail D, Williams RL (1990): Isolation of embryonic stem (ES) cells in media supplemented with recombinant leukemia inhibitory factor (LIF). Dev Biol 141, 344–352

Pekkanen-Mattila M, Pelto-Huikko M, Kujala V, Suuronen R, Skottman H, Aalto-Setälä K, Kerkelä E (2010): Spatial and temporal expression pattern of germ layer markers during human embryonic stem cell differentiation in embryoid bodies. Histochem Cell Biol 133, 595–606

Priori SG, Chen SRW (2011): Inherited Dysfunction of Sarcoplasmic Reticulum Ca2+ Handling and Arrhythmogenesis. Circ Res 108, 871–883

Priori SG, Napolitano C, Memmi M, Colombi B, Drago F, Gasparini M, DeSimone L, Coltorti F, Bloise R, Keegan R, et al. (2002): Clinical and Molecular Characterization of Patients With Catecholaminergic Polymorphic Ventricular Tachycardia. Circulation 106, 69–74

Priori SG, Wilde AA, Horie M, Cho Y, Behr ER, Berul C, Blom N, Brugada J, Chiang C-E, Huikuri H, et al. (2013): HRS/EHRA/APHRS Expert Consensus Statement on the Diagnosis and Management of Patients with Inherited Primary Arrhythmia Syndromes. Heart Rhythm 10, 1932–1963

Ran FA, Cong L, Yan WX, Scott DA, Gootenberg JS, Kriz AJ, Zetsche B, Shalem O, Wu X, Makarova KS, et al. (2015): In vivo genome editing using Staphylococcus aureus Cas9. Nature 520, 186–191

Reid DS, Tynan M, Braidwood L, Fitzgerald GR (1975): Bidirectional tachycardia in a child. A study using His bundle electrography. Br Heart J 37, 339–344

Reinecke H, Studer R, Vetter R, Holtz J, Drexler H (1996): Cardiac Na+/Ca2+ exchange activity in patients with end-stage heart failure. Cardiovasc Res 31, 48–54

Reubinoff BE, Pera MF, Fong C-Y, Trounson A, Bongso A (2000): Embryonic stem cell lines from human blastocysts: somatic differentiation in vitro. Nat Biotechnol 18, 399–404

Richards M, Tan S-P, Tan J-H, Chan W-K, Bongso A (2004): The Transcriptome Profile of Human Embryonic Stem Cells as Defined by SAGE. Stem Cells 22, 51–64

Rosemblit N, Moschella MC, Ondriašová E, Gutstein DE, Ondriaš K, Marks AR (1999): Intracellular Calcium Release Channel Expression during Embryogenesis. Dev Biol 206, 163–177

Rossi D, Sorrentino V (2002): Molecular genetics of ryanodine receptors Ca2+-release channels. Cell Calcium 32, 307–319

Samavarchi-Tehrani P, Golipour A, David L, Sung H, Beyer TA, Datti A, Woltjen K, Nagy A, Wrana JL (2010): Functional Genomics Reveals a BMP-Driven Mesenchymal-to-Epithelial Transition in the Initiation of Somatic Cell Reprogramming. Cell Stem Cell 7, 64–77

Sander JD, Joung JK (2014): CRISPR-Cas systems for genome editing, regulation and targeting. Nat Biotechnol 32, 347–355

Schopperle WM, DeWolf WC (2007): The TRA-1-60 and TRA-1-81 Human Pluripotent Stem Cell Markers Are Expressed on Podocalyxin in Embryonal Carcinoma. Stem Cells 25, 723–730

Schultheiss TM, Burch JB, Lassar AB (1997): A role for bone morphogenetic proteins in the induction of cardiac myogenesis. Genes Dev 11, 451–462

Sheridan SD, Surampudi V, Rao RR (2012): Analysis of Embryoid Bodies Derived from Human Induced Pluripotent Stem Cells as a Means to Assess Pluripotency. Stem Cells Int 2012, 738910

Shui B, Hernandez Matias L, Guo Y, Peng Y (2016): The Rise of CRISPR/Cas for Genome Editing in Stem Cells. Stem Cells Int 2016

Slaymaker IM, Gao L, Zetsche B, Scott DA, Yan WX, Zhang F (2016): Rationally engineered Cas9 nucleases with improved specificity. Science 351, 84–88

Song L-S, Pi Y, Kim S-J, Yatani A, Guatimosim S, Kudej RK, Zhang Q, Cheng H, Hittinger L, Ghaleh B, et al. (2005): Paradoxical Cellular Ca2+ Signaling in Severe but Compensated Canine Left Ventricular Hypertrophy. Circ Res 97, 457–464

Sugiura T, Hibino N, Breuer CK, Shinoka T (2016): Tissue-engineered cardiac patch seeded with human induced pluripotent stem cell derived cardiomyocytes promoted the regeneration of host cardiomyocytes in a rat model. J Cardiothorac Surg 11 (1), 163

Sumitomo N, Harada K, Nagashima M, Yasuda T, Nakamura Y, Aragaki Y, Saito A, Kurosaki K, Jouo K, Koujiro M, et al. (2003): Catecholaminergic polymorphic ventricular tachycardia: electrocardiographic characteristics and optimal therapeutic strategies to prevent sudden death. Heart 89, 66–70

Takahashi K, Yamanaka S (2006): Induction of Pluripotent Stem Cells from Mouse Embryonic and Adult Fibroblast Cultures by Defined Factors. Cell 126, 663–676

Takahashi K, Tanabe K, Ohnuki M, Narita M, Ichisaka T, Tomoda K, Yamanaka S (2007): Induction of Pluripotent Stem Cells from Adult Human Fibroblasts by Defined Factors. Cell 131, 861–872

Takeshima H, Yamazawa T, Ikemoto T, Takekura H, Nishi M, Noda T, Iino M (1995): Ca(2+)-induced Ca2+ release in myocytes from dyspedic mice lacking the type-1 ryanodine receptor. EMBO J 14, 2999–3006

Takeshima H, Komazaki S, Hirose K, Nishi M, Noda T, Iino M (1998): Embryonic lethality and abnormal cardiac myocytes in mice lacking ryanodine receptor type 2. EMBO J 17, 3309–3316

Tang Z-H, Chen J-R, Zheng J, Shi H-S, Ding J, Qian X-D, Zhang C, Chen J-L, Wang C-C, Li L, et al. (2016): Genetic Correction of Induced Pluripotent Stem Cells From a Deaf Patient With MYO7A Mutation Results in Morphologic and Functional Recovery of the Derived Hair Cell-Like Cells. Stem Cells Transl Med 5, 561

Tohyama S, Hattori F, Sano M, Hishiki T, Nagahata Y, Matsuura T, Hashimoto H, Suzuki T, Yamashita H, Satoh Y, et al. (2013): Distinct Metabolic Flow Enables Large-Scale Purification of Mouse and Human Pluripotent Stem Cell-Derived Cardiomyocytes. Cell Stem Cell 12, 127–137

Tsai SQ, Wyvekens N, Khayter C, Foden JA, Thapar V, Reyon D, Goodwin MJ, Aryee MJ, Joung JK (2014): Dimeric CRISPR RNA-guided FokI nucleases for highly specific genome editing. Nat Biotechnol 32, 569–576

Turan S, Farruggio AP, Srifa W, Day JW, Calos MP (2016): Precise Correction of Disease Mutations in Induced Pluripotent Stem Cells Derived From Patients With Limb Girdle Muscular Dystrophy. Mol Ther 24, 685

Tyser RC, Miranda AM, Chen C, Davidson SM, Srinivas S, Riley PR (2016): Calcium handling precedes cardiac differentiation to initiate the first heartbeat. eLife 5, e17113

Valamehr B, Abujarour R, Robinson M, Le T, Robbins D, Shoemaker D, Flynn P (2012): A novel platform to enable the high-throughput derivation and characterization of feeder-free human iPSCs. Sci Rep 2, 213

Warren L, Manos PD, Ahfeldt T, Loh Y-H, Li H, Lau F, Ebina W, Mandal P, Smith ZD, Meissner A, et al. (2010): Highly efficient reprogramming to pluripotency and directed differentiation of human cells using synthetic modified mRNA. Cell Stem Cell 7, 618–630

Wehrens XH, Marks AR (2004): Novel therapeutic approaches for heart failure by normalizing calcium cycling. Nat Rev Drug Discov 3, 565–574

van der Werf C, Wilde AA (2015): Catecholaminergic Polymorphic Ventricular Tachycardia: Disease With Different Faces. Circ Arrhythm Electrophysiol 8, 523–525

Willems E, Cabral-Teixeira J, Schade D, Cai W, Reeves P, Bushway PJ, Lanier M, Walsh C, Kirchhausen T, Belmonte JCI, et al. (2012): Small molecule-mediated TGFβ Type II receptor degradation promotes cardiomyogenesis in embryonic stem cells. Cell Stem Cell 11, 242–252

Wobus AM, Holzhausen H, Jäkel P, Schöneich J (1984): Characterization of a pluripotent stem cell line derived from a mouse embryo. Exp Cell Res 152, 212–219

Yu C, Liu Y, Ma T, Liu K, Xu S, Zhang Y, Liu H, Russa ML, Xie M, Sheng D, Qi LS (2015): Small Molecules Enhance CRISPR Genome Editing in Pluripotent Stem Cells. Cell Stem Cell 16, 142

Yu J, Vodyanik MA, Smuga-Otto K, Antosiewicz-Bourget J, Frane JL, Tian S, Nie J, Jonsdottir GA, Ruotti V, Stewart R, et al. (2007): Induced Pluripotent Stem Cell Lines Derived from Human Somatic Cells. Science 318, 1917–1920

Yusa K, Rashid ST, Strick-Marchand H, Varela I, Liu P-Q, Paschon DE, Miranda E, Ordóñez A, Hannan N, Rouhani FJ, et al. (2011): Targeted gene correction of α1-antitrypsin deficiency in induced pluripotent stem cells. Nature 478, 391–394

Zhang J, Nuebel E, Daley GQ, Koehler CM, Teitell MA (2012): Metabolic Regulation in Pluripotent Stem Cells during Reprogramming and Self-Renewal. Cell Stem Cell 11, 589

Zhang J-H, Adikaram P, Pandey M, Genis A, Simonds WF (2016): Optimization of genome editing through CRISPR-Cas9 engineering. Bioengineered 7, 166

Zhang S, Cui W (2014): Sox2, a key factor in the regulation of pluripotency and neural differentiation. World J Stem Cells 6, 305–311

Zhang X-H, Tee LY, Wang X-G, Huang Q-S, Yang S-H (2015): Off-target Effects in CRISPR/Cas9-mediated Genome Engineering. Mol Ther — Nucleic Acids 4, e264

Zorzato F, Fujii J, Otsu K, Phillips M, Green NM, Lai FA, Meissner G, MacLennan DH (1990): Molecular cloning of cDNA encoding human and rabbit forms of the Ca2+ release channel (ryanodine receptor) of skeletal muscle sarcoplasmic reticulum. J Biol Chem 265, 2244–2256

7 Acknowledgement

I would like to express my sincere gratitude to my supervisor Prof. Dr. Kaomei Guan-Schmidt for the continuous support of my project and research, for her patience, immense knowledge and the professional working environment created throughout the research process.

My appreciation also goes to Dr. Lukas Cyganek for his insightful expertise during the work in the lab, his encouragement to set up this project, his supervision and the performance of the confocal microscopy for the calcium imaging. I appreciated the long distance runs through the Göttinger forest after work and I am truly thankful for the resulting friendship.

My further appreciation goes to Mrs. Dr. Sarah Henze for her supervision and especially for the technical completion of the protein analysis of the RyR2_X4_KO-CMs experiments.

I would like to express my special thanks to the German Centre for Cardiovascular Research (DZHK) for the scholarship granted during my research time in the lab.

I thank my fellow colleagues Mrs. Karolina Sekeres, and Xiaojing Luo for stimulating discussions and brilliant comments as well as all other colleagues of the University Clinic Göttingen (UMG) for the pleasant atmosphere and knowledge.

Finally, I truly thank my parents and grandparents for the support and guidance during my studies.

8 Curriculum vitae

My name is Maximilian Zimmermann. I was born on 2nd July 1989 in Bonn. My parents are Maria Rath-Mainka and Peter Zimmermann.

My school career began at the community primary school Hoffnungsthal in Rösrath. I obtained my general university entrance qualification (*Abitur*) in 2009 after attending the *Freiherr-vom-Stein Gymnasium* in Rösrath. Subsequently, I completed a voluntary social year in Uganda from 08/2009 to 08/2010 as part of the *Weltwärts* program. In the winter semester 2010/2011 I started my studies in International Economics and Development in Bayreuth. In the summer semester 2011 I finally changed the course of studies to the study of human medicine in Göttingen. I successfully completed the study of human medicine in November 2017 with the 3rd state examination and obtained my license to practice medicine (*Approbation*) on 7th December 2017.

In January 2018 I started my further education in internal medicine at the Medical Clinic III, Department of Hematology, Oncology and Rheumatology of the University Hospital Bonn.